

Hadronic Jets

An introduction

Andrea Banfi

University of Sussex, Brighton, UK

Morgan & Claypool Publishers

Copyright © 2016 Morgan & Claypool Publishers

All rights reserved. No part of this publication may be reproduced, stored in a retrieval system or transmitted in any form or by any means, electronic, mechanical, photocopying, recording or otherwise, without the prior permission of the publisher, or as expressly permitted by law or under terms agreed with the appropriate rights organization. Multiple copying is permitted in accordance with the terms of licences issued by the Copyright Licensing Agency, the Copyright Clearance Centre and other reproduction rights organisations.

Rights & Permissions

To obtain permission to re-use copyrighted material from Morgan & Claypool Publishers, please contact info@morganclaypool.com.

ISBN 978-1-6817-4073-7 (ebook)

ISBN 978-1-6817-4009-6 (print)

ISBN 978-1-6817-4201-4 (mobi)

DOI 10.1088/978-1-6817-4073-7

Version: 20160201

IOP Concise Physics

ISSN 2053-2571 (online)

ISSN 2054-7307 (print)

A Morgan & Claypool publication as part of IOP Concise Physics

Published by Morgan & Claypool Publishers, 40 Oak Drive, San Rafael, CA, 94903, USA

IOP Publishing, Temple Circus, Temple Way, Bristol BS1 6HG, UK

To Heather and Luke, my first PhD students

Contents

Preface	ix
Acknowledgments	xi
Author biography	xii
1 Introduction	1-1
1.1 The basics of elementary particle physics	1-4
Bibliography	1-11
2 Jet algorithms	2-1
2.1 Cone or sequential algorithms?	2-4
2.1.1 Cone algorithms	2-4
2.1.2 Sequential algorithms	2-8
2.1.3 Common issues with jet algorithms	2-13
2.2 Novel jet clustering procedures	2-19
Bibliography	2-24
3 QCD for jet physics	3-1
3.1 Collinear splitting in QCD	3-3
3.2 Fixed-order QCD calculations	3-6
3.2.1 Leading-order calculations	3-6
3.2.2 Next-to-leading order (NLO) calculations	3-12
3.2.3 Fixed-order calculations beyond NLO	3-18
3.3 Multi-parton branching	3-19
3.4 At the boundary of perturbative QCD	3-34
Bibliography	3-39
4 Jets as discovery tools	4-1
4.1 Optimising the jet radius	4-3
4.2 Boosted objects and jet substructure	4-8
4.2.1 Groomers and taggers	4-9
4.2.2 Groomers and taggers in QCD	4-14
4.2.3 Event shapes for jet-substructure studies	4-17
4.2.4 The role of interjet radiation	4-18

4.2.5	Quantum jets and volatility	4-19
4.2.6	Jet substructure studies at the LHC	4-21
4.3	Quark–gluon jet discrimination	4-23
4.3.1	Differences between quark and gluon jets	4-24
4.3.2	Quark and gluon jet discrimination at the LHC	4-26
	Bibliography	4-27

Preface

When I was asked to write a concise presentation of hadronic jets, I first thought about what my fresh view on the subject could be. In fact, my research activity considers jets from a specific angle, that of precision calculations, and has the ambition of understanding complicated observables involving jets my means of analytic calculations. This requires a deep understanding of how jets are formed, and what the theoretical and experimental issues behind them are. This is the knowledge I have tried to share with the present book, which can be thought of as a gentle introduction to jet physics. I also asked myself what kind of people might find such reading useful. The book presents the main theoretical and experimental ideas that had made it possible for jet physics to bloom, and to become one of the hot topics in particle physics. It can be then useful to the first kind of readers I thought about, that is physicists not directly involved in the field, in the hope that, seeing how relevant problems in jet physics have been solved, they could find valuable inspiration for their own research. Also, many times during my career I have met students, both graduate and undergraduate, willing to start a project with me on jet physics, but without the proper background in quantum field theory. Such students are not ready to understand a topical review on the subject, or a book on collider physics. These are the second kind of readers I had in mind. Therefore, I chose to present intuitive physical explanations, so that a reader could quickly perceive the main ideas involved. Furthermore, I have described how to perform calculations involving jet observables using simple probabilistic arguments, which are a good starting point to understand more sophisticated theoretical approaches. Last but not least, I thought about the book as pleasant reading, where details could eventually be skipped, and in which each chapter could be read independently from the others.

Let me now describe how the book is organised. The introduction aims to explain what hadronic jets are, and why they are so important for our current understanding of the physics of elementary particles. This also chapter contains an express review of particle physics, so that the reader gets used to the language employed in the rest of the book. This is followed by a chapter on jet algorithms, that describes the procedures that are currently adopted to rigorously define jets. The first two chapters can be understood by a reader with a solid background in fundamental physics, with no detailed knowledge of particle physics required. Chapter 4 is devoted to one of the hot topics in high-energy physics, the search for new particles that decay into jets. This chapter could, in principle, be understood with the material contained in chapter 2. However, the main ideas presented in chapter 4 can be better appreciated by a reader familiar with quantum chromodynamics (QCD), the quantum field theory that provides the theoretical foundations of jet physics. Therefore, I have decided to devote chapter 3 to presenting QCD as the origin of the main theoretical tools that are nowadays used to describe jets. Chapter 3 can be thought of as a gigantic exercise, where every theoretical idea is presented through an example, followed by a review of how the same idea is actually implemented in current theoretical tools. It is my hope that the reader might understand the tasks

that each tool actually performs, and to which physical situations it can be reliably applied. Each chapter contains its own list of references, by no means complete. These are the ones I would suggest an interested reader to go through, so as to have a deeper understanding of the covered topics. Also, the book expresses a personal view on the subject, so I felt free to select which results to present. In fact, in order to help the book flow, I had to sacrifice an important topic like the production of jets with wide angular gaps between them; and relevant concepts like soft-gluon interference, renormalisation and parton density functions are only briefly mentioned.

Lastly, the book was completed just at the beginning of the high-energy runs of the Large Hadron Collider at CERN. This is the place where many of the methods presented here will reveal their full potential. I very much look forward to seeing these ideas put into practice, and hope that a ground-breaking discovery may come out thanks to them.

Acknowledgments

I am deeply grateful to Morgan & Claypool for offering me the possibility to write this book. In particular, I would like to thank Nicki Dennis, the editor in charge, for the very constructive feedback and for her support and advice during the whole writing process, and the editing staff of IOP, in particular Jacky Mucklow, for their infinite patience and invaluable help during the proofreading stage.

This book elaborates on various lectures for PhD students I delivered in Parma, in Freiburg, in Cargese and in Hamburg. I am therefore very grateful to the organising committees of those schools, in particular to Enrico Onofri, Karl Jacobs, Christophe Grojean and Hannes Jung for the invitations and for having given me the possibility to share the physics I love most. I am also grateful to all the students I met there for their questions, comments and valuable discussions and suggestions.

I am deeply indebted to Pino Marchesini and Yuri Dokshitzer, who are the people who have taught me QCD, and have supported me throughout my career. I have also benefited much from my longstanding collaboration with Gavin Salam, Giulia Zanderighi and Mrinal Dasgupta.

Much of the material on jet algorithms and jet substructure is the result of many illuminating discussions with Gavin Salam, Matteo Cacciari, Gregory Soyez, and Mrinal Dasgupta. In particular, I am grateful to Gavin Salam for clarifications on technical details of jet algorithms, and to Matteo Cacciari and Mrinal Dasgupta for comments on the book.

The part on fixed-order calculations reflects what I have learnt from experts in the field I met during my postdoc in Zurich. In particular, I acknowledge very fruitful discussions with Babis Anastasiou, Achilleas Lazopoulos, Thomas Gehrmann and Massimiliano Grazzini.

I also wish to thank my experimental colleagues Fabrizio Salvatore and Iacopo Vivarelli, who gave me valuable comments on the introductory part on detectors, and helped me understand the details of jet calibration.

Author biography

Andrea Banfi



Andrea Banfi is a theoretical particle physicist, expert in the development of theoretical tools for the calculation of observables involving hadronic jets at high-energy colliders. In particular, he is active in the calculation of Higgs production rates in the presence of hadronic jets at the Large Hadron Collider.

He obtained his PhD at the University of Milano in 2002, and then worked as a Research Associate for various institutions in Europe, namely NIKHEF (Amsterdam), the Cavendish Laboratory (Cambridge), the University of Milano-Bicocca, ETH Zurich, and as Assistant Professor by the University of Freiburg. In 2013 he joined the Theoretical Particle Physics group of the University of Sussex, where he is now Senior Lecturer.

Hadronic Jets

An introduction

Andrea Banfi

Chapter 1

Introduction

One of the most striking phenomena that can be observed in high-energy collisions of elementary particles is the production of highly collimated bunches of particles (see figure 1.1). These objects are known as hadronic jets. The word ‘hadronic’ refers to the fact that jets are made up of hadrons, particles which can interact through the strong force, the force that keeps atomic nuclei bound together. If we look inside a jet we might find protons and neutrons, the constituents of nuclei, and other less known hadrons such as pions, which are commonly observed as cosmic rays, as well as kaons, rho mesons, etc. Looking at the list of hadrons in the ‘Review of particle physics’ by the Particle Data Group [1], one finds around 160 pages devoted to mesons, hadrons of integer spin (bosons), such as the pions, and another 50 pages devoted to baryons, hadrons of half-integer spin (fermions), such as protons and neutrons. Given this proliferation of particles, it seems almost a dream to be able to understand anything about jets of hadrons, and even more inconceivable to write a book about them. Surprisingly enough, the main features of hadronic jets, such as their energies and angular distributions, have little to do with their constituent hadrons, but rather with the constituents of the hadrons themselves. It is firmly established that hadrons are not elementary particles, but are bound states of point-like particles, the quarks. These are spin-1/2 particles interacting via the strong force, which is mediated by spin-1 gauge bosons, the gluons. Quarks and gluons are commonly referred to as ‘partons’, using the name that was given to quarks the first time they were probed in inelastic electron–proton collisions at SLAC, in view of the fact that they appeared as parts of the proton [2, 3]. In fact, in every such collision the proton was breaking apart and the angular distribution of the scattered electrons could only be explained by assuming that they hit point-like spin-1/2 particles, carrying a fraction of the proton energy and charge. This behaviour was more pronounced the higher the momentum transferred by the electron in the collision. This means that the hit partons, when probed at high energy, were not tightly bound inside the proton, otherwise the latter would have had recoiled against the electron

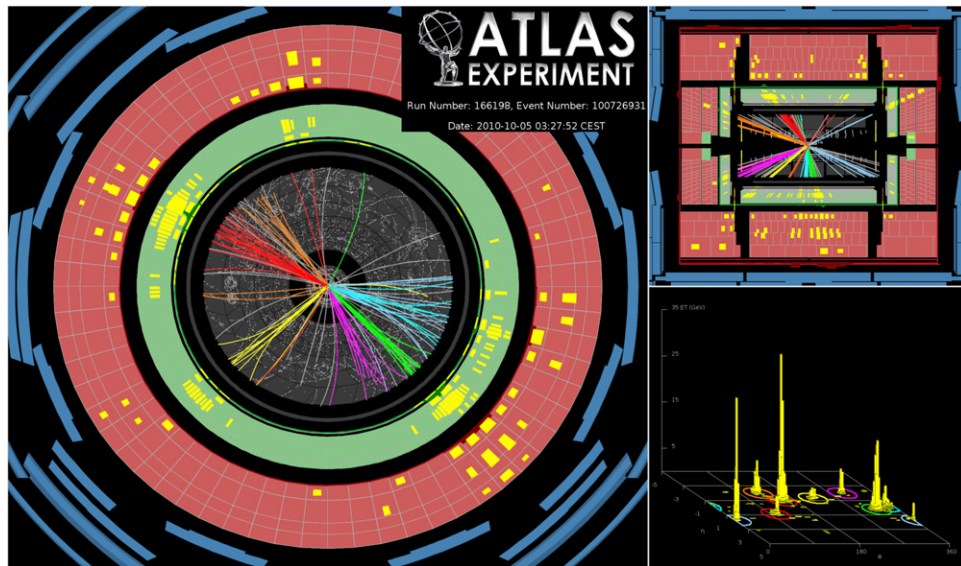


Figure 1.1. A spectacular event with many jets observed by the ATLAS detector at CERN. The picture is taken from the ATLAS public event display repository [4]. ATLAS Experiment, Copyright 2014 CERN.

as a whole. After some time, the partons were identified as quarks, elementary particles whose existence had been hypothesised some years before by Gell-Mann to explain the properties of hadrons [5].

The crucial breakthrough that gave theoretical soundness to the identification of partons with quarks was the discovery that, in some quantum field theories, the effective interaction strength between elementary particles decreases with increasing energy of the particles involved [6, 7]. This property, known as ‘asymptotic freedom’, was assumed to hold for the theory governing the interactions between quarks. Within this framework it is possible to explain inelastic electron–proton collisions. In fact, when the momentum transferred by the electron to the target is small, the quarks interact very strongly and are confined within the proton, which recoils against the electron as a whole. With higher momentum transfer, the quarks inside the proton are probed at high energies and they essentially behave as free particles. This picture was consistent with the behaviour of the electron–proton inelastic collisions observed at SLAC.

More specifically, the theory underlying quark interactions is called quantum chromodynamics (QCD), in that the quarks are supposed to carry a new type of charge, called colour. They interact through the exchange of spin-1 particles, called gluons. The latter obtain their name from the fact that they provide the ‘glue’ that binds quarks together inside hadrons. QCD is quite similar to electromagnetism, with gluons playing the role of photons. The main difference is that gluons carry colour themselves and therefore can interact directly with other gluons¹.

¹ Photons can interact among themselves as well, but their interaction is always mediated by electrically charged particles.

QCD gives a natural explanation for the occurrence of hadronic jets. In fact, in a high-energy collision, quarks and gluons are abruptly produced, and ripped apart. Each parton (quark or gluon) radiates gluons, very much like an electron smashing on a target radiates x-ray photons. This radiation is highly collimated in the directions of the original quarks and gluons produced in the primary collision. Through radiation, quarks and gluons degrade their energies and their interactions become stronger and stronger, until they cluster together to form hadrons, which are the actual ‘final-state’ particles, i.e. the ones we observe in our detectors. The transformation of partons into hadrons, commonly referred to as the ‘hadronisation’ process, does not significantly alter the energy–momentum flow of the original quarks and gluons. Therefore, the jettiness of high-energy hadronic events is to be attributed to the properties of gluon radiation. Jets are thus the footprints of unobservable quarks and gluons in our detectors. Most of their properties can be understood using the language of quarks and gluons, without having to bother with the properties of final-state hadrons.

These speculations were actually confirmed by experiments involving electron–positron collisions. First, events with two jets were observed by the SPEAR collaboration at SLAC [8]. The angular distribution of the jets was compatible with the production of a quark–antiquark pair fragmenting in two bunches of collimated hadrons. The fact that the mechanism of jet formation was indeed due to gluon radiation, as predicted by QCD, was firmly established with the discovery of three-jet events at the Positron–Electron Tandem Ring Facility (PETRA; Positron–Elektron Tandem Ring Anlage) collider at DESY [9–12]. These events were

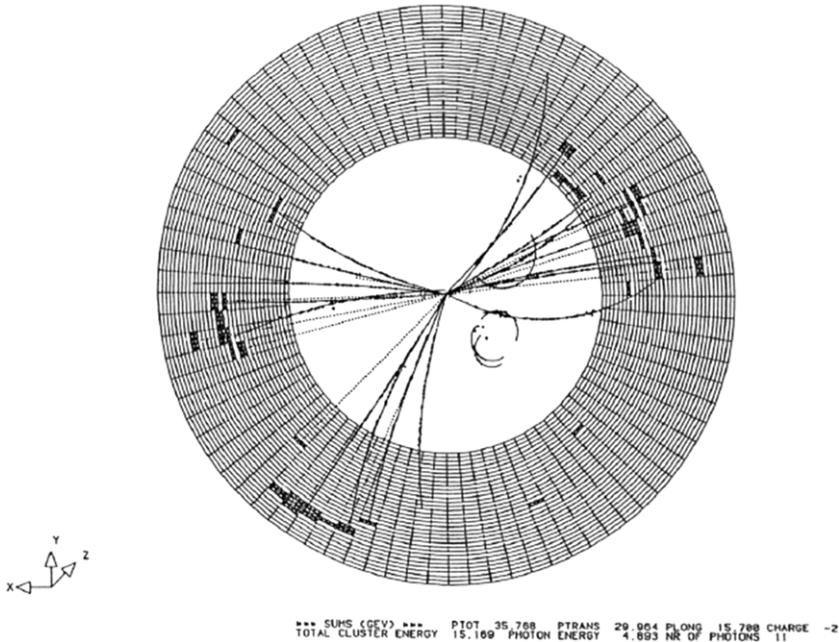


Figure 1.2. A three-jet event as seen by the JADE detector at PETRA. Reproduced from [13] with kind permission from Springer Science+Business Media.

compatible with radiation of an energetic gluon off a quark–antiquark pair. Subsequent studies of jet distributions in three-jet events were able to assess that the gluon had spin-1, and measurements of angular correlations between jets in four-jet events confirmed the existence of gluon self-interactions, as predicted by QCD (see [13] for a historical overview of the discovery of the gluon and its properties). Jets were also observed in hadronic collisions at the Intersecting Storage Rings (ISR) [14] and at the Super Proton Synchrotron (SPS) at CERN [15, 16], thus completing the picture. These and other results established, without any doubt, that QCD provided the correct description of quark–gluon interactions at high energies and that jets are the experimental signature that high-energy QCD is at work.

Jet physics is an incredibly rich subject. This book aims to provide a general overview of this topic to scientists not directly involved in the field. It is not intended to be a review of the most recent advances in jet physics, for which an experienced reader can find good sources elsewhere [17], neither is it a QCD textbook, for which the reader is referred, e.g., to [18, 19]. The general idea of this book is to present the basic experimental and theoretical problems arising when dealing with jets and to describe the solutions proposed in recent years. In this sense it might be very useful for students, both experimentalists and theorists, who are just starting their PhD in high-energy physics.

The book is organised as follows. In chapter 2 we discuss jet algorithms, which are the procedures that are used to rigorously define jets and to extract them from the multitude of hadrons present in a typical final state at high-energy colliders. Chapter 3 will be devoted to QCD, the theory of strong interactions governing the dynamics of quarks and gluons. In particular, we will describe the theoretical tools within QCD that can be used to describe the properties of jets. Finally, in chapter 4 we will discuss how, from a set of observed jets, it is possible to extract information on the elementary event that has produced them. Such techniques are extremely important in the search for new particles, especially when they are expected to decay into quarks and gluons, giving rise to jets as final states. This is the starting point of a new subject, sometimes referred to as ‘jetography’ [17], where jets are the basic ingredients used to describe elementary final states, much as geographic maps are used to describe the Earth.

The reader who is familiar with elementary particle physics is ready to start with chapter 2. In the following sections, basic facts on elementary particles and high-energy colliders are presented. These can be considered as the minimal background required for understanding the rest of the book.

1.1 The basics of elementary particle physics

The known elementary particles, and their interactions, are organised in the so-called Standard Model of elementary particles, summarised in table 1.1.

It represents, in a sense, the actual table of elements. In the language of relativistic quantum mechanics, each particle is associated with a corresponding field. In fact, the energy of each free propagating field is not a continuous quantity, but is quantised, i.e. made up of elementary excitations. These excitations carry both energy and momentum and can be interpreted as particles.

The first building block of the Standard Model is matter particles, carrying spin-1/2. These are further divided into three families of leptons and three families of quarks.

Table 1.1. The Standard Model of elementary particles.

matter particles	ν_e	ν_μ	ν_τ	leptons	γ	force carriers	H
	e	μ	τ		Z		
	u	c	t	quarks	W^\pm		
	d	s	b		g		

Each family of leptons is organised into doublets. We have then the electron e with the electron neutrino ν_e , the muon μ and the muon neutrino ν_μ , and the tau τ with the tau neutrino ν_τ . All neutrinos are electrically neutral, whereas the electron, muon and tau have charge $-e$, with $e \approx 1.6 \times 10^{-19}$ C the magnitude of the charge of the electron. Also quark families are organised into doublets, the first containing the up (u) and down (d) quarks, the second the charm (c) and strange (s) quarks, and the last the top (t) and bottom (b) quarks. All quarks in the top row (up, charm and top) have electric charge $2/3 e$, whereas the ones in the bottom row (down, strange and bottom) have charge $-1/3 e$. The fundamental difference between leptons and quarks is that the former are not subject to strong interactions. Each matter particle has a corresponding anti-particle, having the same mass but opposite charges. For instance, the anti-particle of the electron e^- is the anti-electron or ‘positron’ e^+ . Similarly, the anti-particle of a quark q is an anti-quark, denoted by \bar{q} .

The second part of the table contains force mediators. These are spin-1 particles, whose fields are responsible for the interactions among leptons and quarks. The photon mediates electromagnetic interactions, the W and Z bosons mediate weak interactions, and the gluon mediates strong interactions. All gauge bosons are electrically neutral, except W^\pm , whose electric charge is $\pm e$.

The last part of the Standard Model is the Higgs particle, whose field is responsible for giving mass to all particles, the larger the interaction with the Higgs field, the larger the mass of a particle. The Higgs boson is electrically neutral.

Throughout this book, we will use the system of natural units, in which the Planck constant \hbar and the speed of light c are conventionally set to one. In this system of units the only quantities with dimensions are length, which has the same dimensions as time, and energy, whose dimensions are the inverse of a length. In natural units, all masses have dimensions of energy and are usefully measured in electron-volts (eV).²

Aside from the u quark, the electron, the neutrinos, the gluon and the photon, all particles in the Standard Model are unstable. The inverse of the decay time of a particle in the particle’s rest frame is called ‘width’ and is indicated by Γ . Of course, the larger the width of a particle, the smaller its decay time. In natural units, the width of a particle is measured in electron-volts.

² We recall that one electron-volt is the work done by the electric force to move an electron between two points whose potential difference is one volt.

The elementary particles we observe in high-energy experiments have speeds that are very close to the speed of light, so Lorentz transformations have to be applied to relate quantities measured in one reference frame to another. To simplify equations among the relevant physical quantities appearing in high-energy experiments, it is useful to construct quantities that are invariant with respect to Lorentz transformations. For instance, the energy E and the three-momentum (or impulse) of a particle \vec{p} in a given reference frame can be organised in a four-vector $p = (E, \vec{p})$, with well-defined transformation properties from one frame to another. The quantity

$$p^2 = E^2 - \vec{p}^2, \quad \vec{p}^2 = \vec{p} \cdot \vec{p} = |\vec{p}|^2, \quad (1.1)$$

is invariant under Lorentz transformations. Its square root is equal by definition to the mass of the particle. Similarly, if we consider two four-vectors $a = (a^0, \vec{a})$ and $b = (b^0, \vec{b})$, the ‘dot’ product

$$a \cdot b \equiv (ab) \equiv a^0 b^0 - \vec{a} \cdot \vec{b} \quad (1.2)$$

is also invariant under Lorentz transformations. In order to avoid the complications of performing Lorentz transformations at every corner, it is customary to express all relations between four-momenta (from here on simply ‘momenta’) in terms of relativistically invariant ‘dot’ products. For instance, if p_a and p_b are the momenta of the decay products of a particle, one measures the so-called ‘invariant mass’ of the decay products, defined as the square root of the invariant

$$(p_a + p_b)^2 = (p_a + p_b) \cdot (p_a + p_b). \quad (1.3)$$

It is possible to show using relativistic quantum mechanics that the distribution in the invariant mass of the decay products of an unstable particle has a peak in correspondence to the actual mass of the particle and the width of the peak, which has in fact the dimensions of an energy, is proportional to the unstable particle’s width. Looking for peaks in invariant mass distributions is the standard procedure to search for new particles. For instance, the recently discovered Higgs boson appeared first as a peak in the invariant mass of two photons (figure 1.3, left-hand panel), as well as in that of two Z bosons (figure 1.3, right-hand panel).

The properties of elementary particles are typically investigated through high-energy collisions. Beam particles are stored and accelerated until they reach the desired energy. They then collide at selected collision points where suitable detectors have been placed. From the analysis of the signals in the detectors, experimentalists are able to obtain information on the particles produced in each collision. The main quantities of interest at colliders are cross sections, physical observables that are related to the probabilities that events occur, and are independent of the details of the experimental apparatus. More specifically, for a process $ab \rightarrow X$, where a and b are the colliding particles and X is a selected final state (for instance, a Higgs boson, plus anything else), the number of observed events per unit time dN_X/dt is related to the cross section $\sigma_{ab \rightarrow X}$ via the relation:

$$\frac{dN_X}{dt} = \mathcal{L} \times \sigma_{ab \rightarrow X}. \quad (1.4)$$

The quantity \mathcal{L} is called luminosity, and encodes the information on the intensity of the beams, i.e. the rate of incoming particles per unit area. Cross sections have units of area

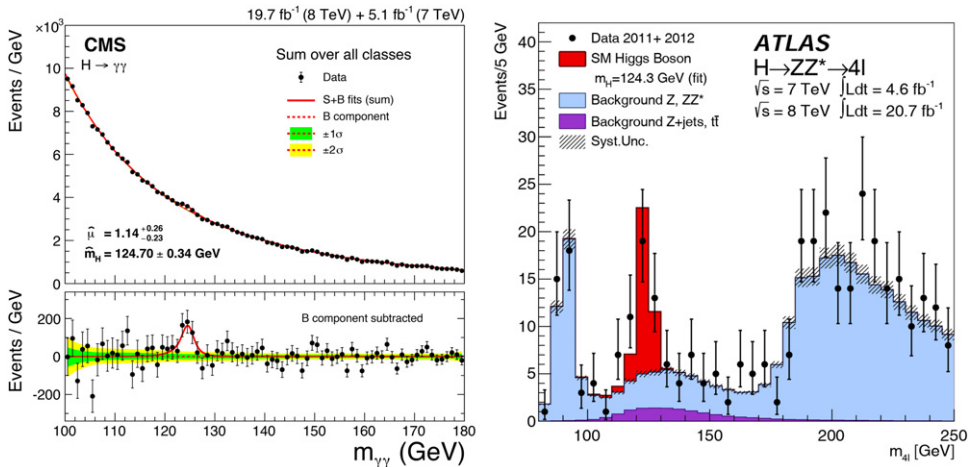


Figure 1.3. Distribution in the invariant mass of two photons ($m_{\gamma\gamma}$) measured by CMS [20] (left) and of two Z bosons (m_{4l}) measured by ATLAS [21] (right), in which a peak corresponding to the production of a particle with a mass around 125 GeV can clearly be seen.

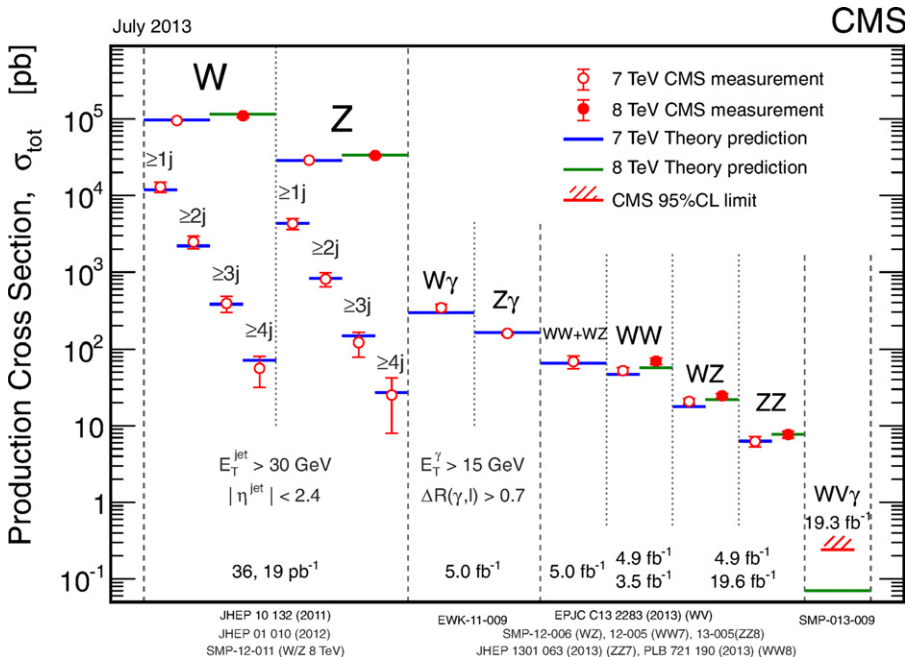


Figure 1.4. Cross sections for various processes involving vector bosons, as observed by the CMS detector during the first run of the LHC.

and are usually measured in barn (b), with $1 \text{ b} = 10^{-28} \text{ m}^2$. One considers also the accumulated luminosity over a period of time, the so-called ‘integrated luminosity’, which is usually measured in b^{-1} . Of course, the higher the integrated luminosity, the better the chances will be of observing rare phenomena. This is illustrated in figure 1.4,

where one can see the cross sections for various processes involving vector bosons at the Large Hadron Collider (LHC). Note that with increasing integrated luminosity more processes become visible. In the following we will describe the different experimental set-ups that can lead to measurements such as the one in figure 1.4. In particular, the two kinds of machines we will consider in this book are electron–positron and hadron–hadron (or simply ‘hadron’) colliders. Furthermore, we will only deal with experimental set-ups that are relevant for jet physics. We will deliberately ignore the extremely important low-energy machines used to observe particular processes, such as rare hadron decays, or to measure selected physical quantities, such as K^0 – \bar{K}^0 mixing parameters, with very high precision.

In electron–positron (e^+e^-) colliders, electron and positron beams are accelerated with various techniques and made to collide. Interesting events occur when an electron and a positron from each beam annihilate, and the energy available in the collision gives rise to new particles. The typical configuration of high-energy e^+e^- colliders is that in which the two beams have the same energy E_{beam} and opposite velocities. In this way no energy is wasted in the motion of the centre-of-mass of the system and a total energy $2E_{\text{beam}}$ is available in the annihilation process. Given the momentum of an electron k_1 and that of a positron k_2 , one introduces the relativistically invariant quantity

$$s = (k_1 + k_2)^2, \quad (1.5)$$

so that, in the case of two opposite beams with energy E_{beam} each, $\sqrt{s} = 2E_{\text{beam}}$ represents the total centre-of-mass energy available for a collision. Examples of high-energy electron–positron colliders are the PETRA accelerator at DESY, with results analysed by the JADE [22], MARK-J, PLUTO, TASSO and CELLO [23] experimental collaborations, and the Large Electron-Positron (LEP) collider at CERN, with the four experiments ALEPH [24], DELPHI [25], L3 [26] and OPAL [27]. One advantage of electron–positron colliders is that they typically produce a limited number of particles in the final state, thus facilitating the interpretation of experimental results. On the other hand, the total available energy is fixed at the start of the experiment and it is generally difficult to increase, because this would require improving the whole accelerator set-up. Furthermore, electrons and positrons, when accelerated, tend to massively lose energy due to electromagnetic radiation, so that it is very difficult to push electron–positron machines towards high energies with current accelerator facilities. Therefore, e^+e^- collisions are not ideal for discovering new particles whose masses are unknown, but are instead useful for precisely measuring the properties of a recently discovered particle. This was the case of the LEP machine in its first run (LEP1), operating at $\sqrt{s} = 91.2$ GeV, the mass of the Z boson, focused on the study of the properties of this particle.

Hadron–hadron collisions are mainly aimed at the discovery of new particles. In fact, at high energies, hadrons break apart and their constituent quarks and gluons undergo elementary highly energetic collisions, producing all sorts of particles. Each parton involved in the collision carries an unknown fraction of the parent hadron’s energy, so that the total energy available in the collision is unknown. This property

makes it possible to span a continuous range of energies up to the centre-of-mass energy of the hadron–hadron collision without changing the experimental set-up as in e^+e^- machines. Furthermore, hadrons such as protons or antiprotons lose less energy than electrons and positrons through electromagnetic radiation and hence can be more effectively accelerated to higher energies. Examples of high-energy hadron colliders are the SPS [28], the Tevatron [29] and the LHC [30]. The SPS, located at CERN, at its time of operation was a proton–antiproton collider and is most famous for the discovery of the W [31, 32] and Z [33, 34] bosons by the two experiments UA1 [35] and UA2 [36]. The Tevatron, at Fermilab, has recently terminated its operations as a high-energy collider. It used proton and antiproton beams, with a centre-of-mass energy of $\sqrt{s} = 1.8$ TeV in its first run and $\sqrt{s} = 1.96$ TeV after an upgrade. Among its most important results is the discovery of the top quark [37, 38]. The LHC is a proton–proton collider located at CERN. It first ran at $\sqrt{s} = 7$ TeV and $\sqrt{s} = 8$ TeV, and has recently been upgraded to reach the centre-of-mass energy of 13 TeV. In its first run, the LHC discovered a spin-0 particle whose properties are compatible with the Higgs boson of the Standard Model [39, 40]. The LHC is the machine which, at the moment, is expected to discover new physics beyond the Standard Model.

The different characteristics of electron–positron and hadron collisions have consequences on the kinematic variables that are typically used in physics analyses. Before discussing these differences, it is useful to quickly review the different parts of a high-energy physics detector. Close to the collision point there is a tracker, which is able to precisely determine the direction of charged particles. This makes it possible to measure charged particle three-momenta by bending their trajectories with a magnetic field. After the tracker there are two detectors called calorimeters devoted to the measurement of particle energies. The first is the so-called ‘electromagnetic’ calorimeter, where photons and electrons lose all their energy. Hadrons, however, lose only part of their energy inside the electromagnetic calorimeter, so their energy determination requires an additional detector, called the ‘hadronic’ calorimeter, where all hadrons are supposed to stop. Muons are the only charged particles that escape the hadronic calorimeter. Their three-momenta are measured through muon detectors, which represent the outermost part of a high-energy detector. Neutrinos are not detected at all and contribute to the so-called missing energy.

Typically, in high-energy electron–positron colliders, the reference frame of the laboratory coincides with the centre-of-mass frame of the collision. Therefore, one naturally stores the energy and the three-momentum of each particle in that reference frame. In hadron collisions, beam particles break apart and the energy of each elementary collision is not known. It is therefore very important to use kinematic variables that transform as simply as possible under Lorentz boosts in the beam direction (which sets for us the z -direction). One of these quantities is the transverse momentum of each particle with respect to the beam, which is invariant with respect to such boosts. For a particle of momentum $p = (E, p_x, p_y, p_z)$, its transverse momentum is identified by its magnitude $p_t = \sqrt{p_x^2 + p_y^2}$ and its

azimuthal angle $\phi = \arctan(p_y/p_x)$. Another useful variable is the rapidity y , defined, given a momentum p , as

$$y = \frac{1}{2} \ln \frac{E + p_z}{E - p_z}. \quad (1.6)$$

If a particle is massless, its rapidity is related to the angle θ that the particle three-momentum forms with the beam axis, as follows

$$y = \frac{1}{2} \ln \frac{1 + \cos \theta}{1 - \cos \theta} = -\ln \tan \frac{\theta}{2}. \quad (1.7)$$

The angular variable $-\ln \tan(\theta/2)$ is called pseudorapidity and is denoted by η . For massless particles, rapidity and pseudorapidity coincide. Therefore, a particle close to the beam setting the positive (negative) z -direction has a large positive (negative) rapidity. Zero rapidity corresponds to a particle whose three-momentum is only transverse to the beam. Under a boost along the beam direction, the rapidity of each particle shifts by a constant quantity, so differences in rapidities are boost-invariant observables. Therefore, in hadron collisions, it is natural to use transverse momentum and rapidity as kinematic variables for each particle. However, since detectors are typically sensitive to particle directions and energy deposits, it is also customary to give information about each particle's pseudorapidity η and transverse energy $E_t = E \sin \theta$, with E the particle's energy. Obviously, the transverse energy of a massless particle is the magnitude of its transverse momentum. An example of how to describe an event in terms of the aforementioned kinematical variables can be seen in the bottom right-hand corner of figure 1.1. There, the horizontal plane corresponds to the pseudorapidity–azimuth plane (η – ϕ). Each point in the plane corresponds to a hadronic calorimeter cell (one of the segments into which the hadronic calorimeter is divided). The vertical axis instead represents the transverse-energy deposit in each cell. All the energy deposits within each of the coloured circles in the η – ϕ plane are considered to build up a jet.

Another difference between e^+e^- and hadron collisions, which is particularly relevant for jet physics, is which hadrons can actually be observed. In e^+e^- colliders, only a negligible fraction of hadrons can fall in the tiny angular region around the beam pipe which is not covered by detectors. Therefore, we can reasonably assume that all hadrons are observed in electron–positron colliders. This is in contrast to high-energy hadronic collisions, where the colliding particles are coloured quarks and gluons. QCD radiation from incoming partons is very collimated around the beam direction, which will contain many interesting hadrons. In hadron collisions, it is therefore important to consider the actual rapidity range spanned by the various parts of a detector. In fact, the tracker is usually placed in a central (pseudo) rapidity region, for instance $|\eta| \lesssim 1.5$ at the Tevatron and $|\eta| \lesssim 2.5$ at the LHC. The hadronic calorimeter extends further, for instance up to $|\eta| \simeq 3$ at the Tevatron and $|\eta| \simeq 5$ at the LHC. The cells of the hadronic calorimeter do not possess the same resolution as the central tracker, especially in the most forward and backward regions, where hadrons from beam fragmentation are most likely to fall. This means that in hadron

collisions, the basic objects that will be measured are not individual particles, but rather pseudo-particles, reconstructed out of the energy deposited in the cells of electromagnetic and hadronic calorimeters. It is then natural to try to construct objects that are independent of the fine details of the detectors. Hadronic jets offer a viable solution to this problem, which is yet another reason why they currently play such an important role in high-energy physics.

Bibliography

- [1] Olive K A *et al* (Particle Data Group Collaboration) 2014 *Chin. Phys. C* **38** 090001
- [2] Breidenbach M *et al* 1969 *Phys. Rev. Lett.* **23** 935
- [3] Feynman R P 1969 *Phys. Rev. Lett.* **23** 1415
- [4] <https://twiki.cern.ch/twiki/bin/view/AtlasPublic/EventDisplayStandAlone>
- [5] Gell-Mann M 1964 *Phys. Lett.* **8** 214
- [6] Gross D J and Wilczek F 1973 *Phys. Rev. Lett.* **30** 1343
- [7] Politzer H D 1973 *Phys. Rev. Lett.* **30** 1346
- [8] Hanson G *et al* 1975 *Phys. Rev. Lett.* **35** 1609
- [9] Brandelik R *et al* (TASSO Collaboration) 1979 *Phys. Lett. B* **86** 243
- [10] Barber D P *et al* 1979 *Phys. Rev. Lett.* **43** 830
- [11] Berger C *et al* (PLUTO Collaboration) 1979 *Phys. Lett. B* **86** 418
- [12] Bartel W *et al* (JADE Collaboration) 1980 *Phys. Lett. B* **91** 142
- [13] Soding P 2010 *Eur. Phys. J. H* **35** 3
- [14] Akesson T *et al* (Axial Field Spectrometer Collaboration) 1982 *Phys. Lett. B* **118** 185
- [15] Arnison G *et al* (UA1 Collaboration) 1983 *Phys. Lett. B* **123** 115
- [16] Banner M *et al* (UA2 Collaboration) 1982 *Phys. Lett. B* **118** 203
- [17] Salam G P 2010 *Eur. Phys. J. C* **67** 637
- [18] Ellis R K, Stirling W J and Webber B R 1996 *QCD and Collider Physics* (Cambridge Monographs on Particle Physics, Nuclear Physics and Cosmology, No. 8) (Cambridge: Cambridge University Press)
- [19] Dissertori G, Knowles I G and Schmelling M 2009 *Quantum Chromodynamics (International Series of Monographs on Physics* vol 115) (Oxford: Oxford University Press)
- [20] Khachatryan V *et al* (CMS Collaboration) 2014 *Eur. Phys. J. C* **74** 3076
- [21] Aad G *et al* (ATLAS Collaboration) 2013 *Phys. Lett. B* **726** 88
Aad G *et al* (ATLAS Collaboration) 2014 *Phys. Lett. B* **734** 406 (corrigendum)
- [22] <https://wwwjade.mpp.mpg.de/>
- [23] Schachter M J *et al* (CELLO Collaboration) 1981 *Phys. Scripta* **23** 610
- [24] <http://aleph.web.cern.ch/aleph/>
- [25] <http://delphiwww.cern.ch/Delphi/Welcome.html>
- [26] <http://l3.web.cern.ch/l3/>
- [27] <http://opal.web.cern.ch/Opal/>
- [28] <http://home.web.cern.ch/about/accelerators/super-proton-synchrotron>
- [29] <http://www.fnal.gov/pub/tevatron/>
- [30] <http://home.web.cern.ch/topics/large-hadron-collider>
- [31] Arnison G *et al* (UA1 Collaboration) 1983 *Phys. Lett. B* **122** 103
- [32] Banner M *et al* (UA2 Collaboration) 1983 *Phys. Lett. B* **122** 476
- [33] Arnison G *et al* (UA1 Collaboration) 1983 *Phys. Lett. B* **126** 398
- [34] Bagnaia P *et al* (UA2 Collaboration) 1983 *Phys. Lett. B* **129** 130

- [35] <http://home.web.cern.ch/about/experiments/ua1>
- [36] <http://home.web.cern.ch/about/experiments/ua2>
- [37] Abe F *et al* (CDF Collaboration) 1995 *Phys. Rev. Lett.* **74** 2626
- [38] Abachi S *et al* (D0 Collaboration) 1995 *Phys. Rev. Lett.* **74** 2632
- [39] Aad G *et al* (ATLAS Collaboration) 2012 *Phys. Lett. B* **716** 1
- [40] Chatrchyan S *et al* (CMS Collaboration) 2012 *Phys. Lett. B* **716** 30

Hadronic Jets

An introduction

Andrea Banfi

Chapter 2

Jet algorithms

Let us consider an event such as the one displayed in the left-hand panel of figure 2.1, in which we recognise the presence of hadronic jets, and ask ourselves how many jets we observe. One might say it is clearly two, but for instance the (pale blue) tracks on the left-hand side of the image can be considered to be a jet by themselves. In fact, this event is classified by ALEPH as a four-jet event, but on what basis? If we nevertheless consider the event as containing two jets, which hadrons have to be included in each jet? If this may be an easy task for the event in the left-hand panel of figure 2.1, what about the event in the right-hand panel, which contains hadrons spread all over the detectors? Suppose we have assigned each hadron to a jet, we have to repeat the same procedure for every event. We definitely need a set of rules to establish how many jets each event has and which hadrons have to be assigned to

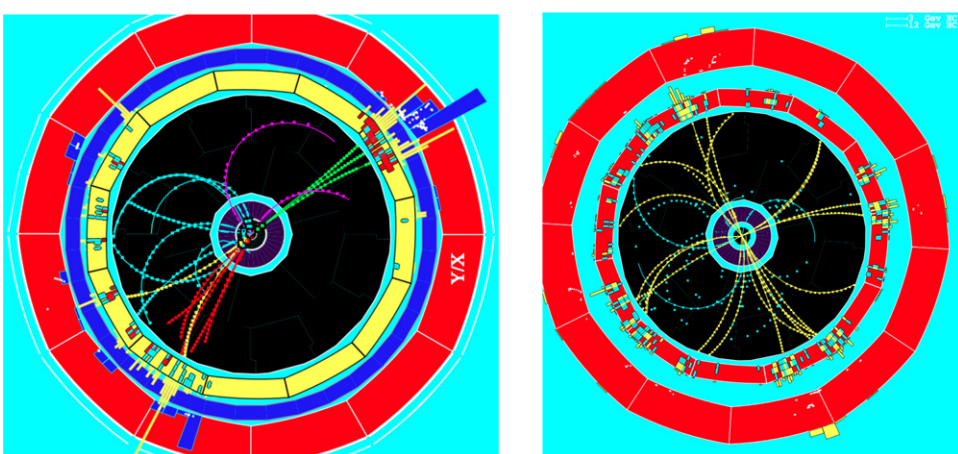


Figure 2.1. Two four-jet events from the event display of the ALEPH collaboration at LEP [1].

each jet. Such a set of rules is called a ‘jet algorithm’. There exist many jet algorithms and choosing one or the other depends crucially on the kind of information that we wish to extract from a set of events. Before going into the details of the various jet algorithms, let us focus on what a jet algorithm should intuitively do. Jet events are originated by the production of highly energetic (hard) quarks and gluons, which later on transform into collimated bunches of hadrons through a mechanism that will be explained in the following chapter. It is natural to require that the number of jets we observe, as well as their energy–momentum flow, reflect the properties of the hard quarks and gluons that were initially produced in the elementary collision. For instance, if an event is generated by the production of a hard quark–antiquark pair in electron–positron annihilation, a good jet algorithm should produce as outputs two jets, with momenta very close to those of the parent quark and antiquark.

Sterman–Weinberg jets. The very first jet algorithm, developed by Sterman and Weinberg [2], is a good example of how to map final-state hadrons into jets. Let us consider for simplicity e^+e^- annihilation. The algorithm works as follows: an event is classified as having two jets if all but at most a fraction ϵ of the total energy of produced hadrons is contained inside two cones of opening angle δ . If ϵ is sufficiently small, the two cones will contain the quark and antiquark produced in the hard collision. This simple example already highlights an important aspect of jet algorithms: they depend on parameters by varying which one changes the fraction of hadrons that are included in each jet. Another important feature of Sterman–Weinberg jets is that, given ϵ and δ , the fraction of events with two jets, the so-called two-jet rate, is a well-defined observable and can be computed using relativistic quantum mechanics within the framework of QCD, the theory of quarks and gluons. What is the property of the jet definition that makes this possible? To answer this question we need to consider jets immediately before the quarks and gluons transform into hadrons. In QCD, the probability of emitting a gluon that has exactly zero energy is infinite. This pathological behaviour is referred to as soft divergence. In fact, the term soft refers to a particle whose energy is much smaller than the typical energy of the other particles. Similarly, one obtains an infinite result if one parton (quark or gluon) splits into a pair of parallel (collinear) partons, giving rise to a collinear divergence. Fortunately, quantum fluctuations (virtual corrections), for instance the fact that a gluon is emitted and is reabsorbed before it is observed, lead to the same kind of divergences, but with opposite sign. Then, if a physical observable is affected in the same way by an infinitely soft gluon and the corresponding quantum fluctuation, the infinities will cancel and a QCD calculation in terms of quarks and gluons will give a finite result. If an observable is to be calculable in QCD, a similar cancellation should occur for collinear divergences as well. For instance, in the case of Sterman–Weinberg jets, for a given value of ϵ and δ , after the addition of a zero-energy gluon the event will still be considered a two-jet event and a quantum fluctuation will also not change the number of jets. Infinites will then cancel between real (gluon emission) and virtual (quantum) corrections. This is illustrated in figure 2.2.

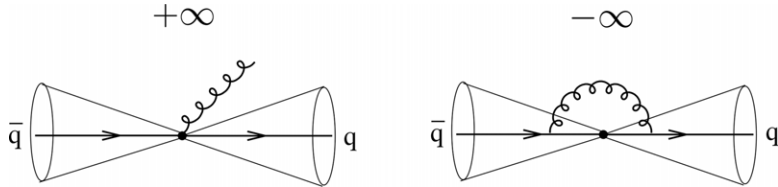


Figure 2.2. The cancellation of soft singularities at work in Sterman–Weinberg jets. The emission of an infinitely soft gluon (left) does not change the amount of energy outside the two cones around the primary quark–antiquark pair. The same happens in the case of a quantum fluctuation (right).

Infrared and collinear safety. As a practical rule, to ensure cancellation of soft and collinear infinities, the number of jets and their momenta should stay the same

1. after the addition of an arbitrary number of infinitely soft partons (infrared safety) and
2. after an arbitrary number of collinear splittings (collinear safety).

Jet algorithms that satisfy both requirements are called infrared and collinear (IRC) safe algorithms. Sterman–Weinberg jets are IRC safe.

IRC safety is the property that ensures that jets defined at the detector level (for instance using calorimetric cells as inputs), at the hadron level (using hadrons with a lifetime up to an agreed value) and at the parton level (obtained from quarks and gluons) are essentially the same. In fact, it is possible to show that, for IRC safe observables, the reshuffling of momenta due to hadronisation leads to effects that are suppressed by inverse powers of the typical momentum scale of the process under consideration, for instance the transverse momentum of a given jet. The higher this scale, the closer hadronic observables will be to the corresponding partonic ones. On the experimental side, a huge issue is the fact that calorimetric cells, especially in hadron colliders and in the forward and backward regions, cannot resolve the energy deposit of single particles. Therefore, jets can only be defined using the transverse energy, the pseudorapidity and the azimuth of individual calorimetric cells as inputs, rather than the momenta of individual hadrons. However, for IRC safe jet algorithms, a soft gluon will give an energy deposit which will not alter the number of jets or their momenta. Similarly collinear splittings, giving energy deposits in the same calorimetric cell, will be clustered inside the same jet. In practice this implies that the IRC safe jet definitions will be independent of the details of the detector, up to corrections that vanish as a power of the detector resolution. The granularity of calorimeters represents such an issue that, in hadron collisions, jets are the main objects that enter physics analyses. To be as insensitive as possible to detector effects, jet algorithms must be IRC safe.

Good jet algorithms. In the early 1990s, a document known as the ‘Snowmass Accord’ [3] summarised the desired features of jet algorithms. Specifically, a good jet algorithm should:

1. be simple to implement in an experimental analysis;
2. be simple to implement in theoretical calculations;
3. be defined at any order of perturbation theory;

4. yield finite cross sections at any order of perturbation theory;
5. yield a cross section that is relatively insensitive to hadronisation.

IRC safety automatically ensures that the last three conditions are satisfied.

Concerning point 2 above, due to the fact that most QCD calculations are performed numerically via Monte Carlo procedures that simulate collider events, a jet clustering algorithm can be arbitrarily complicated. However, in order to have an understanding of the properties of the algorithm, it might be useful if jet observables (e.g. jet rates) could be to some extent computed analytically. This is why procedures understandable to humans are preferred compared to other procedures.

Point 1 deserves special attention. As for point 2, there is no conceptual problem in letting an algorithm crunch a set of particle momenta. However, in environments with lots of particles, such as high-luminosity hadronic colliders, or even heavy-ion colliders, the speed of an algorithm can become an issue. This is why a lot of effort has been put toward designing algorithms that are not only IRC safe, but also scale nicely with the number of input particles. Another typical experimental issue is the elimination of background. This can arise due to particles that have nothing to do with the event under consideration, for instance coming from secondary collisions occurring close in time to a primary collision of interest (the so-called ‘pile-up’ (PU)), or simply from detector noise. Such backgrounds are easier to eliminate if jets have a fixed shape, for instance if each jet is enclosed in a circle in the η - ϕ plane. Achieving this last property is a highly non-trivial task, as will become clear at the end of section 2.1.1.

Given this general overview, we will now discuss different jet algorithms. In section 2.1, we will present the two main families of algorithms currently in use, namely cone and sequential algorithms. Rather than giving a historical overview, we will concentrate on the distinctive features of both families. In section 2.2, we will present some of the most recent ideas on jet algorithms, which have not been exploited in experimental analyses, but that nevertheless have intriguing properties that might be useful to investigate in the future.

2.1 Cone or sequential algorithms?

2.1.1 Cone algorithms

When looking at events containing jets, it is natural to draw cones around the most energetic deposits in detectors and identify a jet as the set of particles within one of those cones. In hadron colliders, one looks at events in the two-dimensional space defined by pseudorapidity and azimuth (the η - ϕ plane), where particles appear as spots, having activated a number of calorimetric cells. Figure 2.3 includes, in the bottom right-hand corner, a so-called ‘lego’ plot, in which not only is it possible to see the active calorimetric cells in the η - ϕ plane, but also the corresponding transverse energy deposit, represented by the height of the tower above each cell.

Fixed cones. A natural way of finding jets is to start by drawing a circle around the most energetic spot in an event and consider all the particles inside each circle to build up a jet. More rigorously, one considers a list of pseudo-particles, which can be individual particles, calorimetric cells, or even jets resulting from some earlier

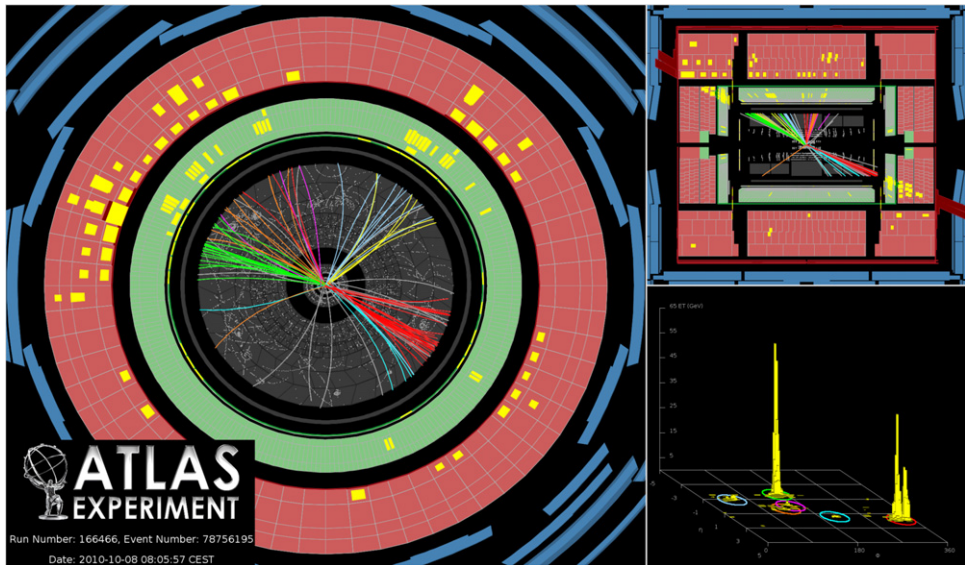


Figure 2.3. The display of an event recorded by the ATLAS detector at CERN. The bottom right-hand corner shows the lego plot of the event [4]. ATLAS Experiment, Copyright 2014 CERN.

clustering procedure. One then takes the pseudo-particle with the largest transverse momentum (or transverse energy) and draws around it a circle of radius R , the jet radius, in the η - ϕ plane. All pseudo-particles within that circle are considered to build up a jet. These pseudo-particles are then removed from the original list and the procedure is repeated until all pseudo-particles have been assigned to a jet. This is the first example of a cone algorithm, which is commonly referred to as a ‘fixed-cone’ jet algorithm. This simple example already highlights one of the main problems of cone algorithms, which is how to draw cones so as to obtain an IRC safe procedure. The cone algorithm we have just described, similar to the ones used by the UA1 and UA2 experiments at the SPS [5], is unfortunately collinear unsafe. In fact, the highest transverse momentum particle can change after collinear splittings, whereas nothing happens in the presence of quantum fluctuations¹. Hence real and virtual corrections can give rise to different jets and infinities will not cancel. This non-cancellation is illustrated pictorially in figure 2.4. Note that the quantity that should not change in an IRC safe cone algorithm in hadron collisions is not the number of jets, but rather the momenta of jets that have a transverse momentum above a given threshold, which we call the ‘hard’ jets. In fact, nothing can prevent an infinitely soft gluon sufficiently far away from all the other jets giving rise to an infinitely soft jet. This, however, does not change the momenta of the hard jets.

Stable cones. A more refined procedure aiming at having an IRC safe cone algorithm involves the concept of a stable cone of radius R , which is the set of all

¹This is strictly true only if the inputs of the algorithm are individual particles, or calorimetric cells, but not if they are jets defined with some IRC safe procedure.

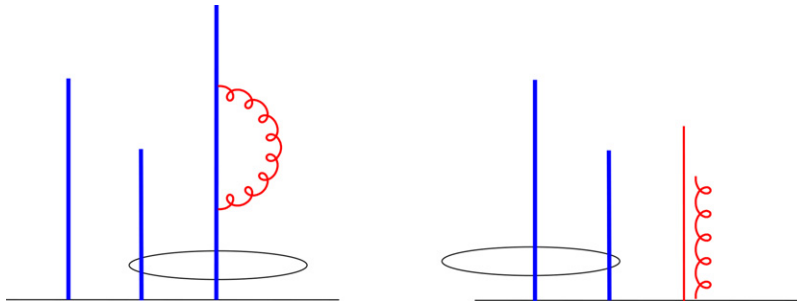


Figure 2.4. A collinear unsafe jet algorithm. Each line represents a parton and the height of each line is proportional to the parton transverse energy. The horizontal axis can be thought of as the pseudorapidity axis at a fixed azimuth, or vice versa. With a virtual correction, the parton on the right is the most energetic, so that a jet is formed by this parton and the central one. If a collinear splitting occurs, the parton on the left becomes the most energetic and will then form a jet with the central parton. Adapted from [31].

pseudo-particles p_i which are within a distance R in the rapidity–azimuth ($y-\phi$) plane from a jet axis p_J (with rapidity y_J and azimuth ϕ_J)²:

$$(y_i - y_J)^2 + (\phi_i - \phi_J)^2 < R^2, \quad (2.1)$$

with the jet axis constructed out of the momenta of the particles inside the stable cone. Its direction can be, for instance, that of the vector sum of the momenta of the selected pseudo-particles. Other popular definitions involve the weighted combinations

$$p_{tJ} = \sum_i p_{ti}, \quad y_J = \frac{\sum_i w_i y_i}{\sum_i w_i}, \quad \phi_J = \frac{\sum_i w_i \phi_i}{\sum_i w_i}, \quad (2.2)$$

where w_i can be p_{ti} or p_{ti}^2 and all sums extend to all pseudo-particles inside the region identified by (2.1). In practice, a stable cone is a circle in the $y-\phi$ plane with its centre coinciding with the jet axis.

Neither a collinear splitting nor a soft emission can change the position or momentum of a *hard* stable cone. Therefore, if we identify each stable cone with a jet, the momentum of the jets with transverse momentum above a given threshold is an IRC safe quantity. A way to look for all stable cones is to consider all possible circles of radius R that one can draw and for each one check if the position of the corresponding jet axis in the $(y-\phi)$ plane coincides with the centre of the circle: then we have found a stable cone. In practice this is not feasible, so that more efficient procedures have to be devised. One possibility might be to use the momenta of all pseudo-particles as trial directions for the jet axis. Such trial directions are known as seeds [6]. One starts with any pseudo-particle and constructs the jet axis out of the

²In the rest of this chapter we will use transverse momenta and rapidity to describe particles in hadron collisions, since these quantities have simple transformation rules under Lorentz boosts. All the quantities that we will introduce can be redefined in terms of transverse energy and pseudorapidity, without changing any of the conclusions we will draw.

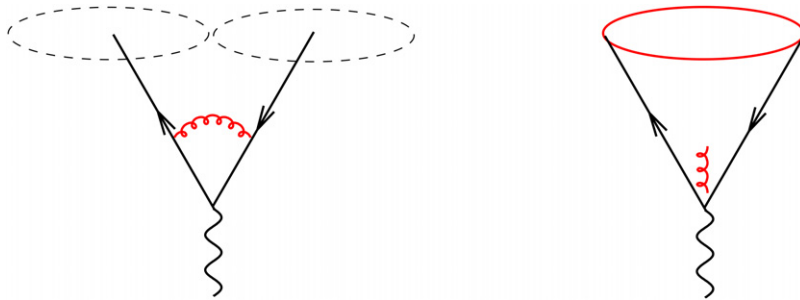


Figure 2.5. Infrared unsafety of the midpoint seeded cone algorithm. With virtual corrections (left), the algorithm finds two hard stable cones (dashed), centred around the two hard partons; when an infinitely soft gluon is emitted between the two hard partons (right), an extra hard stable cone (solid, red) is found. Adapted from [31]

momenta of all pseudo-particles within a distance R from it in the $y-\phi$ plane. The resulting axis is a new trial direction, and the procedure is repeated until the pseudo-particle content of the set does not change any more. Then we have found a stable cone and another pseudo-particle is used as a seed, until all trial directions have been used. Such algorithms are commonly referred to as ‘iterative-cone’ finders. Unfortunately, the procedure we have just described is not able to find all hard stable cones, because it will definitely miss those centred at the midpoint of two pseudo-particles with similar transverse momentum. This cone will be found only after the emission of a soft particle between the two energetic ones. The algorithm is thus infrared unsafe, because the quantum corrections cancelling the infinity coming from soft gluon emission cannot be used as seeds to find the new hard stable cone [7] (see figure 2.5)³. An attempt to fix this problem could be to add more seeds, for instance also considering the midpoint between any pair of pseudo-particles as an additional trial direction [8]. Unfortunately, as explained for instance in [9], even for this choice of seeds it is always possible to find configurations in which the addition of an infinitely soft gluon leads to finding a new hard stable cone. At the moment there exists no IRC safe seeded cone algorithm, although a no-go theorem stating that it is impossible to have an IRC cone algorithm with a *finite* number of trial directions for stable cones has never been openly formulated.

The problem of finding all stable cones has been solved in a general way using seedless algorithms. From an experimental point of view, one can draw circles centred in each cell of the hadronic calorimeter and check whether each corresponds to a stable cone [8]. This is the closest equivalent to a seedless algorithm that draws all possible circles, but is quite expensive from a computational point of view, because it requires $\mathcal{O}(N_{\text{cells}}n)$ steps, where N_{cells} is the number of calorimetric cells and n the typical number of particles within a cone. If one has information of the momenta of all pseudo-particles, one can consider all possible subsets of pseudo-particles and check whether each subset gives a stable cone [10]. In this case it is obvious that all stable cones will be found. However, the number of subsets that can be formed out of

³ As for fixed cones, a workaround for this problem might be to use IRC safe jets as seeds. However, this makes the procedure inefficient from a computational point of view.

N pseudo-particles is 2^N , so the algorithm becomes computationally impractical for a large number of particles. A much faster procedure to find stable cones is provided by the seedless infrared safe cone (SISCone) algorithm [9]. The main idea behind SISCone is to exploit methods borrowed from computational geometry to efficiently move circles of radius R around the y - ϕ plane until all stable cones are found. In fact, this can be performed in $O(Nn \ln n)$ steps. Furthermore, it is possible to show that the hard stable cones found with the SISCone procedure are IRC safe.

Overlapping cones. After all the stable cones have been found, many of them will have particles in common, i.e. they will overlap. One then needs a procedure to decide how to move from a set of stable cones, which at this stage are commonly referred to as ‘proto-jets’, to the list of the final jets. The current way to deal with overlapping cones is the split–merge procedure [8]. One starts with the proto-jet for which the scalar sum of the transverse momenta of its constituents (i.e. the first sum in (2.2)) is the largest. Let us call this proto-jet p_a and look for the closest (in the y - ϕ plane) proto-jet p_b that overlaps with p_a . If this is not found, p_a is considered to be a jet and is removed from the list of proto-jets. Otherwise, the two proto-jets are merged into a single proto-jet if the scalar sum of transverse momenta of the shared particles is more than a fraction f (normally chosen to be 0.5 or 0.75) of the scalar sum of transverse momenta of proto-jet p_b . If this is not the case, the shared particles are assigned to either of the proto-jets, currently each particle to the jet whose axis is closer. This is repeated until the hard proto-jet has no overlap with any other proto-jet, in which case it is called a jet and removed from the list of proto-jets. The split–merge procedure continues with the other proto-jets until no proto-jets are left. A viable alternative is the split–drop procedure [11], in which the shared particles are attributed to the proto-jet with the largest scalar sum of constituents’ transverse momenta and the remaining particles belonging to the jets with a smaller scalar sum of the constituents’ transverse momenta are simply eliminated. This is an example of a procedure in which ‘dark towers’ are created, i.e. objects that are not clustered with any jet. Dark towers are common in cone algorithms and have been dealt with in a number of different ways [12]. The simplest seems to be to run the jet algorithm over and over until no dark towers are left unclustered [13].

An unwanted feature of the split–merge procedure is that, in the presence of many soft particles, the shapes of well-separated hard cones are not perfect circles in the y - ϕ plane, as shown in figure 2.6. Not only is their shape irregular, but it is also known only after the whole jet-finding procedure is terminated. This makes it difficult to subtract a known uniform background on an event-by-event basis, as will be discussed in more detail at the end of this section. Surprisingly enough, circular cones can instead be achieved using sequential algorithms, the topic of the next subsection.

2.1.2 Sequential algorithms

Sequential algorithms reconstruct jets by clustering particles pairwise until no particles are left. We will first discuss the general features of sequential algorithms developed for e^+e^- collisions and later introduce their counterparts in hadron collisions. As for

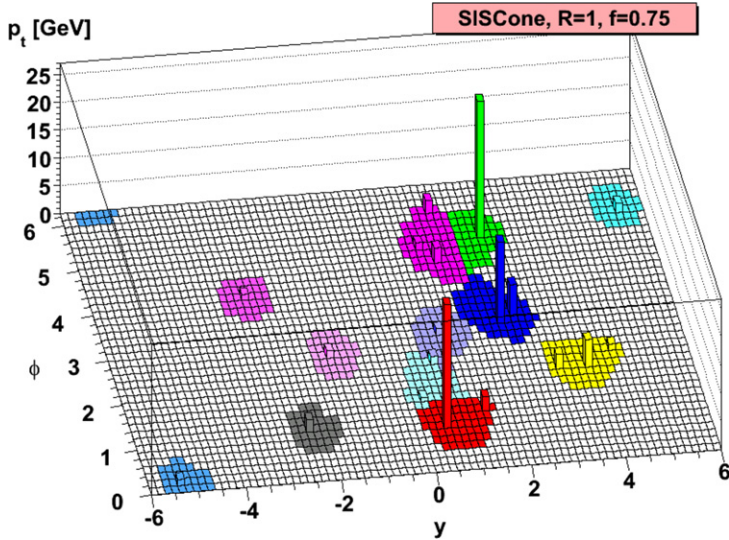


Figure 2.6. Jets reconstructed with the SIScone algorithm, with radius $R = 1$ and a split–merge procedure to deal with overlapping cones corresponding to $f = 0.75$ [14]. Cells with the same colour are clustered within the same jet.

cone algorithms, the starting point is a set of pseudo-particles, which can be either true particles, or the result of the recombination of one or more particles.

Electron–positron annihilation. In e^+e^- sequential algorithms, one considers all pairs of pseudo-particles and finds p_i and p_j , the ones for which a suitable distance measure y_{ij} is the smallest. The two pseudo-particles are then recombined into a new pseudo-particle, for instance by simply adding their four-momenta p_i and p_j . The procedure is repeated until no pseudo-particles are left. If we have N initial particles, the algorithm goes through N steps. At each step, one stores the minimum distance between all pairs of particles and calls it y_n , with $n = 1, \dots, N$. One then introduces a resolution y_{cut} and, if $y_n > y_{\text{cut}}$, classifies an event as having n jets, whose momenta are those of the n pseudo-particles left at the n th stage of the clustering procedure. The n -jet rate $R_n(y_{\text{cut}})$ is defined as the fraction of events having $y_n > y_{\text{cut}}$.

The two main ingredients that determine the behaviour of sequential jet algorithms are the distance measure and the recombination procedure. A simple example of a distance measure is the invariant mass of p_i and p_j . This is implemented in the JADE algorithm [15]:

$$y_{ij}^{(J)} = \frac{(p_i + p_j)^2}{Q^2}, \quad (2.3)$$

where Q is the centre-of-mass energy of the e^+e^- collision. This measure is by construction IRC safe, because it vanishes when either p_i or p_j is soft, or when the pair is collinear. Unfortunately the JADE algorithm has an unwanted feature, which is

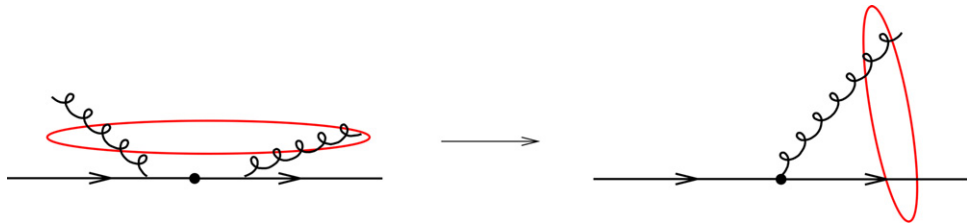


Figure 2.7. Creation of a soft large-angle jet out of two gluons with the JADE algorithm. The red hoops indicate which partons will be clustered together by the jet algorithm. The gluon on the left is not clustered with the parton to which it is collinear.

easily understood if one considers a configuration in which a hard quark–antiquark pair, flying in opposite directions, is accompanied by two soft gluons, one collinear to the quark and the other to the antiquark. In this situation, depicted in figure 2.7, it is possible that the algorithm, instead of clustering each gluon to the parton to which it is collinear, clusters the two gluons together, creating a soft large-angle pseudo-particle, which later on will be clustered either with the quark or with the antiquark. Therefore, one of the two gluons will be attracted towards a particle which is far away in angle. This is not ideal, because the momenta of each jet should closely correspond to those of the partons which have initiated them, in particular by including as much as possible the corresponding successively radiated partons. This feature also creates complications from the point of view of all-order QCD calculations, as will be discussed in the next chapter. An improved distance that provides a solution to the problem of the JADE algorithm is provided by the Durham algorithm [16]:

$$y_{ij}^{(D)} = 2 \frac{\min(E_i^2, E_j^2)}{Q^2} (1 - \cos \theta_{ij}), \quad (2.4)$$

with E_i and E_j the energies of pseudo-particles p_i and p_j and θ_{ij} their relative angle. The above distance is, as needed, IRC safe, and at small angles reduces to the relative transverse momentum (squared) of the softer particle with respect to the harder. The Durham algorithm does not create spurious large-angle jets, so collinear bunches of particles are clustered into the same jet. A more sophisticated variant of the Durham algorithm is the Cambridge algorithm [17]. This clustering procedure is aimed at reconstructing the typical sequence of gluon emissions, which occur predominantly at successively decreasing angles. At each step, the Cambridge algorithm finds the pair of pseudo-particles with the smallest *angular* distance $y_{ij} = (1 - \cos \theta_{ij})$. Then, one computes their distance $y_{ij}^{(D)}$, as given by (2.4). If $y_{ij}^{(D)} < y_{\text{cut}}$, the two particles are merged, otherwise the object with the smaller energy is stored as a jet and removed from the list of pseudo-particles.

Hadron collisions. Both the Durham [18] and the Cambridge [19] algorithms have been generalised to hadron collisions. In this context, the algorithms are usually run in a different way with respect to e^+e^- annihilation, in that, as for cones, one is interested in the number of jets in an event, even without having specified a jet

resolution [20]. Let us consider the Durham algorithm first, which is called the k_t algorithm in the context of hadron collisions. At each step, one considers the pair of pseudo-particles p_i and p_j with the smallest distance (which we call the ‘ k_t distance’)

$$d_{ij} = \min(p_{ti}^2, p_{tj}^2) \frac{\Delta R_{ij}^2}{R^2}, \quad \Delta R_{ij}^2 = (y_i - y_j)^2 + (\phi_i - \phi_j)^2, \quad (2.5)$$

where R is a parameter that plays the role of a jet radius⁴. One then finds the distance of p_i and p_j from the beam:

$$d_{iB} = p_{ti}^2, \quad d_{jB} = p_{tj}^2. \quad (2.6)$$

If the minimum among d_{ij} , d_{iB} , d_{jB} is the mutual distance d_{ij} , then p_i and p_j are recombined into a single pseudo-particle. Otherwise, if that minimum is d_{iB} (or d_{jB}), pseudo-particle p_i (or p_j) is removed from the list of pseudo-particles and added to the list of jets. Similarly, for the Cambridge algorithm, known as the Cambridge/Aachen algorithm in this context [19], the distance d_{ij} is given by just $\Delta R_{ij}^2/R^2$ and $d_{iB} = d_{jB} = 1$ and the procedure runs in the same way as for the k_t algorithm. Note that, in hadron collisions, the distance measures do not need to be infrared safe. In fact, as for cone algorithms, the quantity that has to be IRC safe is the momenta of the jets that have a transverse momentum above a given threshold.

As can be seen from the above discussion, sequential algorithms are easier to understand from a theoretical point of view, in that they are manifestly IRC safe and do not present the issue of the same pseudo-particle being assigned to different jets, as happens for overlapping cones. In practice, until very recently, sequential algorithms had some practical issues which made them less attractive than cone algorithms for hadron collisions. The first issue is that a naive implementation of sequential algorithms scales as N^3 with the number of initial particles N . In fact, computing the minimum of the mutual distances between pairs of particles requires N^2 numbers and this minimisation has to be performed N times, until no pseudo-particles are left. However, the particles p_i and p_j that have the smallest distance need to be nearest neighbours in the $y-\phi$ plane. This fact is evident for the Cambridge/Aachen, and has been shown for the k_t algorithm in [21]. In fact, if $p_{ti} < p_{tj}$, if there exists another particle p_l such that $\Delta R_{il} < \Delta R_{ij}$, then necessarily $d_{il} = \min(p_{ti}^2, p_{tl}^2) \Delta R_{il}^2/R^2 < d_{ij}$, in contradiction with the fact that d_{ij} is the minimum of the k_t distances. This finding triggered a huge improvement in the speed of implementations of sequential algorithms [21]. One can in fact use methods from computational geometry to look for nearest neighbours in the $y-\phi$ plane and reduce the overall problem of finding jets with the k_t and the Cambridge/Aachen algorithms to scale as $N \ln N$ [21]. The second problem with sequential algorithms such as the k_t or the Cambridge/Aachen is that, in the presence of many soft particles, the boundary of each hard jet in the $y-\phi$ plane is very irregular, as can be seen from the examples in figure 2.8. Furthermore, this boundary is known only *a posteriori*, after the algorithm has finished reconstructing all the jets. This makes it painful to subtract from each jet the contribution of a uniform

⁴Note that, unlike in e^+e^- annihilation, the distance in (2.5) is dimensionful, given the fact that, in hadron collisions, it is not immediate to identify a typical hard scale.

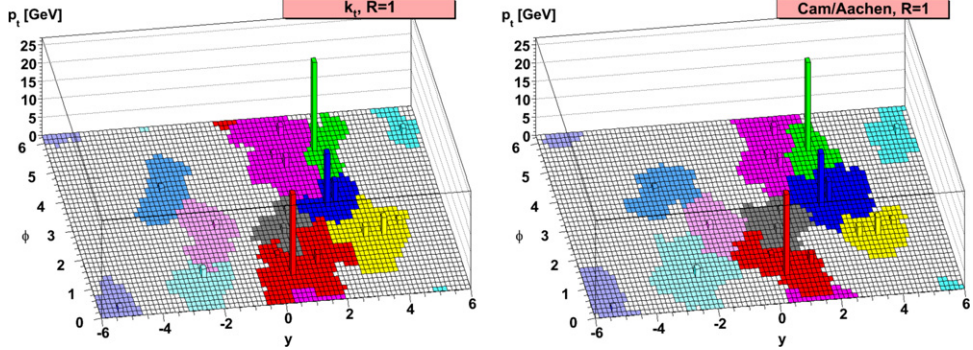


Figure 2.8. Jets reconstructed with the k_t (left) and the Cambridge/Aachen (right) algorithms, corresponding to the same jet radius $R = 1$ [14]. Cells with the same colour are clustered within the same jet.

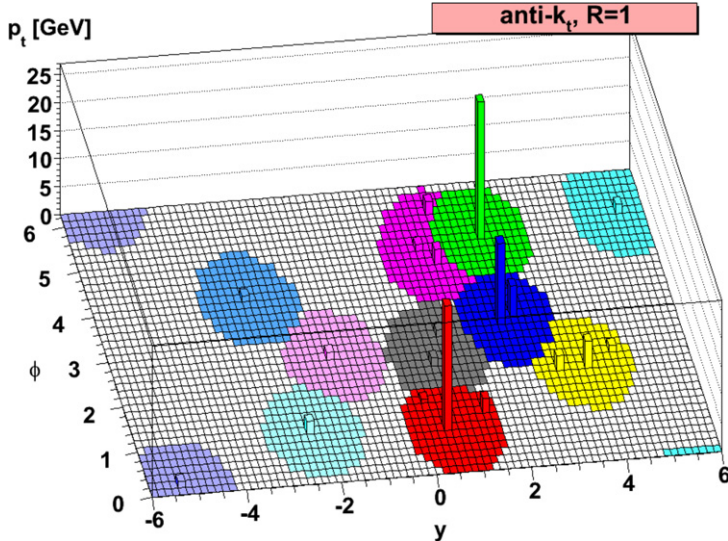


Figure 2.9. Jets reconstructed with the anti- k_t algorithm [14]. As in previous examples, cells with the same colour are clustered in the same jet.

background noise. However, this problem has been elegantly solved by considering the family of generalised k_t algorithms identified by the distances

$$d_{ij} = \min(p_{ti}^{2p}, p_{ij}^{2p}) \frac{\Delta R_{ij}^2}{R^2}, \quad d_{iB} = p_{ti}^{2p}, \quad d_{jB} = p_{ij}^{2p}, \quad (2.7)$$

with p a parameter. For $p = 1$ and $p = 0$ one obtains the k_t and Cambridge/Aachen algorithms, respectively. For $p = -1$ one obtains a novel procedure, called the ‘anti- k_t ’ algorithm. Even in the presence of many soft particles, well-separated hard jets obtained with the anti- k_t algorithm, as shown for instance in figure 2.9, have precisely the shapes of circles in the y - ϕ plane [14]! An intuitive explanation of this fact resides in that, while the k_t algorithm starts clustering particles starting from the softest ones, the anti- k_t does the opposite, i.e. it clusters soft particles around the hardest ones, which remain more or less fixed. This unexpected feature explains why

all LHC experiments use the anti- k_t as a default choice. In spite of its practical advantages, the anti- k_t clustering procedure is somehow unrelated to the pattern of QCD radiation, which was one of the motivations for introducing sequential algorithms. For instance, one cannot introduce a jet resolution parameter based on the anti- k_t distance to define jet rates, because this would be infrared unsafe. The standard procedure to define jet rates is to find all anti- k_t jets and classify an event as having n jets, if only n jets have transverse momenta above a given threshold. For experimental analyses in which it is important to understand the substructure of jets (e.g. in boosted object searches, see chapter 4), other algorithms, such as the Cambridge/Aachen, have been exploited. In fact, LHC experiments consider a variety of jet algorithms and do not stick to the anti- k_t .

2.1.3 Common issues with jet algorithms

We end this section by discussing two issues that are common to all jet algorithms. The first is the problem of determining the correct ‘jet energy scale’, i.e. assessing the ‘true’ value of a jet’s momentum out of what is observed in the detectors. The second is the effect of the recombination scheme, the procedure used to determine the momentum of a jet out of the momenta of its components.

Jet energy scale and removal of a uniform background. Since jets are the main objects that enter physics analyses in hadron collisions, it is crucial to be able to reconstruct their momenta as accurately as possible from the information obtained from the detectors. In fact, jet distributions, for instance those in jet transverse momentum or invariant mass, fall steeply with the increase of these variables, so that a migration of events between bins of such distributions due to an incorrect assignment of the energy of a jet has a huge effect on their overall shapes, undermining their correct interpretation. For instance, a peak in the invariant mass of two jets might reveal the presence of a new particle that decays hadronically, such as a Z' , a heavier partner of the Z boson, decaying into a quark–antiquark pair. The effect of a mis-measurement of the transverse momentum of jets might result in a broadening of the peak, which therefore becomes indistinguishable from QCD jet production.

The first serious issue is the correct determination of the energy of a jet out of the corresponding calorimetric deposits, which is commonly referred to as the problem of ‘jet energy scale’. In practice, one tries to find the correction factor to be applied to the observed transverse momentum (or transverse energy) of a jet, to obtain its actual value, the one to be used in physics analyses. This procedure, commonly referred to as ‘calibration’, is very complicated, has to be repeated for each jet algorithm and is strongly dependent on the specific experimental set-up. This is why we will not attempt to describe all the experimental procedures needed to perform jet calibration, for which the interested reader is referred to experimental notes (e.g. [8, 22, 23]). Here we will instead highlight the main sources of uncertainties and discuss in some detail one detector-independent issue, the removal of a uniform background.

From a purely experimental point of view, one needs to take into account, for instance: the segmentation of calorimeters, whose cells have a finite size, which might be different in the central and in the forward/backward regions; the availability of tracking information, i.e. the fact that charged particle momenta

can be reconstructed only in a central region; noise in the detectors, as well as imperfections, such as cracks, transition regions, or even faults; and unstable particles, whose decay products might fall in different parts of the detector. These are just examples of the many issues that experiments have to face when performing jet calibration. Some of these problems can be tackled offline, for instance by sending a beam of hadrons of known energy against the detectors and studying their response. Such offline tests have to be validated when the experiment is running. One common procedure consists in checking that the transverse momentum of a jet is the same as that of a well-measured object (e.g. a photon) recoiling against it.

Even if the momentum of jets is known with infinite precision, all jet observables in hadron collisions are contaminated by a large background that has nothing to do with the high-energy collisions one is interested in. A first source of background is the so-called PU, secondary low-energy collisions that occur at every crossing of the beams. The size of this effect at a high-luminosity machine such as the LHC can be appreciated from figure 2.10, where one can see the peak number of interactions per beam crossing, as recorded by the CMS detector as a function of time during the first high-energy runs of the LHC. These numbers will increase in the second run of the LHC, with 55 PU events expected for an instantaneous luminosity $\mathcal{L} = 2 \times 10^{34} \text{ cm}^{-2}\text{s}^{-1}$ and as many as 200 PU events at $\mathcal{L} = 7 \times 10^{34} \text{ cm}^{-2}\text{s}^{-1}$. Another source of background is the so-called ‘underlying event’ (UE), i.e. beam-remnant interactions. These happen because, in every hadronic collision, the remainders of the collision of the incoming hadrons are coloured particles and hence can interact via the strong force. Only rarely can these interactions give rise to a secondary hard collision, this occurrence being referred to as ‘double-parton scattering’. More commonly, the remnants undergo a number of low-energy collisions, producing a large number of soft hadrons, many of which can be observed in regions of the detectors where hard jets are typically tagged. These are known as the ‘diffuse’ component of the UE, whereas double-parton scattering is

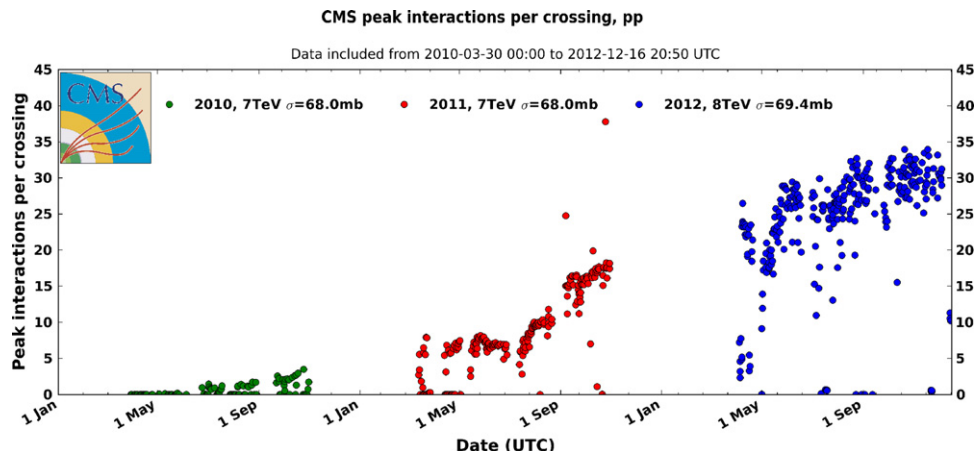


Figure 2.10. The peak number of interactions per beam crossing recorded by the CMS experiment during the first high-energy runs of the LHC [24].

referred to as its ‘point-like’ component. PU and UE have in common the fact that they produce a yield of particles that is roughly uniform in rapidity and azimuth. Just to give an idea of the size of these effects, at its highest energy, the UE at the LHC will produce up to 10–15 GeV of transverse momentum per unit rapidity, whereas the effect of PU in the higher luminosity phase of the LHC is estimated to be of the order of 100 GeV per unit rapidity [25].

The effects of detector noise, PU and UE cannot be cleanly separated and have to be dealt with concurrently. A problem that can be solved in a detector-independent way is the removal of a ‘uniform’ background, i.e. giving a fixed amount of transverse momentum ρ per unit rapidity and unit azimuth. If ρ is known with infinite precision, and each jet p_J is just a patch of fixed area A in the y – ϕ plane, we have

$$p_{t,J}^{\text{true}} \simeq p_{t,J}^{\text{meas}} - \rho A, \quad (2.8)$$

where $p_{t,J}^{\text{true}}$ is the actual value of the transverse momentum of the jet and $p_{t,J}^{\text{meas}}$ is its measured value⁵. In practice, however, ρ and A are not known *a priori*. Therefore, one needs to find a way to assess the sensitivity of a jet to a uniform background and a sensible strategy to measure ρ .

A recent proposal to quantify a jet’s sensitivity to a uniform background is through the notion of ‘active area’ [25]. This is defined by generating a set g of ultra-soft ‘ghost’ particles $\{g_i\}$, with ν_g ghost particles per unit area in the y – ϕ plane and average transverse momentum $\langle g_i \rangle$, and considering, for each hard jet p_J , the quantity

$$A(J| \{g_i\}) = \frac{N_g(J)}{\nu_g}, \quad (2.9)$$

where $N_g(J)$ is the number of ghost particles of the set g clustered within the jet ‘J’. One then defines the active area of jet ‘J’ in terms of the following limit:

$$A_J = \lim_{\nu_g \rightarrow \infty} \left\langle A(J| \{g_i\}) \right\rangle_g, \quad (2.10)$$

where the average is over all possible sets of ghosts, provided $\nu_g \langle g_i \rangle$ stays much smaller than the transverse momentum of the considered hard jets. This procedure gives an idea of how ‘catchy’ a given jet algorithm is when many soft particles are present.

The second problem one has to solve is how to estimate the size of the background transverse momentum density ρ . The proposal that is currently used by LHC experiments is based on the observation that, in a busy environment with a few hard jets and many soft jets, the ratio between the transverse momentum of most jets and their area is roughly constant. The only exception to this scaling is constituted by hard jets. In fact, if all jets were produced by a uniform background,

⁵For simplicity, we have neglected the fact that the transverse momentum is a two-dimensional vector. Therefore, the procedure in (2.8) is strictly correct only if the transverse momentum of a jet is reconstructed through the scalar sum of its constituents’ transverse momenta, as in (2.2).

the transverse momentum of each jet would be proportional to the jet area. Since in a regime with a high PU the number of soft jets is much larger than that of hard jets, one can use the following estimator [26]:

$$\rho = \text{median}_j \left(\frac{p_{tJ}}{A_j} \right), \quad (2.11)$$

and correspondingly find estimators for the standard deviation of ρ . Note that, in the absence of PU, the above equation provides a measurement of the size of the diffuse component of the UE. Then one can obtain, on an event-by-event basis, the subtracted transverse momentum of a jet by replacing, in (2.8), the generic area A by A_j , the jet area defined in (2.10). The subtraction can be improved by taking into account the vectorial nature of transverse momentum [26]. Also, if performed before jet calibration, the procedure described above eliminates all detector noise that gives a uniform background.

Let us now look in more detail at the active area of the algorithms we have defined so far, in particular of jets defined with SIScone with a split–merge procedure, and with the k_t , Cambridge/Aachen and anti- k_t sequential algorithms. The active area of an isolated hard jet defined with a seedless cone algorithm (such as e.g. SIScone) with radius R is not πR^2 , as one would naively expect. In fact, simulations of dijet events show that the active area of each hard jet is a mild function of the jet's transverse momentum, with an average around $\pi R^2/2$ (see the left-hand panel of figure 2.11). The reason for this value relies on the split–merge procedure of cone algorithms and is better understood by considering the example of an isolated stable cone containing a single hard parton [25]. If we add a uniform background of ghost particles, we obtain new soft stable cones made up of only ghost particles. The maximum overlap between the hard cone and a soft stable cone corresponds to the situation where the boundary of the soft cone touches the centre of the hard cone, as depicted in the right-hand panel of figure 2.11. From geometrical considerations, one finds that the fraction of particles that is contained in both cones is $f_{\max} = \frac{2}{3} - \frac{\sqrt{3}}{2\pi} \simeq 0.391$, which is below the commonly chosen overlap thresholds $f=0.5$ or $f=0.75$. This means that the common particles will be assigned to either jet, according to which jet axis is closer. Indeed, if one considers all possible ghost stable

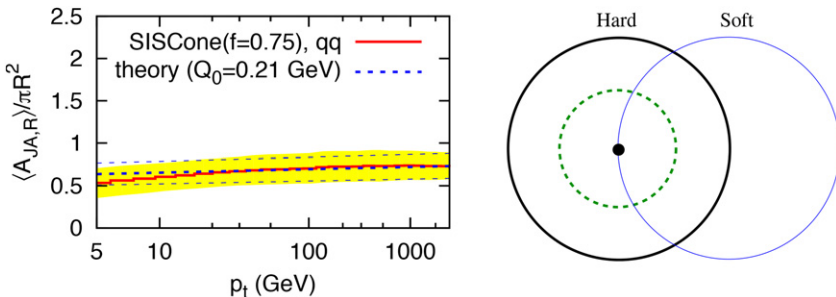


Figure 2.11. Left: the average area of a jet defined with the SIScone algorithm, as a function of the jet transverse momentum [25]. Right: maximal overlap between a hard stable cone, ('Hard', black) and a cone made up of ghost particles ('Soft', blue). The picture, drawn by the author, is adapted from [25].

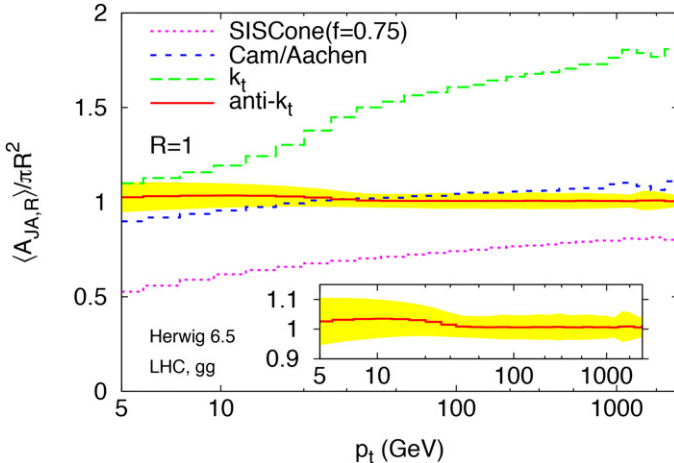


Figure 2.12. The mean value of the active area of the four algorithms described in the text, for jets initiated by gluons [14].

cones that have a maximal overlap with the hard cone, only particles within a radius $R/2$ from the axis of the hard cone will be part of the hard jet, which will have now an active area $A_j = \pi R^2/4$. Addition of extra QCD radiation increases this value, so the average area of hard jets is close to $\pi R^2/2$ with mild fluctuations. As expected, the average active area of jets obtained from the k_t and the Cambridge/Aachen algorithms has a greater dependence on the transverse momentum of the jets, as can be seen from the corresponding curves in figure 2.12, and large fluctuations (not shown). This is not the case for the anti- k_t algorithm, which confirms the intuitive picture of figure 2.9. The average active area of anti- k_t hard jets is πR^2 with very small fluctuations and basically no dependence on the jet transverse momentum [14]. Note that it is possible to have circular hard jets in the $y-\phi$ plane using cone algorithms as well, at the cost of abandoning the split-merge procedure. For instance, one can use SIScone to find all stable cones and a progressive removal approach to deal with overlapping cones [27]. This procedure looks for the hardest stable cone and calls it a jet. This cone is then removed from the list of stable cones and its particles are removed from the list of particles. The procedure is then repeated until no stable cones are left. SIScone with progressive removal scales as $N^2 \ln N$ for N input particles. Therefore, it performs slightly worse than anti- k_t , whose current implementation scales at most as $N^{3/2}$ [14].

Having a quantitative notion of the area of a jet, the procedure of subtracting a uniform background becomes possible on an event-by-event basis for any jet algorithm, not only for those whose jets have a fixed area. However, one needs to take into account that background is not completely uniform in rapidity. For instance, detector noise is different according to which parts of the experimental apparatus, in particular of the calorimeters, one considers. One can in principle devise rapidity-dependent estimators for ρ , for instance by dividing the $y-\phi$ plane into regions that are small enough to have a smooth function of y , but enough jets so that the estimate in (2.11) can be trusted. It is, however, more complicated to

determine the correct jet energy scale for jets that cluster pseudo-particles in an unpredictable way, as happens for the k_t and Cambridge/Aachen algorithms. This is why the anti- k_t , whose jets are localised in the $y-\phi$ plane, is the preferred algorithm for measurements involving hard-jet transverse momenta.

Recombination schemes. We conclude this section by discussing various procedures that can be used to merge different particles into a single pseudo-particle. These procedures are known as ‘recombination schemes’. At each step of a sequential algorithm, the recombination scheme determines how the momenta p_i and p_j of two pseudo-particles have to be recombined into a new pseudo-particle of momentum p_{ij} . Three recombination schemes use the particles’ energies and three-momenta, as follows:

- E -scheme: $p_{ij} = p_i + p_j$, i.e. addition of pseudo-particles’ four-momenta.
- $E0$ -scheme: $E_{ij} = E_i + E_j$ and $\vec{p}_{ij} = (\vec{p}_i + \vec{p}_j)/E_{ij}$, so that the resulting jet is massless.
- P -scheme: $\vec{p}_{ij} = \vec{p}_i + \vec{p}_j$ and $E_{ij} = |\vec{p}_{ij}|$, so as to have again a massless jet.

Other recombination schemes determine the transverse momentum $p_{t,ij}$, the rapidity y_{ij} and the azimuthal angle ϕ_{ij} of the new pseudo-particle out of the transverse momenta, rapidities and azimuths of the parent pseudo-particles [3]. They can all be obtained from the relations

$$\begin{aligned} p_{t,ij} &= p_{ti} + p_{tj}, \\ y_{ij} &= \frac{w_i y_i + w_j y_j}{w_i + w_j}, \\ \phi_{ij} &= \frac{w_i \phi_i + w_j \phi_j}{w_i + w_j}, \end{aligned} \tag{2.12}$$

where w_i can be, for instance, p_{ti} or p_{ti}^2 . More recombination schemes can be obtained by replacing transverse momenta with transverse energies, and rapidities with pseudorapidities. The above schemes can be generalised to any number of recombined particles and are not specific to sequential algorithms. In fact, they can be used with cone algorithms to obtain the axis of a cone out of the momenta of the pseudo-particles inside it, as shown in (2.2).

One of the effects of the recombination scheme is that of changing the sensitivity of physical observables to the energy-momentum flow inside each jet. For instance, variables such as the azimuthal angle between two jets are insensitive to QCD radiation inside each jet if the recombination scheme adds three-momenta vectorially, but not if it performs any of the weighted recombinations in (2.12) [28]. Although very interesting theoretically, changing the recombination scheme might not be ideal from an experimental point of view. This is specifically due to the fact that the transverse momentum of a jet depends on the recombination procedure, so that jet energy-scale calibration has to be repeated for each recombination procedure within the same jet algorithm. Since jet calibration is a complicated procedure, experiments select not

only a default jet algorithm, but also a default recombination scheme. For instance, the LHC default is the anti- k_t algorithm with the E recombination scheme. Note that the two main LHC experiments, ATLAS and CMS, adopt slightly different choices for the jet radius, so as to exploit the sensitivity of their detectors as much as possible [22, 29]. It has to be stressed that there is nothing that prevents an experiment from using a different jet algorithm for a specific analysis, or exploring a different recombination scheme within the same jet algorithm.

Both this and the previous section have shown how difficult it is to move from the intuitive concept of a jet as a huge deposit of energy in a detector to its rigorous formulation in terms of an algorithmic procedure. The algorithms we have described so far are the ones that have actually been used in high-energy physics experiments. Their properties have been thoroughly tested and are well understood. In recent years, however, in particular to make better use of jets as tools to discover new particles, novel and sometimes unconventional ideas for reconstructing jets have been proposed. The next section is devoted to presenting a number of these recent developments, so as to give the reader a sense of how the field might evolve in the future.

2.2 Novel jet clustering procedures

With more and more experimental analyses exploiting the properties of jets, it is very difficult to follow closely the development of jet algorithms. As a basic reference for the interested reader, many algorithm definitions and codes can be found in the computer library FASTJET [30]. For an overview of novel jet algorithms, as an alternative to those presented in the previous sections, the reader is referred to topical reviews on jet physics such as [31]. In this section we wish to present some ideas on how it is possible to ‘play’ with jet definitions so as to be able to extract useful information about the observed jets. The examples we have chosen aim to highlight various complementary ways to approach the problem of finding and characterising jets.

Inclusive jet algorithms in e^+e^- annihilation. Let us consider for instance the k_t -algorithm in hadron collisions. The way it reconstructs jets is referred to as ‘inclusive mode’. There is however the possibility of running the k_t -algorithm in ‘exclusive mode’, in which one fixes a jet resolution d_{cut} and each event is classified as having n jets if and only if the minimum of the mutual distances d_{ij} and of the distance of each particle with the beam d_{iB} is larger than d_{cut} . All algorithms we have presented for e^+e^- annihilation work in exclusive mode, whereas inclusive mode is the typical way of reconstructing jets in hadron collisions. Due to the fact that e^+e^- colliders represent a less intricate environment, it might be very useful to have inclusive jet algorithms defined there as well. How this is possible can be understood by considering, in a hadron collider, particles that are quasi-central, i.e. whose rapidity is very close to zero. The energy of these particles is almost equal to their transverse momentum. In particular, considering two particles p_i and p_j that are very close in angle, we can approximate

$$2(p_i p_j) = 2E_i E_j (1 - \cos \theta_{ij}) \simeq p_i p_j \Delta R_{ij}^2, \quad (2.13)$$

so that we can identify ΔR_{ij}^2 with the angular distance $2(1 - \cos \theta_{ij}) \simeq \theta_{ij}^2$. Therefore, a suitable definition of inclusive generalised k_t algorithms in e^+e^- annihilation involves a distance between pairs of pseudo-particles

$$d_{ij} = \min(E_i^{2p}, E_j^{2p}) \frac{1 - \cos \theta_{ij}}{1 - \cos R}, \quad (2.14)$$

as well as a distance with a ‘beam’, which is given by $d_{iB} = E_i^{2p}$ [30, 32]. Then the algorithm works as in hadron collisions: if, at any step, the minimum of all distances is d_{iB} , pseudo-particle p_i is considered as a jet and removed from the list of pseudo-particles. If the minimum distance is d_{ij} , pseudo-particles p_i and p_j are recombined as in the exclusive mode of the algorithm. The procedure stops when no pseudo-particles are left. Similarly, it is also possible to devise an e^+e^- version of SISCone [32]. With these adaptations, one can study the behaviour of jet algorithms in a simpler environment than hadron collisions. For instance, in e^+e^- annihilation it is possible to compute jet rates in QCD with high precision [32], or even gain an analytical understanding of the properties of various algorithms, and exploit this knowledge to devise better algorithms for hadron colliders [33].

Quantum jets. As explained at the beginning of the chapter, the main purpose of a jet algorithm is that of mapping a set of final-state particles into a small number of jets, whose momenta should be close to those of the primordial hard quarks and gluons produced in a high-energy collision. This perfect match is only guaranteed in a case where the initial hard partons are accompanied by a set of infinitely soft emissions and collinear splittings. In real life, it might happen that the number of jets an event is mapped into does not reflect the original hard event and moreover that this result depends on the jet algorithm. A notion that emphasises this intrinsic uncertainty in the interpretation of events is that of ‘quantum jets’, or simply ‘Q-jets’ [34]. They are constructed out of a ‘quantum’ jet algorithm, in which an event is not mapped into a number of jets with certainty, but with a given probability. More specifically, a quantum jet algorithm is similar to a ‘classical’ sequential algorithm, with the following modifications occurring at each stage:

1. A weight ω_{ij} is computed for every pair of pseudo-particles p_i and p_j .
2. A pair p_i and p_j is chosen with probability $\Omega_{ij} = \omega_{ij}/\sum_{k < l} \omega_{kl}$ and merged into a single pseudo-particle.

The classical procedure is recovered if $\omega_{ij} = \delta(d_{ij} - d_{\min})$, where d_{ij} is an arbitrary IRC safe distance measure and d_{\min} is its smallest value among all possible pairs of pseudo-particles. The procedure is repeated N_{tree} times, each time giving a ‘tree’ of clusterings, the probability of each tree being $\prod_{\text{mergings}} \Omega_{ij}$. A particularly interesting class of weights is

$$\omega_{ij} = \exp \left[-\alpha \frac{d_{ij} - d_{\min}}{d_{\min}} \right]. \quad (2.15)$$

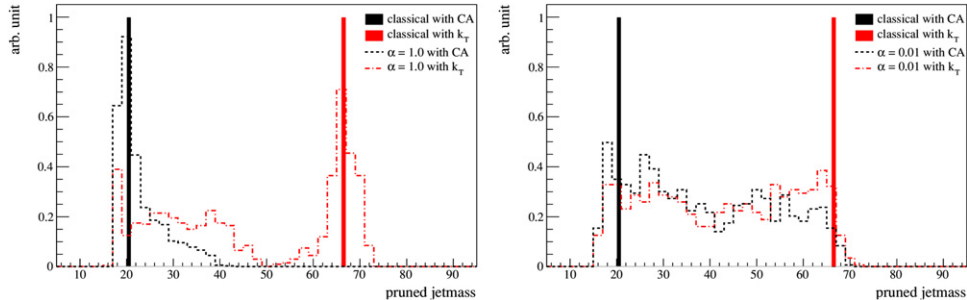


Figure 2.13. The distribution in the invariant mass of a pruned jet for the classical k_t and Cambridge/Aachen algorithms and their quantum versions with $\alpha = 1.0$ (left) and $\alpha = 0.01$ (right) [34].

with α a positive number called ‘rigidity’. Note that, for $\alpha \rightarrow \infty$ the pair with the minimum d_{ij} will always be chosen, thus recovering the corresponding classical sequential algorithm. This is very close to what happens in quantum mechanics, where quantum trajectories are distributed according to a probability that is peaked around classical trajectories, with the role of the parameter α played by the constant $1/\hbar$. The trees constructed out of this probabilistic interpretation are called Q-jets. The effect of classical versus quantum jets can be appreciated by considering observables that are sensitive to the clustering sequence. One of these observables is the so-called pruned-jet mass, the invariant mass of a jet in which, at each clustering stage, one of the two particles that is to be merged is discarded or kept according to some ‘pruning’ criterion, which will be discussed in detail in chapter 4. The number of pseudo-particles that will enter each jet will be strongly affected by the clustering sequence, and hence the value of the pruned-jet mass will be very different according to the chosen sequential algorithm. This can be appreciated in figure 2.13, where one can see the distribution in the invariant mass of a pruned jet, obtained by running several times the classical and quantum versions of the k_t and Cambridge/Aachen jet algorithms. One can see that the classical versions of the algorithms give the same values of jet mass for each of the considered trees. Note that the two values are different, highlighting the strong dependence on the algorithm of this observable. In the quantum case, for $\alpha = 1.0$, closer to the classical limit, one obtains two distributions, peaked around the corresponding classical values. In a deeper quantum regime, for $\alpha = 0.01$, the difference between the two jet algorithms is somewhat washed out and one obtains two very similar distributions. It seems then that quantum jets point to physical features of an event, rather than being sensitive to artefacts induced by the choice of a specific jet algorithm. More properties of Q-jets will be discussed in the context of the use of jets as discovery tools in chapter 4.

Jet-finding as an optimisation procedure. Let us consider, as a starting point, a two-jet event in e^+e^- annihilation. In line with the intuitive idea of a jet as a region where energy deposit is maximised, one can find the direction that maximises the scalar sum of the projection of momenta along it. This maximum is called the thrust

$$T = \max_{\vec{n}_T} \frac{\sum_i |\vec{p}_i \cdot \vec{n}_T|}{\sum_i |\vec{p}_i|}, \quad (2.16)$$

and the direction \vec{n}_T maximising the sum in the above equation is called the thrust axis. In e^+e^- annihilation, for each event, one can cluster all particles into two back-to-back jets as follows: the thrust axis can be identified with the jet axis and particles can be assigned to either jet according to whether $\vec{p}_i \cdot \vec{n}_T$ is larger or smaller than zero. An analogous procedure, which coincides with that in (2.16) for two back-to-back jets but which is generalisable to an arbitrary jet configuration, is to *minimise* a quantity called 2-jettiness $\mathcal{T}_2(n_1, n_2)$, with $n_i = (1, \vec{n}_i)$ two light-like vectors. The 2-jettiness is defined as

$$\mathcal{T}_2(n_1, n_2) = \frac{1}{\sum_i |\vec{p}_i|} \sum_i \min\{2n_1 \cdot p_i, 2n_2 \cdot p_i\}. \quad (2.17)$$

One can introduce a jet radius R and a ‘beam jet’ that collects all particles that are not clustered with the two jets by redefining the 2-jettiness as follows:

$$\mathcal{T}_2(n_1, n_2) = \frac{1}{\sum_i |\vec{p}_i|} \sum_i \min\left\{E_i, \frac{2n_1 \cdot p_i}{R^2}, \frac{2n_2 \cdot p_i}{R^2}\right\}. \quad (2.18)$$

Once the two directions \vec{n}_1 and \vec{n}_2 have been found, particle p_i is assigned to either jet, or to the beam jet, according to which is the minimum between $2(n_1 p_i)/R^2$, $2(n_2 p_i)/R^2$ and E_i . Similarly, one can find N jets $\{n_1, n_2, \dots, n_N\}$ by minimising N -jettiness, defined as [35, 36]

$$\mathcal{T}_N(n_1, n_2, \dots, n_N) = \frac{1}{\sum_i |\vec{p}_i|} \sum_i \min\left\{E_i, \frac{2n_1 \cdot p_i}{R^2}, \frac{2n_2 \cdot p_i}{R^2}, \dots, \frac{2n_N \cdot p_i}{R^2}\right\}. \quad (2.19)$$

The procedure can also be defined iteratively, first finding one jet of radius R by minimising 1-jettiness, then removing all particles within that jet and repeating the procedure with the remaining particles, until no particles are left. In this case one finds that isolated hard jets are perfect cones of radius of order R .

Another proposal [37] that exploits a maximisation procedure consists in defining the momentum of a jet p_J by considering all possible sets of particles α and for each set constructing the total momentum of the set

$$p_\alpha = \sum_{i \in \alpha} p_i. \quad (2.20)$$

The momentum of a jet p_J is the vector p_α that maximises a certain ‘jet function’ $J(p_\alpha)$, with

$$J(p_\alpha) = f\left(E_\alpha, \frac{m_\alpha^2}{E_\alpha}\right), \quad m_\alpha^2 = p_\alpha^2. \quad (2.21)$$

In order to match the intuitive idea of a jet as the footprint of a massless parton, $J(p_\alpha)$ should increase with increasing energy and decrease with increasing mass. A suitable proposal for e^+e^- annihilation is then⁶

$$J(p_\alpha) = E_\alpha - \frac{1}{R^2} \frac{m_\alpha^2}{E_\alpha}. \quad (2.22)$$

The algorithm then proceeds by iteration. One finds the momentum p_α that maximises $J(p_\alpha)$, calls it a jet with momentum p_j and removes all the particles belonging to the set α . The procedure is then repeated with the remaining particles until no particles are left. Jets defined with this procedure are again cones of nearly fixed radius R . It has been noted that, with this algorithm, energy is very localised inside these cones, with only infinitely soft particles allowed to live at the cone boundaries.

It has remarkably been shown that [37], in e^+e^- annihilation, the minimisation of 1-jettiness and the maximisation of the above jet-function lead to the same jets. Moreover, the two procedures are equivalent to the SISCone jet algorithm, when progressive removal is applied to deal with overlapping cones. In fact, one can construct the following function of a candidate jet momentum $p_\alpha = (E_\alpha, \vec{p}_\alpha)$, and of a light-like jet axis $n = (1, \vec{n})$:

$$M(p_\alpha, n) = E_\alpha - \frac{2n \cdot p_\alpha}{R^2}. \quad (2.23)$$

It is possible to show [35] that maximising M over all possible p_α and n simultaneously yields a maximum for the jet function $J(p_\alpha)$, a minimum for the 1-jettiness $T_1(n)$ and a hard stable cone. This property makes it possible to use the methods of computational geometry to find jets defined with an optimisation procedure. In fact, one can first find all stable cones and then determine the one that maximises the jet-function, or minimises 1-jettiness. Note that the extension of the three procedures to hadron collisions does not lead to the same jets, due to different ways of defining the transverse momentum of a jet. However, jets are still nearly fixed cones with a radius of order R .

There are many lessons that one can learn from the above discussion. An important one is that there can be different procedures that lead to qualitatively similar jets. It is then only a matter of finding which one makes it possible to achieve the goals it was designed for in the fastest and most efficient way. Exploring different jet-finding philosophies makes it easier to find new procedures that can lead to jets that are qualitatively different from those already known. This in turn can lead to even more possibilities to exploit jets as tools for high-energy physics.

⁶In the original source [37], R^2 is called $1/\beta$. As suggested in [35], we change the notation in analogy with that in use for other jet algorithms.

Bibliography

- [1] <http://aleph.web.cern.ch/aleph/dali/>
- [2] Sterman G F and Weinberg S 1977 *Phys. Rev. Lett.* **39** 1436
- [3] Huth J E *et al* 1990 *Proc. FERMILAB Conf. Summer Study on High Energy Physics—Research Directions for the Decade (Snowmass, CO, June 25–July 13)* FERMILAB-Conf-90-249 <http://inspirehep.net/record/303065/files/fermilab-conf-90-249.pdf>
- [4] <https://twiki.cern.ch/twiki/bin/view/AtlasPublic/EventDisplayPublicResults>
- [5] Arnison G *et al* (UA1 Collaboration) 1983 *Phys. Lett. B* **132** 214
- [6] Abe F *et al* (CDF Collaboration) 1992 *Phys. Rev. D* **45** 1448
- [7] Seymour M H 1998 *Nucl. Phys. B* **513** 269
- [8] Blazey G C *et al* 2000 arXiv: hep-ex/0005012 <http://inspirehep.net/record/538825/files/fermilab-pub-00-297.pdf>
- [9] Salam G P and Soyez G 2007 *J. High Energy Phys.* JHEP05(2007)086
- [10] Kidonakis N, Oderda G and Sterman G F 1998 *Nucl. Phys. B* **531** 365
- [11] Seymour M H and Tevlin C 2006 *J. High Energy Phys.* JHEP11(2006)052
- [12] Ellis S D, Huston J and Tonnesmann M 2001 *eConf C* **010630** P513
- [13] Albrow M G *et al* (TeV4LHC QCD Working Group Collaboration) 2006 arXiv: [hep-ph/0610012](http://arxiv.org/abs/hep-ph/0610012)
- [14] Cacciari M, Salam G P and Soyez G 2008 *J. High Energy Phys.* JHEP04(2008)063
- [15] Bartel W *et al* (JADE Collaboration) 1986 *Z. Phys. C* **33** 23
- [16] Catani S, Dokshitzer Y L, Olsson M, Turnock G and Webber B R 1991 *Phys. Lett. B* **269** 432
- [17] Dokshitzer Y L, Leder G D, Moretti S and Webber B R 1997 *J. High Energy Phys.* JHEP08(1997)001
- [18] Catani S, Dokshitzer Y L, Seymour M H and Webber B R 1993 *Nucl. Phys. B* **406** 187
- [19] Wobisch M and Wengler T 1999 *Proc. Workshop on Monte Carlo Generators for HERA Physics* pp 270–9
- [20] Ellis S D and Soper D E 1993 *Phys. Rev. D* **48** 3160
- [21] Cacciari M and Salam G P 2006 *Phys. Lett. B* **641** 57
- [22] CMS Collaboration 2010 *CERN Report CMS-PAS-JME-10-003*
- [23] Aad G *et al* (ATLAS Collaboration) 2013 *Eur. Phys. J. C* **73** 2304
- [24] <https://twiki.cern.ch/twiki/bin/view/CMSPublic/LumiPublicResults>
- [25] Cacciari M, Salam G P and Soyez G 2008 *J. High Energy Phys.* JHEP04(2008)005
- [26] Cacciari M and Salam G P 2008 *Phys. Lett. B* **659** 119
- [27] <https://siscone.hepforge.org/usage.html>
- [28] Banfi A, Dasgupta M and Delenda Y 2008 *Phys. Lett. B* **665** 86
- [29] Aad G *et al* (ATLAS Collaboration) 2009 arXiv: [0901.0512](http://arxiv.org/abs/0901.0512)
- [30] Cacciari M, Salam G P and Soyez G 2012 *Eur. Phys. J. C* **72** 1896
- [31] Salam G P 2010 *Eur. Phys. J. C* **67** 637
- [32] Weinzierl S 2011 *Eur. Phys. J. C* **71** 1565
Weinzierl S 2011 *Eur. Phys. J. C* **71** 1717 (erratum)
- [33] Dasgupta M, Fregoso A, Marzani S and Powling A 2013 *Eur. Phys. J. C* **73** 2623
- [34] Ellis S, Hornig A, Roy T, Krohn D and Schwartz M 2012 *Phys. Rev. Lett.* **108** 182003
- [35] Thaler J 2015 *Phys. Rev. Lett.* **D 92** 074001
- [36] Stewart I, Tackmann F, Thaler J, Vermilion C and Wilkason T 2015 *J. High Energy Phys.* JHEP11(2015)072
- [37] Georgi H 2014 arXiv: [1408.1161](http://arxiv.org/abs/1408.1161)

Hadronic Jets

An introduction

Andrea Banfi

Chapter 3

QCD for jet physics

One the most amazing features of jet physics is that, despite jets being complicated objects constructed out of many hadrons, their basic properties can be understood in terms of the elementary degrees of freedom of QCD, i.e. quarks and gluons. A formal introduction to QCD is beyond the scope of this book and is now textbook material [1, 2]. Here we will review the aspects of QCD that are crucial for jet physics.

QCD is a quantum field theory describing the interactions of elementary fermions, the quarks, mediated by spin-1 gauge particles, the gluons. As explained in the introduction, the known quarks are six, organised in three families. Their properties are summarised in table 1.1.

Besides electric charge (and weak isospin), each quark possesses an additional conserved charge, the colour. More specifically, each quark has three colours (say red, green and blue). Coloured particles, such as quarks, can interact with the strong force in a similar way to which electrically charged particles interact with the electromagnetic force. The strong force is mediated by spin-1 particles, the gluons, like the electromagnetic force is mediated by photons. There is, however, a fundamental difference between the electromagnetic and the strong force. When an electron emits a photon, it does not change its electric charge, whereas a quark emitting a gluon changes its colour. This means that gluons can take away colour and are colour-charged themselves, whereas photons are electrically neutral. Specifically, the gluons can have eight different colours. Therefore, while in quantum electrodynamics (QED) the transition amplitude for an electron emitting a photon is only proportional to the electron charge e , in QCD one has to specify not only the strong interaction coupling constant g_s (the analogue of e), but also the probability that a quark of a colour j transforms into a quark of a colour i after the emission of a gluon. This gives rise to a transition matrix t_{ij}^a , where a is the colour of the

emitted gluon. We have then eight transition matrices, which form a Lie algebra under commutation, namely:

$$[t^a, t^b] = if^{abc}t^c. \quad (3.1)$$

Their commutation relations are those of the generators of the Lie group $SU(3)$, which is in fact the gauge group of QCD. The symbol f^{abc} , totally antisymmetric in the indices a, b, c , embodies the so-called ‘structure constants’ of the group $SU(3)$.

Before discussing jet formation, we need to address the fact that no coloured particles are observed in our detectors. Despite this, for high-energy processes, we can compute hadronic cross sections using transition probabilities between unobserved quarks and gluons, and surprisingly we obtain extremely good agreement with experimental data. The key property that makes QCD predictive is asymptotic freedom. The strength of the interactions in QCD is the strong coupling $\alpha_s = g_s^2/(4\pi)$, the analogue of the fine structure constant $\alpha = e^2/(4\pi)$ in QED. As in any quantum field theory, the value of α_s that rules the magnitude of a given transition probability depends on the typical scale of that transition. For instance, the total production rate of hadrons in electron–positron annihilation depends on $\alpha_s(\sqrt{s})$, with \sqrt{s} the centre-of-mass energy of the electron–positron collision. The coupling α_s decreases for increasing momenta and vanishes for asymptotically large momenta, giving rise to non-interacting quarks. QED has the opposite behaviour, with the fine structure constant tending to the fixed value 1/137 for vanishingly small momenta. What happens at low momenta for QCD? The coupling α_s grows, until a point at which we cannot calculate any further. In fact, except for rare exceptions, in quantum field theory we can calculate only small deviations from the free behaviour through perturbative expansions in the coupling. When the latter is large, such expansions become meaningless and one needs to know how the full theory behaves. In QCD, at low momenta quarks and gluons interact so strongly that they can no longer exist as quasi-free objects, but are doomed to live confined to form colourless objects, the hadrons.

We are now in a position to qualitatively understand jet formation. Suppose a quark is produced in a high-energy process. The fact that it is ripped off from the vacuum results in a huge instantaneous acceleration, similar to that experienced by fast electrons colliding on a target. Similarly to how these electrons emit bremsstrahlung photons, e.g. x-rays, an accelerated quark radiates gluons. In fact, at high energy the QCD coupling is small and, except for the colour matrices t^a , QCD closely resembles classical electromagnetism. As in classical electrodynamics, gluons are radiated preferably with small energies, collinear to their emitter, with a probability density

$$dP(E, \theta) \sim \alpha_s(E\theta) \frac{dE}{E} \frac{d\theta^2}{\theta^2}, \quad (3.2)$$

where E is the energy of the emitted gluon and θ is its angle relative to the emitting quark. Note that the coupling α_s is to be evaluated at the scale $E\theta$, the transverse momentum of the radiated gluon with respect to the emitting quark. The most likely configurations are those in which gluons are emitted at subsequently decreasing angles. This gives an ensemble of highly collimated partons. This ‘branching’

process stops when the angle and/or the energy of the last emitted parton are so small that $\alpha_s(E\theta)$ becomes large. At this point, the quark feels a strong interaction from the neighbouring partons and hadrons are formed. We do not know how hadronisation actually takes place. What we know is that models in which only partons whose momenta are of similar size form hadrons provide the best description of collider data. We can safely assume that, when the QCD coupling becomes large, neighbouring partons gather together to form hadrons, without a significant reshuffling of energy and momenta with respect to the parent partons. This is why a highly energetic quark gives rise to a jet of highly collimated hadrons. Of course, the momenta of the hadrons in a jet will be related to that of the parent quark or gluon. More specifically, the change in the transverse momentum of a jet induced by hadronisation is of the order of a small hadronisation scale (~ 1 GeV), so that the relative corrections (~ 1 GeV/ $p_{t,\text{jet}}$) are expected to decrease with increasing $p_{t,\text{jet}}$. Furthermore, with increasing jet transverse momenta, given that the gluon emission probability in (3.2) is proportional to $\alpha_s(E\theta) \sim \alpha_s(p_{t,\text{jet}}\theta)$, the angle of emitted gluons such that the QCD coupling becomes of order one and hadronisation takes place becomes smaller and smaller. This is why, at high transverse momenta, jets are so collimated that their momenta are very close to those of the individual quarks or gluons that have initiated them.

This very qualitative picture of jet formation is confirmed by the excellent agreement between QCD theoretical predictions and experimental data. The rest of this chapter will thus be devoted to presenting the basics of QCD that are needed to understand jet physics and to describing the state-of-the art of QCD theoretical tools.

3.1 Collinear splitting in QCD

The most important quantity for jet physics that can be computed in QCD is the probability that a parton of type a (quark q , or gluon g) splits into two partons of type b and c . The reader might be surprised that it is possible to isolate an elementary subprocess in a quantum theory, in which probabilities are computed by squaring transition amplitudes. Consider then a parton of type a with a given four-momentum p_a . By collinear splitting we mean the production of two partons p_b and p_c , quasi-parallel to p_a , as displayed in figure 3.1. All partons can be considered to be quasi-massless, in the sense that their invariant masses are much smaller than their energies and momenta. In this case the probability to produce partons p_b and p_c factorises into the product of the probability of producing p_a , times a universal factor, which can be interpreted as the elementary probability for the splitting

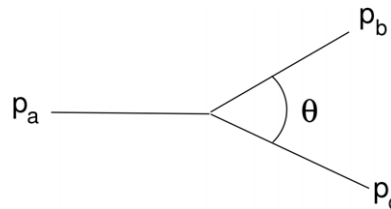


Figure 3.1. Pictorial representation of the splitting $a \rightarrow bc$.

$a \rightarrow bc$ [1, 2]. The splitting probabilities depend only on the type of parton involved (quarks or gluons) and can be expressed as

$$dP_{a \rightarrow bc}(z, \theta) = \frac{d\theta^2}{\theta^2} dz P_{ba}(z) \frac{\alpha_s(z(1-z)\theta E)}{2\pi}. \quad (3.3)$$

In the above expression, θ is the angle between partons p_b and p_c , E is the energy of parton p_a and z is the fraction of the energy E carried by parton p_b . By momentum conservation, the energy of parton p_c will be $(1-z)E$. For the splitting to take place, parton p_a needs to have a positive invariant mass squared, which is approximately given by

$$p_a^2 = (p_b + p_c)^2 \simeq z(1-z)\theta^2 E^2. \quad (3.4)$$

Note that the coupling has to be evaluated at the scale $z(1-z)\theta E$, which is of the order of the relative transverse momentum of partons p_b and p_c . The splitting probability in (3.3) is large when the angle between p_b and p_c is small, i.e. p_b and p_c are quasi-collinear. In this situation $p_a^2 \ll E^2$. In the collinear limit $\theta \rightarrow 0$, the splitting probability diverges. This is precisely the collinear divergence of QCD matrix elements introduced in the previous chapter in the discussion about IRC safety.

There are four basic splitting functions in QCD, $P_{qq}(z)$, $P_{gq}(z)$, $P_{qe}(z)$ and $P_{gg}(z)$. Their expressions are [1]

$$\begin{aligned} P_{qq}(z) &= C_F \frac{1+z^2}{1-z}, & P_{gq}(z) &= C_F \frac{1+(1-z)^2}{z}, \\ P_{qe}(z) &= T_F [z^2 + (1-z)^2], & P_{gg}(z) &= C_A \left[\frac{z}{1-z} + \frac{1-z}{z} + z(1-z) \right]. \end{aligned} \quad (3.5)$$

Some comments are in order. First of all, the prefactors C_F , T_F , C_A are related to the gauge group of the theory. In particular, for a gauge theory based on the Lie group $SU(N_c)$, with N_c the number of colours, we have

$$\text{Tr}(t^a t^b) = T_F \delta^{ab}, \quad \sum_{a=1}^{N_c^2-1} t_{ik}^a t_{kj}^a = C_F \delta_{ij}, \quad f^{acd} f^{bcd} = C_A \delta^{ab}. \quad (3.6)$$

The value of T_F is conventional, and sets the normalisation of the matrices t^a . We adopt the convention $T_F = 1/2$, giving

$$C_F = \frac{N_c^2 - 1}{2N_c}, \quad C_A = N_c. \quad (3.7)$$

For $N_c = 3$ we have $C_F = 4/3$ and $C_A = 3$. Similar expressions hold in QED, with the only difference that $T_F = 1$, $C_F = 1$ and $C_A = 0$, so that the splitting of a photon into two photons cannot occur. Both QED and QCD share the fact that splitting functions can become singular when z is close to zero or one. This corresponds to the fact that one gauge boson (gluon or photon) has vanishingly small energy, i.e. becomes infinitely soft. This is precisely the soft divergence that was discussed when the concept of IRC safety was introduced.

The basics of jet physics can be understood by analysing the splitting probability in (3.3) and the splitting functions of (3.5). Suppose that an energetic

parton p_a (quark or gluon) is produced in a high-energy (i.e. ‘hard’ as opposed to soft) collision and a splitting $a \rightarrow bc$ occurs. We have three possible scenarios:

1. $\theta \ll 1$, z arbitrary: this is the basic process underlying jet formation. Parent parton p_a splits into two partons p_b and p_c , close in angle. These will subsequently branch to produce a cascade of quasi-collinear partons, which will turn into highly collimated bunches of hadrons. An IRC safe jet algorithm will likely cluster these hadrons as a single jet.
2. $\theta \sim 1$, $z(1 - z) \ll 1$, and either parton b or parton c is a gluon: a soft gluon is emitted at a large angle. This soft gluon is in general coherently emitted by all the hard partons in the event. Soft gluons at wide angles give rise to soft hadrons in the region between the jets, whose angular distribution reflects the colour connections of the hard emitters, the so-called ‘colour flow’ of the event (see [1] for the exact definition of what a colour connection is). The fate of such hadrons is either to be clustered with the nearest jet or, if too far away, give rise to soft jets.
3. $\theta \sim 1$, $z \sim 1$: a hard parton is produced, well separated from all other hard partons in the event. This will further split into a bunch of collinear partons, which will later hadronise and give rise to an extra jet.

QCD, in its perturbative formulation, is best suited to describe the third scenario. It costs a power of the coupling α_s to produce an extra jet. The requirement that all jets are energetic (hard) and well separated in angle ensures that jet production rates can be expressed as perturbative series in powers of α_s , which at high energies is indeed a small expansion parameter. In this region, the collinear approximation we have discussed so far gives only a qualitative picture of the behaviour of hadronic jets. Instead, for a given order in α_s , one needs to compute the necessary QCD amplitudes (generally through Feynman-diagram techniques [1, 2]), square them and integrate over the momenta of all particles in the final state, the so-called multi-particle phase space. Such perturbative calculations are extremely important for the quantitative understanding of the dynamics of hadronic jets. In recent years, theoretical methods to perform perturbative QCD calculations have seen enormous progress. Given the importance of the topic, section 3.2 will be devoted to a general overview of the ideas underlying perturbative QCD calculations and to an illustration of the most recent advances. Despite the enormous success of such calculations in describing jet production rates, many interesting measurements involve looking inside the jets to unravel their structure. Such measurements normally require fixing a resolution parameter whose size is much smaller than the typical energy of the jets. In such situations, a naive application of QCD perturbation theory leads, in general, to series that are poorly convergent. This is due to the appearance of large logarithms of two widely separated energy scales at all orders in perturbative expansions. In this regime, multiple soft and collinear branchings become relevant and one can use the universality of splitting functions to obtain approximate predictions for interesting jet observables, either through analytical techniques (resummation) or through numerical simulations (the so-called ‘parton-shower’ event generators). The relevant features of both approaches will be discussed in section 3.3. The final aspect that

needs to be discussed is the fact that jets are made of hadrons, not of quarks and gluons. It is legitimate therefore to ask the question: given a prediction for a jet observable in terms of quarks and gluons, will this be close to what we measure experimentally? In other words, what is the effect of phenomena, such as hadronisation, which are beyond the domain of perturbative QCD? It is not possible to give a mathematically rigorous formulation of the problem. Nevertheless, it is possible to build realistic phenomenological models that, if successful in describing data, give some insight on the dynamics of intrinsically non-perturbative phenomena. Their implications for jet physics will be discussed in section 3.4.

3.2 Fixed-order QCD calculations

In this section we discuss the main theoretical techniques used for fixed-order QCD calculations. These are predictions that are truncated at a given order in the QCD coupling α_s . Before discussing the general features of fixed-order calculations, we discuss some elementary examples which, however, contain the relevant issues of such calculations.

3.2.1 Leading-order calculations

Jet rates in e^+e^- annihilation. We consider e^+e^- collisions, in particular events containing hadrons in the final state. Most such events are characterised by the presence of two jets that are quasi-back-to-back, i.e. point in opposite directions. They originate from the production of a quark and an antiquark, which undergo several collinear splittings and then hadronisation. A relevant fraction of events (around 10–20%) is characterised by the presence of three energetic and well-separated jets. Here we wish to quantify this fraction. First, QCD tells us that these events are due to the emission of a hard gluon from the original quark–antiquark pair. Therefore, what we have to do is to first compute the probability for such an emission to occur, differential in suitable kinematic variables spanning the phase space of the emitted gluon. This is achieved by computing two contributions, represented pictorially by the two Feynman diagrams of figure 3.2. Their sum gives the quantum mechanical amplitude for the process under consideration, at the lowest order in QCD perturbation theory. This order is called the leading order (LO). The obtained amplitude has to be squared and suitably integrated over all

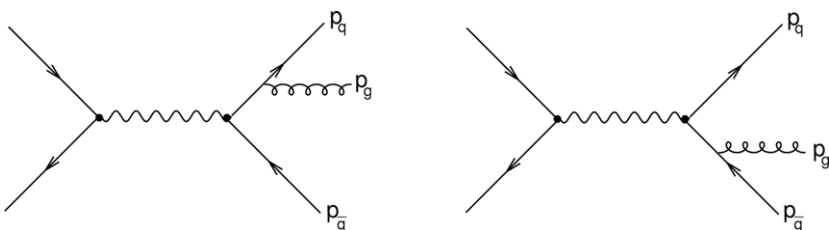


Figure 3.2. The two Feynman diagrams that give the quantum mechanical amplitude for $e^+e^- \rightarrow 3$ jets at the lowest order in QCD perturbation theory. The two lines with an arrow on the left-hand side of each diagram represent the incoming electron and positron, while the internal wavy line represents the sum of the contributions of all vector bosons (here a photon and a Z) that can mediate the interaction [1, 2].

possible values of the momenta in the final state, according to a Lorentz-invariant measure, which is known as multi-particle phase space. Denoting by p_q , $p_{\bar{q}}$ and p_g the momenta of the quark, anti-quark and gluon, respectively, it is customary to introduce the kinematic variables

$$x_q = \frac{2(p_q q)}{Q^2}, \quad x_{\bar{q}} = \frac{2(p_{\bar{q}} q)}{Q^2}, \quad q = p_q + p_{\bar{q}} + p_g, \quad Q^2 \equiv q^2, \quad (3.8)$$

with $Q = \sqrt{s}$ the centre-of-mass energy of the e^+e^- collision. One can then compute the differential cross section in x_q and $x_{\bar{q}}$, normalised to the total cross section σ for the process $e^+e^- \rightarrow \text{hadrons}$ [1, 2]:

$$\frac{1}{\sigma} \frac{d\sigma}{dx_q dx_{\bar{q}}} = C_F \frac{\alpha_s}{2\pi} \frac{x_q^2 + x_{\bar{q}}^2}{(1 - x_q)(1 - x_{\bar{q}})}. \quad (3.9)$$

What is the physical interpretation of the kinematic variables x_q and $x_{\bar{q}}$? From basic kinematics considerations based on momentum conservation one obtains

$$1 - x_q = \frac{(p_{\bar{q}} + p_g)^2}{Q^2}, \quad 1 - x_{\bar{q}} = \frac{(p_q + p_g)^2}{Q^2}, \quad x_q + x_{\bar{q}} - 1 = \frac{(p_q + p_{\bar{q}})^2}{Q^2}. \quad (3.10)$$

As expected, the differential cross section in equation (3.9) is singular when p_g is collinear to p_q ($x_{\bar{q}} \rightarrow 1$) or to $p_{\bar{q}}$ ($x_q \rightarrow 1$), or when p_g becomes soft (both x_q and $x_{\bar{q}}$ tend to 1). To compute the fraction of events in which three jets are observed, the so-called three-jet rate, one needs a variable that discriminates between two- and three-jet events. For instance, we can cluster events into jets using the JADE algorithm described in section 2.1.2, introduce a jet resolution y_{cut} and say we have three jets whenever $y_3 > y_{\text{cut}}$. In this case $y_3 = \min[1 - x_q, 1 - x_{\bar{q}}, x_q + x_{\bar{q}} - 1]$, giving for the three-jet rate

$$R_3(y_{\text{cut}}) = C_F \frac{\alpha_s}{2\pi} \int_0^1 dx_q \int_0^1 dx_{\bar{q}} \frac{x_q^2 + x_{\bar{q}}^2}{(1 - x_q)(1 - x_{\bar{q}})} \Theta(x_q + x_{\bar{q}} - 1) \times \Theta(\min[1 - x_q, 1 - x_{\bar{q}}, x_q + x_{\bar{q}} - 1] - y_{\text{cut}}). \quad (3.11)$$

The region of integration can be visualised in the plot of figure 3.3. There one sees that the regions in which the integrand is singular do not contribute to the three-jet rate. We can then perform safely the integral in (3.11) and obtain

$$R_3(y_{\text{cut}}) = C_F \frac{\alpha_s}{2\pi} \left[2 \ln^2 \left(\frac{y_{\text{cut}}}{1 - y_{\text{cut}}} \right) + (3 - 6y_{\text{cut}}) \ln \left(\frac{y_{\text{cut}}}{1 - 2y_{\text{cut}}} \right) + \frac{5}{2} - \frac{\pi^2}{3} - 6y_{\text{cut}} - \frac{9y_{\text{cut}}^2}{2} + 4 \operatorname{Li}_2 \left(\frac{y_{\text{cut}}}{1 - y_{\text{cut}}} \right) \right] \Theta \left(\frac{1}{3} - y_{\text{cut}} \right). \quad (3.12)$$

For instance, at the LEP1 energy $Q = 91.2$ GeV, using $\alpha_s(Q) = 0.118$, we can evaluate that for $y_{\text{cut}} = 0.1$, around 10% of events will be classified as three-jet events, and this

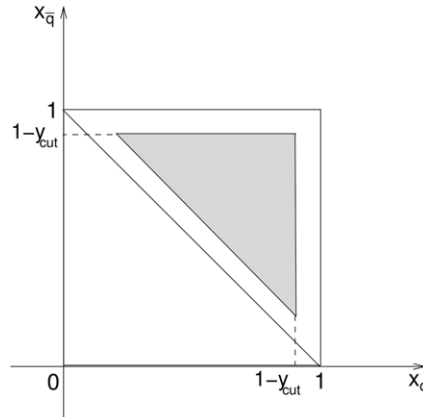


Figure 3.3. Allowed phase space for gluon emission from a $q\bar{q}$ pair in e^+e^- annihilation. The shaded region corresponds to the three-jet selection cut of (3.11).

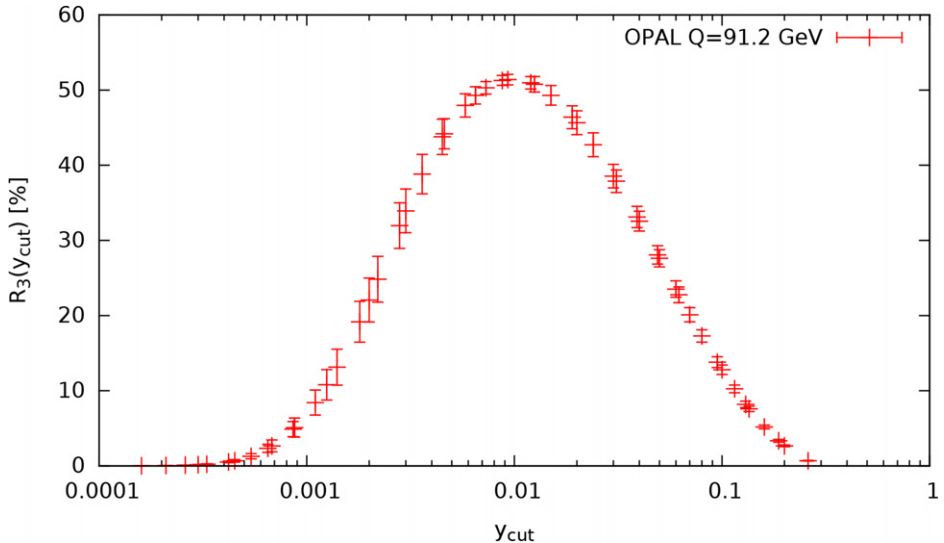


Figure 3.4. The JADE three-jet rate, as measured by the OPAL collaboration at LEP1 [3].

number increases to about 20% for $y_{cut} = 0.05$. This is very close to what is observed in experimental data (see figure 3.4), thus confirming the picture that jet momenta are very close to those of their parent partons. Note that this agreement is obtained by simply performing the lowest order QCD calculation giving rise to a third *partonic* jet, which in this case is just a single energetic gluon. Note also that the agreement breaks down for y_{cut} around 0.01, revealing the need for higher order corrections.

Jet cross sections in hadron collisions. The calculation of jet cross sections in hadron collisions proceeds in a similar fashion, with small modifications due to the presence of hadrons in the initial state. These can again be discussed using an example. Suppose we wish to study Z production plus one additional jet. At the lowest order in QCD

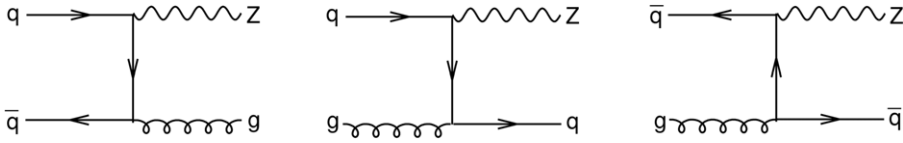


Figure 3.5. Representative Feynman diagrams for the three partonic subprocesses contributing to Z production plus one jet.

perturbation theory this jet can be either a quark or a gluon. What about the initial state? If two hadrons collide at high energy, jet production requires that they break apart and two partons, one extracted from each hadron, give rise to an elementary collision. Therefore, if our final state is Z plus one jet, we need to consider all possible subprocesses in which two partons extracted from the initial-state hadrons collide and produce a Z boson plus an extra parton. There are three partonic subprocesses that can give rise to this final state, $q\bar{q} \rightarrow Zg$, $qg \rightarrow Zq$ and $\bar{q}g \rightarrow Z\bar{q}$, represented pictorially in figure 3.5. The cross section for each subprocess is called the partonic cross section and is normally identified by the incoming partons (i.e. the incoming ‘channel’). Then, the cross section for two hadrons h_A and h_B to produce a Z boson plus an extra parton is the sum of the cross sections for each incoming channel, each one weighted by the probability of finding one incoming parton in hadron h_A and the other in hadron h_B . More precisely, given a hadron h_A with momentum P_A it is possible to define a parton density function (PDF) $f_{a/A}(x_a, \mu_F)$, giving the probability density for finding a parton of type $a = q, \bar{q}, g$ with momentum $p_a = x_a P_A$ inside hadron h_A [1, 2]. The scale μ_F , called the factorisation scale, is an arbitrary energy scale on which each PDF depends and represents the fact that our observable is insensitive to all partons with a transverse momentum (with respect to the beam) below μ_F . If we denote symbolically by $d\sigma_{ab \rightarrow Zc}[p_a, p_b]$ the cross section for the partonic subprocess $ab \rightarrow Zc$, fully differential in the momenta of the final-state particles, the hadronic cross section for Z plus one jet, at the lowest order in QCD perturbation theory, is given by

$$\begin{aligned}
 d\sigma_{h_A h_B \rightarrow Z + \text{jet}} = & \int_0^1 dx_a \int_0^1 dx_b \\
 & \times \left\{ \sum_q \left(f_{q/A}(x_a, \mu_F) f_{\bar{q}/B}(x_b, \mu_F) d\sigma_{q\bar{q} \rightarrow Zg}[x_a P_A, x_b P_B] \right. \right. \\
 & + f_{\bar{q}/A}(x_a, \mu_F) f_{q/B}(x_b, \mu_F) d\sigma_{q\bar{q} \rightarrow Zg}[x_b P_B, x_a P_A] \Big) \\
 & + \sum_q \left(f_{q/A}(x_a, \mu_F) f_{g/B}(x_b, \mu_F) d\sigma_{qg \rightarrow Zg}[x_a P_A, x_b P_B] \right. \\
 & + f_{g/A}(x_a, \mu_F) f_{q/B}(x_b, \mu_F) d\sigma_{qg \rightarrow Zg}[x_b P_B, x_a P_A] \Big) \\
 & + \sum_{\bar{q}} \left(f_{\bar{q}/A}(x_a, \mu_F) f_{g/B}(x_b, \mu_F) d\sigma_{\bar{q}g \rightarrow Zg}[x_a P_A, x_b P_B] \right. \\
 & \left. \left. + f_{g/A}(x_a, \mu_F) f_{\bar{q}/B}(x_b, \mu_F) d\sigma_{\bar{q}g \rightarrow Zg}[x_b P_B, x_a P_A] \right) \right\}. \quad (3.13)
 \end{aligned}$$

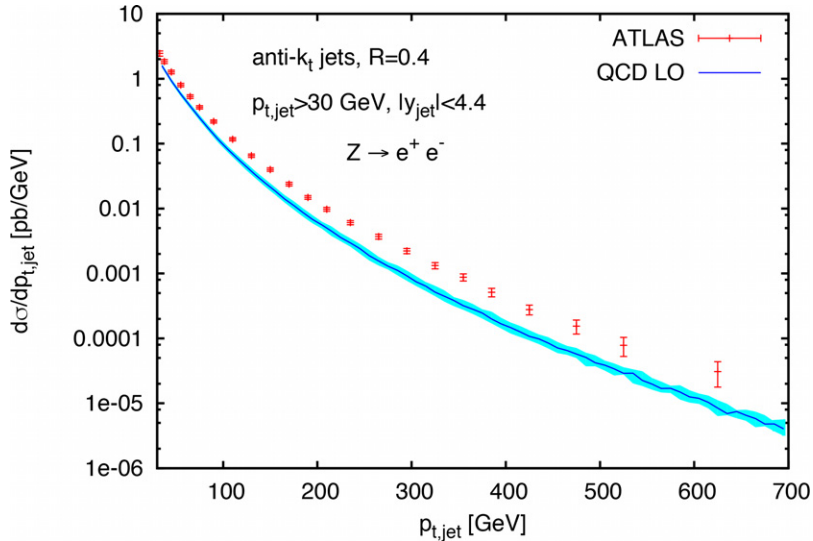


Figure 3.6. The distribution in the transverse momentum of the leading jet in Z plus one events, as measured by the ATLAS collaboration [4], compared to an LO QCD prediction.

In the above expression, the sum over q extends to all the quarks that can be found in the proton at a scale below μ_F . For instance, if μ_F is of the order of some tenths of giga-electron-volts, $q = u, d, c, s, b$. In hadronic collisions, jet cross sections are usually presented as differential in the transverse momentum of the jet with respect to the beam axis $p_{t,jet}$ and of the rapidity of the jet y_{jet} . If we wish to compute the hadronic Z plus one jet cross section, differential in $p_{t,jet}$ and y_{jet} , we need to compute $d\sigma_{ab \rightarrow Zc}[p_a, p_b]/(dp_{t,jet} dy_{jet})$ for each partonic subprocess contributing to our observable and weigh each cross section with the appropriate parton densities. In figure 3.6 we show the result of this procedure. There, the computed $p_{t,jet}$ distribution, obtained by the author using the program MCFM [5], is compared to LHC data by the ATLAS collaboration [4]. The central theoretical prediction is obtained by choosing $\mu_R = \mu_F = \sqrt{p_{t,jet}^2 + M_Z^2}$, with μ_R the so-called ‘renormalisation scale’, i.e. the scale at which the strong coupling is to be evaluated. The band represents an estimate of the theoretical uncertainty, obtained by varying $\mu_R = \mu_F$ by a factor of two around the chosen central value, as such variation produces predictions that differ by a quantity of order α_s^2 from the central one. The PDFs have been chosen from the CT10 set [6]. We note first that the lowest order QCD prediction is close in shape to data, but underestimates them over the whole range of values of $p_{t,jet}$. The discrepancy points to the fact that we do need missing higher orders to accurately describe the leading jet transverse momentum distribution. The arbitrariness in the choice of μ_R and μ_F is a ubiquitous characteristic of QCD calculations in hadron collisions and calls again for the computing of higher orders. The main reason for this is that the centre-of-mass of each partonic collision is not known, so there is no unambiguous way to assign a hard scale to a cross section. One normally chooses a scale that is of the order of the transverse momentum of the jets involved, or of the masses of the

heavy particles produced. The scale we have chosen gives predictions that are close to experimental data, suggesting that higher order corrections are not too big for this choice of scales. Despite their difficulties in describing data, lowest order calculations contain a lot of information on the physics of jet events. For instance, they give approximately the right shape for jet transverse momentum distributions, as well as jet angular correlations. Such observables, as in the case we have analysed, are in general not distorted in a significant way by higher order corrections, unless one looks into very specific configurations of final-state particles. This is why it is extremely important to be able to perform LO calculations in a general, fast and reliable way.

Tree-level techniques. LO calculations such as the ones outlined above are called ‘tree-level’, as opposed to loop calculations, whose representation in terms of Feynman diagrams involves particles forming loops. The latter incorporate quantum corrections to tree-level amplitudes. Comparisons of tree-level calculations with experimental data have lead to an enormous amount of information on the nature of quarks and gluons. For instance, from angular correlations between pairs of jets in four-jet events in e^+e^- annihilation it was possible to confirm the existence of gluon self-interactions. The remarkable success of tree-level calculations pushed QCD practitioners to improve the technical tools for computing tree-level amplitudes with an increasing number of final-state particles (or ‘legs’). On one hand, one needs an automated method to generate and evaluate Feynman diagrams. This can be achieved, for instance, with software packages such as QGRAF [7], FEYNARTS [8], or CALCHEP [9]. On the other hand, one needs techniques to integrate the resulting amplitude squared over the phase space of all particles in the final state. As carried out for the amplitude squared for the emission of a gluon from a $q\bar{q}$ pair, one usually parameterises this phase space in terms of a set of variables that assume values between zero and one, i.e. live inside a multi-dimensional hyper-cube. Actual experimental cuts on final-state particles restrict the range of integration to a multi-dimensional hyper-surface, whose boundary is generally so complicated that the integration cannot be performed using analytical methods, but only with Monte Carlo techniques. These procedures work as follows. One generates a sequence of random numbers (x_1, \dots, x_m) between zero and one. Then, one checks if this point is inside the hyper-surface allowed by experimental cuts. If yes, the product of the amplitude squared and of the phase-space Jakobian is the event weight, which is added to the histograms corresponding to the cross sections one wishes to compute. At the end of the Monte Carlo procedure, the average over the number of generated events of the total weight in each histogram represents an estimator for the physical cross section. Note that each point in the hypercube corresponds to a set of final-state momenta. Therefore, a Monte Carlo integrator for tree-level matrix elements is in fact an event generator, because the sequence of generated random numbers (x_1, \dots, x_m) can be translated into a sequence of final-state momenta (p_1, \dots, p_n) . At this point, one can check directly if the produced final-state momenta pass the required experimental cuts ($y_3 > y_{\text{cut}}$ in our example in e^+e^- annihilation). If so, the event is accepted and its weight is stored in the appropriate histogram. In particular for processes with many legs in the final state, it is essential to speed up this

procedure as much as possible. On one hand, this is achieved by improving the efficiency of event generation. This is done by using adaptive techniques such as importance sampling (see e.g. [10]) or VEGAS [11], which aim to generate the most events where the integrand has the largest value, so as to make the Monte Carlo procedure converge faster to the actual value of the integral we wish to compute. These techniques are implemented in all tree-level event generators currently in use, such as the aforementioned CALCHEP and MADGRAPH [12, 13]. The latter is a fully automated framework that generates tree-level amplitudes for all processes in the Standard Model, as well as some models of yet undiscovered new physics. MADGRAPH is also able to square amplitudes and feed them into a Monte Carlo event generator which provides histograms as requested by the user.

Another important aspect that requires consideration is the fact that the number of Feynman diagrams needed to compute an amplitude with a given number of legs grows factorially with the number of legs. This immediately creates a computational problem if we wish to describe jet events at the LHC, where one expects to see events with a large number of jets. To give an idea, an amplitude for producing eight gluons in the final state results from the sum of more than one million Feynman diagrams! A viable alternative to Feynman diagrams is helicity techniques [14, 15]. Gluons and quarks have two possible states of helicity, the component of the spin along the particle three-momentum. One decomposes the amplitude into all possible helicity states. As a first outcome, one obtains that many of these amplitudes are related, which reduces the number of contributions to be computed. Second, some helicity amplitudes can vanish, which information cannot be easily obtained by just looking at Feynman diagrams. For instance, it can be shown that, if one considers gluons only, amplitudes in which all gluons have the same helicity vanish. This also happens when a single gluon has the opposite helicity with respect to the others. The first non-vanishing gluon amplitudes are the so-called maximally helicity-violating amplitudes, in which two gluons have opposite helicity with respect to all the others. Such amplitudes actually reduce to only one term [16] and more and more compact formulae are being found for all other helicity amplitudes (see e.g. [17–19]). Furthermore, one can exploit the factorisation properties of amplitudes to devise recursion relations that link amplitudes with a different number of particles [20–24]. Discussing these techniques is beyond the scope of this book. They constitute a very important topic in theoretical physics, on which the interested reader can find a review in [25].

3.2.2 Next-to-leading order (NLO) calculations

Jet-rates in e^+e^- annihilation. Let us consider again jet production in e^+e^- annihilation. This time we wish to study the two-jet rate, the fraction of events that will be classified as two jets. We use again the JADE algorithm to cluster final-state particles in two jets. At order α_s we have either zero or one extra gluon in the final state. As a consequence, according to the value of y_{cut} , we have two or three jets. In this situation, the two-jet rate $R_2(y_{\text{cut}})$ is just one minus the three-jet rate $R_3(y_{\text{cut}})$ in (3.11). Although trivial in this case, we wish to investigate how this result arises in fixed-order perturbation theory. Let us define $\sigma(y_{\text{cut}})$, the cross section for events with $y_3 < y_{\text{cut}}$, and σ_{tot} the total cross section

for e^+e^- into hadrons¹. Each of these cross sections has an expansion in powers of α_s , evaluated at a renormalisation scale μ , as follows

$$\sigma = \sigma^{(0)} + \sigma^{(1)} + \sigma^{(2)} + \dots, \quad (3.14)$$

where $\sigma^{(n)}$ is of relative order α_s with respect to $\sigma^{(n-1)}$. In this case, omitting for simplicity interactions mediated by a Z boson, we get

$$\sigma_{\text{tot}}^{(0)} = N_c \frac{4\pi\alpha}{3s} \sum_q Q_q^2, \quad \sigma_{\text{tot}}^{(1)} = \frac{\alpha_s}{\pi} \sigma_{\text{tot}}^{(0)}, \quad (3.15)$$

where the sum extends to all quasi-massless quarks (each carrying electric charge $Q_q e$) that can be produced for a given value of s . For instance, at LEP1 energies, $\sqrt{s} = 91.2$ GeV, hence $q = u, d, c, s, b$. The two-jet rate can be expressed in terms of $\sigma(y_{\text{cut}})$ and σ_{tot} as follows

$$R_2(y_{\text{cut}}) = \frac{\sigma(y_{\text{cut}})}{\sigma_{\text{tot}}} = \frac{\sigma^{(0)}(y_{\text{cut}}) + \sigma^{(1)}(y_{\text{cut}}) + \sigma^{(2)}(y_{\text{cut}}) + \dots}{\sigma_{\text{tot}}^{(0)} + \sigma_{\text{tot}}^{(1)} + \sigma_{\text{tot}}^{(2)} + \dots}. \quad (3.16)$$

Strict fixed order for R_2 requires expanding the denominator, giving

$$R_2(y_{\text{cut}}) = \frac{\sigma^{(0)}(y_{\text{cut}}) + \sigma^{(1)}(y_{\text{cut}}) - \sigma_{\text{tot}}^{(1)} + \dots}{\sigma_{\text{tot}}^{(0)}}. \quad (3.17)$$

At the lowest order, all events have two jets, irrespective of the value of y_{cut} , hence $\sigma^{(0)}(y_{\text{cut}}) = \sigma_{\text{tot}}^{(0)}$. Therefore, at LO $R_2(y_{\text{cut}}) = 1$ as expected. To compute $R_2(y_{\text{cut}})$ at the next perturbative order, the so-called next-to-LO (NLO), we need to know $\sigma^{(1)}(y_{\text{cut}})$ and $\sigma_{\text{tot}}^{(1)}$. In fact, we only have to compute the difference between the two cross sections, which is simply given by $-\sigma_{\text{tot}}^{(0)} R_3(y_{\text{cut}})$, with $R_3(y_{\text{cut}})$ in (3.12). However, for the sake of illustration, we discuss the calculation of $\sigma^{(1)}(y_{\text{cut}})$. The contribution of this cross section from the emission of a gluon from the original quark–antiquark pair is given by

$$\begin{aligned} \sigma_R^{(1)}(y_{\text{cut}}) &= \sigma_{\text{tot}}^{(0)} C_F \frac{\alpha_s}{2\pi} \int_0^1 dx_q \int_0^1 dx_{\bar{q}} \frac{x_q^2 + x_{\bar{q}}^2}{(1-x_q)(1-x_{\bar{q}})} \Theta(x_q + x_{\bar{q}} - 1) \\ &\quad \times \Theta(y_{\text{cut}} - \min[1-x_q, 1-x_{\bar{q}}, x_q + x_{\bar{q}} - 1]). \end{aligned} \quad (3.18)$$

The integral above diverges when x_q and/or $x_{\bar{q}}$ equal one. This divergence occurs when the gluon becomes collinear to the quark ($x_{\bar{q}} \rightarrow 1$), to the antiquark ($x_q \rightarrow 1$) and/or when the gluon is soft ($x_q, x_{\bar{q}} \rightarrow 1$). As explained in the previous chapter, soft and collinear divergences cancel against quantum corrections arising when a gluon is emitted and then reabsorbed by the quark–antiquark pair. Such gluons are called

¹ We compute both cross sections using partons as the final states, keeping in mind that they always turn into hadrons. Corrections induced by hadronisation will be discussed in section 3.4.

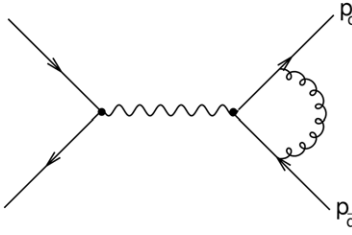


Figure 3.7. Feynman diagram representing virtual corrections to the two-jet rate at order α_s .

‘virtual’ because they do not appear in the final state, as opposed to ‘real’ particles, representing observable objects. We now discuss the explicit cancellation of soft and collinear divergences of the real cross section $\sigma_R^{(1)}(y_{\text{cut}})$ against the contribution of the one-loop diagram in figure 3.7. Soft and collinear divergences are conveniently regularised by computing both real and virtual corrections in a number of space–time dimensions D that slightly differs from four, namely $4 - 2\epsilon$. Virtual corrections are given as analytic functions of ϵ , with poles for $\epsilon \rightarrow 0$. In particular, each soft or collinear divergence gives a $1/\epsilon$ pole. In our case, these virtual corrections are given by $\sigma_V^{(1)}(y_{\text{cut}}) = V(\epsilon)\sigma_{\text{tot}}^{(0)}$ with²

$$V(\epsilon) = \frac{C_F \alpha_s}{2\pi} \left(\frac{4\pi\mu_R^2}{Q^2} \right)^\epsilon \frac{1}{\Gamma(1-\epsilon)} \left(-\frac{2}{\epsilon^2} - \frac{3}{\epsilon} + \pi^2 - 8 + \mathcal{O}(\epsilon) \right). \quad (3.19)$$

Correspondingly, computing the correction due to real emission in (3.18) in $4 - 2\epsilon$ dimensions gives [1, 2]

$$\begin{aligned} \sigma_R^{(1)}(y_{\text{cut}}) &= \sigma_{\text{tot}}^{(0)} C_F \frac{\alpha_s}{2\pi} \left(\frac{4\pi\mu_R^2}{Q^2} \right)^\epsilon \frac{1}{\Gamma(1-\epsilon)} \int_0^1 dx_q \int_0^1 dx_{\bar{q}} \\ &\times \frac{(x_q^2 + x_{\bar{q}}^2) - \epsilon(2 - x_q - x_{\bar{q}})^2}{(1 - x_q)^{1+\epsilon} (1 - x_{\bar{q}})^{1+\epsilon} (x_q + x_{\bar{q}} - 1)^\epsilon} \Theta(x_q + x_{\bar{q}} - 1) \\ &\times \Theta(y_{\text{cut}} - \min[1 - x_q, 1 - x_{\bar{q}}, x_q + x_{\bar{q}} - 1]). \end{aligned} \quad (3.20)$$

This expression has up to two poles in $1/\epsilon$, which can be extracted using the following relation among distributions:

$$\frac{1}{x^{1+\epsilon}} = -\frac{1}{\epsilon} \delta(x) + \sum_{n=0}^{\infty} (-1)^n \epsilon^n \left(\frac{\ln^n x}{x} \right)_+, \quad (3.21)$$

²In addition to infra-red and collinear divergences, virtual corrections might have additional $1/\epsilon$ poles due to ultra-violet divergences, arising when the momenta of the particles in the loops become very large. However, these divergences can be removed via a suitable redefinition of the parameters of the theory, for instance the coupling and the masses. From now on we will thus assume that ultra-violet divergences have been removed from virtual corrections. This procedure, called ‘renormalisation’, ultimately results in the fact that the QCD coupling has to be defined in terms of some renormalisation scheme, and depends on an arbitrary renormalisation scale μ_R .

where the ‘plus’ prescription for distributions is defined through the relation

$$\int_0^1 dx \left(\frac{\ln^n x}{x} \right)_+ f(x) = \int_0^1 dx \left(\frac{\ln^n x}{x} \right) (f(x) - f(0)). \quad (3.22)$$

This gives

$$\sigma_R^{(1)}(y_{\text{cut}}) = \sigma_{\text{tot}}^{(0)} C_F \frac{\alpha_s}{2\pi} \left(\frac{4\pi\mu_R^2}{Q^2} \right)^{\epsilon} \frac{1}{\Gamma(1-\epsilon)} \left(\frac{2}{\epsilon^2} + \frac{3}{\epsilon} + 7 - \frac{2}{3}\pi^2 + F(y_{\text{cut}}) + O(\epsilon) \right) \quad (3.23)$$

with $F(y_{\text{cut}})$ finite for $\epsilon \rightarrow 0$ ³. We see that the poles in the real correction cancel exactly against those in the virtual correction. We can then take the limit $\epsilon \rightarrow 0$, and obtain

$$\sigma^{(1)}(y_{\text{cut}}) = \sigma_V^{(1)}(y_{\text{cut}}) + \sigma_R^{(1)}(y_{\text{cut}}) = \sigma_{\text{tot}}^{(0)} C_F \frac{\alpha_s}{2\pi} \left(\frac{\pi^2}{3} - 1 + F(y_{\text{cut}}) \right). \quad (3.24)$$

Let us consider for a moment the expression for $F(y_{\text{cut}})$.

$$F(y_{\text{cut}}) = \int_0^1 dx_q \int_0^1 dx_{\bar{q}} \frac{x_q^2 + x_{\bar{q}}^2}{(1-x_q)_+(1-x_{\bar{q}})_+} \Theta(x_q + x_{\bar{q}} - 1) \times \Theta(y_{\text{cut}} - \min[1-x_q, 1-x_{\bar{q}}, x_q + x_{\bar{q}} - 1]). \quad (3.25)$$

Expanding all plus distributions we obtain

$$\begin{aligned} F(y_{\text{cut}}) &= \int_0^1 \frac{dx_q}{1-x_q} \int_0^1 \frac{dx_{\bar{q}}}{1-x_{\bar{q}}} \\ &\times \left[(x_q^2 + x_{\bar{q}}^2) \Theta(y_{\text{cut}} - \min[1-x_q, 1-x_{\bar{q}}, x_q + x_{\bar{q}} - 1]) \Theta(x_q + x_{\bar{q}} - 1) \right. \\ &\left. - (1+x_q^2) - (1+x_{\bar{q}}^2) + 2 \right] = \frac{5}{2} - \frac{\pi^2}{3} - R_3(y_{\text{cut}}). \end{aligned} \quad (3.26)$$

After dividing by σ_{tot} and expanding the denominator in powers of α_s the expected result is

$$R_2(y_{\text{cut}}) = 1 - R_3(y_{\text{cut}}).$$

Most importantly, the expression in (3.26) has a clean physical interpretation. The second line in the equation represents the contribution of true events, each with a given value of x_q and $x_{\bar{q}}$, corresponding to some kinematic configuration of the qqg system, whose three-jet resolution is given by $\min[1-x_q, 1-x_{\bar{q}}, x_q + x_{\bar{q}} - 1]$. The last line represents instead the contribution of counter-events, in which the emitted gluon is either collinear to the quark ($x_{\bar{q}} \rightarrow 1$), or to the antiquark ($x_q \rightarrow 1$), or soft

³ Note that, both in $\sigma_V^{(1)}$ and $\sigma_R^{(1)}$, the cross section $\sigma_{\text{tot}}^{(0)}$ is understood to be calculated in $4 - 2\epsilon$ dimensions. However, since singularities cancel exactly between real and virtual corrections, so do the ϵ -dependent pieces of $\sigma_{\text{tot}}^{(0)}$. This is why we have decided not to change notation with respect to the LO case.

(both $x_q, x_{\bar{q}} \rightarrow 1$). In all these cases $y_3 = 0$, so that the counter-events live exactly where the real matrix element becomes singular, with a weight that is equal and opposite. Therefore, in actual calculations, soft and collinear singularities do not cancel against virtual corrections, but against counter-events! Only now can we appreciate the importance of the IRC safety of a jet algorithm. If the algorithm were IRC unsafe, singular real events would not contribute to the two-jet rate and hence they would generate an infinite contribution that does not cancel with that of the corresponding counter-events.

In hadron collisions we meet an additional complication. In fact, the $1/\epsilon$ poles of collinear origin do not cancel completely between real and virtual corrections. The reason is that a collinear emission from one of the initial-state partons takes a sizeable amount of energy from the emitting parton. Therefore, the total available centre-of-mass energy of the elementary partonic collision will be different for real and virtual corrections, causing a non-cancellation of collinear divergences. These divergences can, however, be reabsorbed in a redefinition of PDFs. In practice, one introduces extra universal counter-terms, one for each initial-state parton, proportional to $1/\epsilon$, which cancel against the surviving collinear singularities. One then repeats the same procedure as in e^+e^- annihilation and, for an IRC safe observable, finds a finite result after the addition of real contributions, virtual corrections and the collinear counter-terms.

The procedure outlined above is general enough to be applied to any fixed-order calculation. One maps the phase space for extra-gluon emissions onto a multi-dimensional hyper-cube and for each independent variable performs an expansion in plus distributions as in (3.21). Although general, this procedure has the disadvantage that it has to be performed for each different process. It also requires analytical control over matrix elements, which can be very complicated, especially for a large number of legs. The most popular solution to this problem is to introduce universal counter-terms, which have the same singularities as real matrix elements, but are simpler to handle analytically. In this case, real matrix elements can be computed in four dimensions and their singularities are cancelled by the universal counter-terms. Singularities of virtual corrections cancel against the integral of the counter-terms over their full phase space. The latter needs to be performed analytically in $4 - 2\epsilon$ dimensions. This last requirement restricts the possible choice of counter-terms. In fact, only two procedures are widely used to perform NLO calculations, the first introduced by Frixione, Kunszt and Signer [26], the other by Catani and Seymour [27]. Thanks to subtraction procedures, it is possible to construct NLO Monte Carlo event generators that are fully differential in the momenta of final-state particles. These momenta can then be used to compute physical observables which are stored in the form of histograms.

Interestingly enough, the jet physics we have seen so far provides us with yet another method to eliminate divergences in real matrix elements. Let us consider the expression of the two-jet cross section for small values of y_{cut} :

$$\sigma^{(1)}(y_{\text{cut}}) \simeq \sigma_{\text{tot}}^{(0)} \frac{C_F \alpha_s}{2\pi} \left(-2 \ln^2 \frac{1}{y_{\text{cut}}} + 3 \ln \frac{1}{y_{\text{cut}}} + \frac{\pi^2}{3} - 1 \right). \quad (3.27)$$

We now generate events and compute the value of y_3 . If it is less than y_{cut} we consider the gluon as unresolved, i.e. the event will have the kinematics of a tree-level quark–antiquark event, and its weight will be given by (3.27). If $y_3 > y_{\text{cut}}$, the gluon is resolved and the kinematics will be that of a qqg event. Suppose that we want to compute an observable in which the weight of resolved emissions with $y_3 \gtrsim y_{\text{cut}}$ is binned in the same histogram as unresolved emissions. This happens for instance in the case of σ_{tot} , the total cross section for $e^+e^- \rightarrow \text{hadrons}$. The weight of resolved emissions will have up to two logarithms of y_{cut} , but these logarithms will cancel exactly those coming from unresolved emissions, displayed in (3.27), with a leftover that vanishes as y_{cut} becomes small. Therefore, for small-enough values of y_{cut} , any histogram in which resolved and unresolved emissions contribute as above will be independent of y_{cut} within the numerical precision. This procedure is called phase-space slicing and can be performed with any IRC safe resolution variable that is different from zero when gluon emission occurs. Due to the presence of the vanishing leftover, phase-space slicing is used less than subtraction methods. However, the method has been recently resurrected in the context of next-to-NLO (NNLO) calculations, as explained in section 3.2.3. It is amazing how a basic knowledge of jet physics has already led to a number of important applications!

At the moment, NLO constitutes the state-of-the-art for fixed-order calculations. NLO calculations are usually available in the form of Monte Carlo event generators, producing a finite number of partons in the final state. The most popular are EVENT2 [27] for e^+e^- annihilation, NLOJET++ [28], containing a selected number of processes in e^+e^- and hadron collisions, and MCFM [5], encoding many calculations for relevant processes in hadron colliders, such as W, Z, H and heavy-quark production. NLO calculations constitute essentially a solved problem, the only issue being that of constructing efficient event generators that accommodate a large number of processes and an arbitrary number of emitting legs. Practical limitations are the increasing number of Feynman diagrams that one has to compute and the numerical stability of phase-space integrations. Among the most recent advances in this field, we cannot avoid mentioning the so-called ‘unitarity’ techniques, which solve the problem of computing one-loop amplitudes in a general and fast way. Any one-loop amplitude in QCD can be decomposed into a basis of ‘master’ integrals, called boxes, triangles and bubbles because of their graphical representation in terms of Feynman diagrams for spin-0 particles. Until very recently, such decomposition had to be performed for each Feynman diagram using the Passarino–Veltman technique [29], consisting basically in its expansion into all possible Lorentz-covariant tensor structures. The main advance came from [30], where the coefficients of the decomposition in ‘master’ integrals were related to physical amplitudes, which could be computed numerically using tree-level techniques, such as the helicity formalism discussed in the previous section. This led to a huge simplification in the calculation of virtual diagrams and opened the way for efficient computation of QCD amplitudes with a large number of legs (see [31] for a review on the subject). These techniques made it possible, for instance, to compute for the first time the W production rate plus three jets at NLO [32]. Currently, unitarity techniques are implemented in a variety of computer programs that automatically

generate virtual corrections. The most widely used are BLACKHAT [33], GoSAM [34] and HELAC [35]. BLACKHAT encodes W production up to five jets [36], Z production plus four jets [37] and four-jet production in hadron collisions [38]. In its current implementation, BLACKHAT is in fact responsible for the generation of virtual amplitudes, whereas subtracted real matrix elements with an extra parton are computed with the tree-level generator SHERPA [33]. GoSam is a publicly available package that automatically generates code for one-loop QCD amplitudes. It has been used for a number of multi-leg NLO calculations, including Higgs production plus three jets [39]. In the current version, GoSam can be interfaced with both SHERPA and MADGRAPH. HELAC is a fully contained package for NLO calculations, including the efficient generation of real matrix elements using spinor-helicity amplitudes. One of its most important results is the NLO calculation of the cross section for $t\bar{t}bb$ production [40], which is an important background to Higgs production, when the Higgs decays into a pair of W bosons. Note that $t\bar{t}bb$ has also been computed with Feynman-diagram techniques, using automated reduction of one-loop amplitudes with the Passarino–Veltman method [41]. Unitarity techniques are also embedded in the package aMC@NLO, a fully automated framework which, combined with MADGRAPH, makes it possible to, in principle, compute NLO corrections to an arbitrary process [13]. This package is also able to interface NLO calculation with parton-shower event generators, as explained in section 3.3.

3.2.3 Fixed-order calculations beyond NLO

There are several reasons why one would wish to compute jet cross sections beyond NLO, the most compelling one is clearly that of reducing the uncertainty of theoretical predictions, which for NLO calculations is still around 10–20%. Pushing this accuracy to the percent level requires even higher-order corrections. Notably, such an accuracy is comparable, for instance, to that which will be achieved by LHC experiments for many relevant cross sections at the end of the LHC second run. Furthermore, for many processes, including Higgs production plus jets, NLO corrections are as large as the LO contribution, suggesting a slow convergence of the QCD perturbative series. Improving such convergence requires, in many cases, applying additional cuts to the final-state jets, for instance vetoing jets with transverse momentum above a given threshold. Precise predictions in the presence of tight kinematic cuts nevertheless requires control of higher order corrections. This explains the general interest in NNLO calculations.

The first problem that arises at NNLO is the calculation of two-loop amplitudes. At the moment a basis of two-loop master integrals is not known. Therefore, one has to compute two-loop amplitudes on a case-by-case basis. These are known for all processes involving at most four external particles (see e.g. [42–45]).

The other problem is how to construct the counter-terms to eliminate soft and collinear divergences in real-emission matrix elements. A general subtraction scheme with universal counter-terms has been proposed [46] and all the counter-terms are currently available [47]. Another general subtraction procedure, the so-called antenna subtraction method [48], is available, but the counter-terms have to be computed analytically for each process. The antenna method has been

successfully applied to build a fully exclusive NNLO Monte Carlo event generator for $e^+e^- \rightarrow 3$ jets [49], as well as for hadronic dijet production and Higgs production plus one jet in the incoming gluon–gluon channel [50].

Alternatively, a straightforward, though computationally involved, procedure is to map the $4 - 2\epsilon$ -dimensional phase space for all real emissions into a multi-dimensional hypercube and perform an expansion in powers of ϵ . The construction of counter-terms proceeds as for NLO calculations if all singularities appear in a factorised form. Otherwise, it is possible to systematically split integrals in such a way that in each integral all singularities are factorised. This method is known as sector decomposition and can be applied generally to any integral in any number of dimensions [51, 52]. This is how the first exclusive NNLO Monte Carlo event generators for Higgs [53] and vector boson [54] production in hadron collisions were constructed. An improvement on this line of thought consisted in a general phase-space parametrisation that makes it possible to perform the ϵ expansion only on the singular limits of real-emission contributions [55]. This method has been used recently to obtain a NNLO generator for $t\bar{t}$ production [56] and Higgs production plus one jet [57].

A third alternative is to use a generalisation of the phase-space slicing technique described at NLO. Suppose we have an IRC safe observable V , a function of all final-state parton momenta that vanishes at tree-level and such that the cross section for $V < v$ is known at NNLO, up to corrections that vanish as v goes to zero. In this case, one can split the real-emission phase space so that configurations having $V > v_{\min}$ are resolved, hence giving rise to partons in the final state, whereas configurations with $V < v_{\min}$ are unresolved, their weight being just the analytic cross section for $V < v_{\min}$. A Monte Carlo event generator constructed in this way gives finite cross sections, independent of v_{\min} up to corrections that vanish for $v_{\min} \rightarrow 0$. One of these observables is the transverse momentum p_t of a Higgs or of a vector boson in hadron collisions. Knowledge of the most singular terms of the cross-section for $p_t < p_{t,\min}$ has been used to devise NNLO event generators for Higgs [58] and vector boson [59] production, and has been generalised to the production of any colourless particle in hadron collisions, notably to Higgs plus vector boson [60, 61] and vector–boson pair production [62, 63]. The method has been generalised to events with an arbitrary number of jets using N -jettiness, defined in (2.19), as a cut-off variable [64, 65].

The construction of NNLO Monte Carlo event generators, fully differential in all final-state momenta, is the frontier of QCD higher order calculations. Having many of these calculations available is crucial for exploiting the full potential of the LHC, especially to understand the nature of possible deviations of data from Standard Model predictions.

3.3 Multi-parton branching

Let us consider again the cross section for $y_3 < y_{\text{cut}}$ in (3.18). This cross section contains logarithms of y_{cut} that diverge when y_{cut} becomes vanishingly small. This limit corresponds to having two extremely narrow jets, because events with any extra gluons will be classified as three-jet events and hence discarded. Such logarithms arise from the fact that one restricts the phase space available to real emissions, so

that the cancellation of soft and collinear real and virtual contributions is not complete, but occurs only up to momentum scales of the order of $y_{\text{cut}} Q$. Since both the energy and the angle of the extra gluon are logarithmically divergent, we obtain at most two logarithms of y_{cut} for any power of α_s . Such a divergence for $y_{\text{cut}} \rightarrow 0$ is a signal of the breakdown of perturbation theory, in other words of the fact that considering a single extra gluon is not enough to obtain a physically sensible prediction for $\sigma(y_{\text{cut}})$ when y_{cut} is close to zero.

Notably, in the JADE algorithm, the three-jet resolution is closely related to the invariant mass of each jet. Hence, $y_{\text{cut}} \ll 1$ corresponds to the situation in which we require that the invariant mass of each jet be much less than its energy, which in two-jet events is of the order of the e^+e^- centre-of-mass energy Q . This is a very common situation in many experimental analyses. Suppose for instance that we are looking for a heavy particle (e.g. the Higgs) that decays hadronically, such that its decay products are clustered into the same jet. This happens when the transverse momentum of the jet is much larger than its invariant mass, so that the decay products of the heavy particle receive a huge boost in the jet direction. On top of the jets originating from the decay of the heavy particle, there will be background jets, whose invariant mass is dynamically produced through QCD radiation. It is therefore important to have theoretical tools that are able to tell us not only how likely it is that jets are produced, but also how their inner structure is determined by subsequent parton emissions. This is normally investigated by considering a jet resolution parameter and making it much smaller than the typical energy of the jets. Such analyses are then characterised by two scales, one being the typical energy of jets and the other the small resolution parameter. Another situation characterised by the presence of two energy scales is cross sections with a jet-veto. There are situations in which one rejects events with jets with a transverse momentum above a given threshold. This is carried out, for instance, to suppress background from heavy coloured particles, such as top quarks, which will tend to produce many jets. The two scales here are the transverse momentum threshold and the total invariant mass produced.

The physics of two-scale processes can again be understood from the simple example of the two-jet rate. When $y_{\text{cut}} \ll 1$ we expect to find events with a quark and an antiquark without any accompanying gluons. But this is impossible, because a quark and an antiquark abruptly ripped off the vacuum will experience a huge instantaneous acceleration and, since they possess a colour charge, will radiate gluons. Hence we expect the two-jet rate to be exactly zero for $y_{\text{cut}} = 0$. This behaviour cannot be obtained at any fixed order in perturbation theory, but only after collecting logarithmically enhanced contributions to all orders in the perturbative expansion. A naive resummation of the largest (leading) logarithms at all orders gives, for the JADE two-jet rate,

$$R_2(y_{\text{cut}}) \simeq e^{-\frac{\alpha_s}{\pi} \ln^2 \frac{1}{y_{\text{cut}}}} \rightarrow 0 \quad y_{\text{cut}} \rightarrow 0. \quad (3.28)$$

The configurations that give rise to the exponential in the above equation contain an arbitrary number of soft gluons, collinear either to the quark or to the antiquark. Furthermore, the emissions collinear to each leg are strongly ordered in invariant mass, i.e. if k_1, \dots, k_n are collinear to the quark, we have $(k_1 p_q) \gg (k_2 p_q) \gg \dots \gg (k_n p_q)$.

Last but not least, the emission providing the largest invariant mass has to determine the value of y_3 , i.e. $y_3 Q^2 \sim \max(\max_i\{2(k_i p_{q_i})\}, \max_j\{2(k_j p_{q_j})\})$, with $\{k_i\}$ collinear to the quark and $\{k_j\}$ collinear to the antiquark. Unfortunately, for the JADE algorithm, not all configurations that are strongly ordered in invariant mass have this last property. Hence the resummation of the leading logarithms does not lead to an exponential, and (3.28) is only approximate [66]. In practice, this is reflected in the fact that the JADE algorithm can recombine soft gluons collinear to two different hard legs, as explained in section 2.1.2, and illustrated in figure 2.7. This is the main reason behind QCD practitioners devising ‘exponentiating’ jet algorithms, such as the Durham and Cambridge algorithms. In both cases, resummation of the leading logarithms leads to an exponential similar to that in (3.28).

Exponentials such as the one in (3.28) are called Sudakov form factors and represent the probability of having no emissions above a given scale (represented for instance by a jet resolution). To understand how such exponentials emerge, we will abandon jet rates for a while and discuss a simpler, and theoretically more transparent, example. In e^+e^- it is always possible to divide final-state hadrons in two sets, called hemispheres, such that, at tree-level, the produced quark and antiquark belong to different hemispheres. Let us call a jet the set of all particles belonging to one hemisphere and constrain the invariant mass (squared) of one hemisphere to be less than a given resolution $Q_0^2 \ll Q^2$. Suppose that this jet contains the hard quark originating from the e^+e^- collision and that the quark emits a single collinear gluon. If z is the splitting fraction and θ the opening angle between the final-state quark and the emitted gluon, in the small-angle limit the invariant mass (squared) of the jet is $q^2 \sim z(1-z)\theta^2 Q^2$ (see section 3.1). Therefore, the probability $\Sigma(Q_0^2)$ that the mass of this jet is below Q_0^2 is just one minus the probability that its mass is above Q_0^2 :

$$\begin{aligned} \Sigma(Q_0^2) &\simeq 1 - \int \frac{d\theta^2}{\theta^2} dz P_{qq}(z) \frac{\alpha_s}{2\pi} \Theta[z(1-z)\theta^2 Q^2 - Q_0^2] \\ &= 1 - \int_{Q_0^2}^{Q^2} \frac{dq^2}{q^2} \int dz P_{qq}(z) \frac{\alpha_s}{2\pi}, \end{aligned} \quad (3.29)$$

where we have changed a variable from θ^2 to $q^2 = z(1-z)\theta^2 Q^2$ and used the fact that the invariant mass of a jet cannot exceed Q^2 .

If in a hemisphere we have only collinear splittings with successively decreasing values of q^2 , we have that $\Sigma(Q_0^2)$ is, in a first crude approximation, the probability of having no emissions with $q^2 > Q_0^2$. Let us split then the interval $[Q_0^2, Q^2]$ into n subintervals $[Q_{i-1}^2, Q_i^2]$, with $Q_n^2 = Q^2$. If these intervals are infinitesimally small, only one emission can have q^2 in any given interval and, therefore, the probability of not emitting anything in that interval is just

$$dP(Q_i^2, Q_{i-1}^2) = 1 - \int_{Q_{i-1}^2}^{Q_i^2} \frac{dq^2}{q^2} \int dz P_{qq}(z) \frac{\alpha_s}{2\pi}. \quad (3.30)$$

The total probability of having no emission with $Q_0^2 < q^2 < Q^2$ is the product of the elementary probabilities in (3.30):

$$\Delta_q(Q^2, Q_0^2) = \lim_{n \rightarrow \infty} \prod_{i=1}^n dP(Q_i^2, Q_{i-1}^2) = \exp \left[- \int_{Q_0^2}^{Q^2} \frac{dq^2}{q^2} \int dz P_{qq}(z) \frac{\alpha_s}{2\pi} \right]. \quad (3.31)$$

Working out the correct kinematic boundaries for z , this reduces to a double logarithmic exponent such as the one in (3.28).⁴

Not all configurations in which the mass of a jet is less than Q_0^2 are made up of strongly ordered emissions, so $\Sigma(Q_0^2)$ is only approximately equal to $\Delta_q(Q^2, Q_0^2)$. Corrections can be computed by introducing the jet invariant mass distribution $J_a(Q^2, k^2)$, the probability that a jet initiated by a parton of type $a = q, g$ has an invariant mass k^2 , provided k^2 is less than Q^2 . If we consider the mass of a jet as generated dynamically through subsequent collinear splittings, we observe that there are only two ways to produce a jet with invariant mass k^2 . In fact, either no emissions occur and the invariant mass of the jet is zero, or there is at least one splitting with opening angle θ and splitting fraction z , giving rise to two jets, each with an invariant mass below $q^2 = z(1-z)\theta^2 E^2$, with $E = Q/2$ the energy of the quark and antiquark produced in the hard e^+e^- collision. If a jet is initiated by a quark the various possibilities are illustrated in the figure 3.8. In formulae

$$J_q(Q^2, k^2) = \Delta_q(Q^2, 0) \delta(k^2) + \int_0^{Q^2} \frac{dq^2}{q^2} \Delta_q(Q^2, q^2) \int dz P_{qq}(z) \frac{\alpha_s}{2\pi} \\ \times \int_0^\infty dq_1^2 J_q(q^2, q_1^2) \int_0^\infty dq_2^2 J_g(q^2, q_2^2) \delta(k^2 - q^2 - q_1^2 - q_2^2), \quad (3.32)$$

and an analogous equation holds for J_g . In the above equation we have left unspecified the boundaries of the z integration, since they are irrelevant for the current discussion. We have also assumed that there exists some well-defined procedure (e.g. dimensional regularisation) to regularise the otherwise vanishing Sudakov form factor $\Delta_q(Q^2, 0)$. Also, from now on we will implicitly assume that all Sudakov form factors we will introduce are regularised.

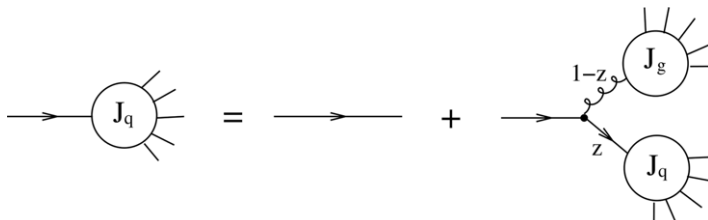


Figure 3.8. Pictorial representation of the evolution equation (3.32).

⁴The correct limiting value for z is obtained by imposing an upper bound on the splitting angle $\theta = q^2/[z(1-z)Q^2] < \theta_{\max} \sim 1$ [66]. Since a double logarithm is obtained only in the soft limit $z \rightarrow 1$, the bound on θ translates into $z \lesssim 1 - q^2/Q^2$.

Integrating this equation with respect to k^2 from 0 to Q_0^2 we obtain

$$\Sigma(Q_0^2) = \Delta_q(Q^2, Q_0^2) \left\{ \Delta_q(Q_0^2, 0) + \int_0^{Q^2} \frac{dq^2}{q^2} \Delta_q(Q_0^2, q^2) \int dz P_{qq}(z) \frac{\alpha_s}{2\pi} \right. \\ \left. \times \int_0^\infty dq_l^2 J_q(q^2, q_l^2) \int_0^\infty dq_g^2 J_g(q^2, q_g^2) \Theta(Q_0^2 - q^2 - q_l^2 - q_g^2) \right\}. \quad (3.33)$$

The expression in brackets has a finite expansion in powers of α_s and, as will be clear later, contains fewer logarithms per power of α_s than the Sudakov form factor $\Delta_q(Q^2, Q_0^2)$, which therefore represents the dominant contribution to $\Sigma(Q_0^2)$.

Given the fact that distributions such as the one in the invariant mass of a jet are ubiquitous in all studies aiming to understand the inner structure of jets, QCD practitioners have tried to describe such observables with the highest possible accuracy. This requires accounting for logarithmically enhanced contributions to all orders in QCD perturbation theory. There are two ways in which this theoretical programme is actually carried out, one is parton-shower event generators, the other is analytical resummations. In the following we will try to explain the philosophy underlying the two methods, highlighting advantages and limitations.

Parton-shower event generators. The equations for J_q , and for J_g , can be solved iteratively. Each iteration consists in a further collinear splitting and corresponds to what is done in parton-shower event generators. These computer programs simulate successive collinear splittings, ordered in some variable q^2 proportional to the splitting opening angle θ^2 (q^2 can be the invariant mass of the parent parton, but it does not need to be so). The i th splitting in the cascade, of type $a \rightarrow bc$ is generated with probability

$$dP_{a \rightarrow bc} \sim \frac{dq^2}{q^2} \Delta_a(q'^2, q^2) dz P_{ba}(z) \frac{\alpha_s}{2\pi} \Theta(q'^2 - q^2), \quad (3.34)$$

with $\Delta(Q^2, Q_0^2)$ the generalized Sudakov form factor

$$\Delta_q(Q^2, Q_0^2) = \exp \left[- \int_{Q_0^2}^{Q^2} \frac{dq^2}{q^2} \int dz P_{qq}(z) \frac{\alpha_s}{2\pi} \right], \\ \Delta_g(Q^2, Q_0^2) = \exp \left[- \int_{Q_0^2}^{Q^2} \frac{dq^2}{q^2} \int dz [P_{gg}(z) + n_f P_{qg}(z)] \frac{\alpha_s}{2\pi} \right], \quad (3.35)$$

where n_f is the number of quasi-massless quark-antiquark pairs a gluon is kinematically allowed to split into.

The different ordering variable is reflected in the boundaries of the z integration, which have been left intentionally unspecified in (3.34). Once q^2 and z have been generated, one can reconstruct the full kinematics of the splitting, i.e. the momenta p_a , p_b and p_c . During this procedure the ordering variable decreases until it reaches a minimum value, where the procedure stops, leaving a set of final-state partons.

These partons are then transformed into final-state hadrons by means of a hadronisation model and these hadrons are used as inputs for the physical observable under consideration. For instance, if we wish to compute the sum of the invariant masses of the two hemispheres in e^+e^- annihilation, we first produce a quark and an anti-quark, let them split subsequently and produce a set of final-state partons and then hadrons. Then, the hadron momenta are separated in two hemispheres and the sum of the invariant masses of the two hemisphere is calculated. A parton shower program also returns the weight of each event, which can then be suitably used to produce histograms. Parton-shower event generators are among the most widely used tools in high-energy physics. Their strengths are twofold:

- they describe correctly an arbitrary number of collinear splittings and
- they produce realistic simulated events, whose final states correspond to actually observed particles.

The last point is particularly important for experimental analyses. The final-state momenta produced by parton-shower event generators can be sent directly to a detector simulator, which returns the signals that would be observed in an actual detector, given the input momenta. It is these reconstructed momenta that constitute the input for physics analyses in high-energy experiments. Therefore, the ideal parton-shower event generator should be able to simulate events with the same probability as they would occur in reality. Of course, this is not possible, not only from a theoretical, but also from a practical point of view. However, current event generators do give a satisfactory description of experimental data. This success relies on several improvements with respect to the naive formulation we have presented above.

Many improvements concern the modification of the splitting probability of (3.34), so as to account for the largest number of logarithmically enhanced contributions. These arise not only when emissions are collinear, but also when they are soft. Soft gluon emission does not admit a simple probabilistic interpretation, in that it depends crucially on the colour structure of all the energetic emitters. One crucial simplification is the fact that a soft gluon emitted from a set of collinear partons sees only the total colour charge of the collinear ensemble rather than the individual colour charges (see e.g. [68], and references therein). This ‘coherence’ property can be accounted for if the generation of collinear splittings is ordered in the splitting angle rather than in the invariant mass of the products of the splitting, as happens for the configuration shown in figure 3.9. This observation is the basis of the so-called ‘coherent branching’ algorithm, implemented in the event generator HERWIG [67, 69, 70]. Another widely used event generator is PYTHIA [71]. Its original version uses the invariant mass as an ordering variable for collinear splittings and corrects the phase space of

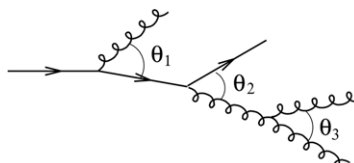


Figure 3.9. Three subsequent collinear splittings, with successively decreasing splitting angle $\theta_1 > \theta_2 > \theta_3$.

emitted partons to account for coherence. Another parton-shower algorithm has been devised which uses the relative transverse momentum of each splitting as an ordering variable [72]. This is the algorithm implemented in the most recent versions of PYTHIA [73]. Other branching algorithms, such as those implemented in HERWIG ++ [74] and SHERPA [75], are similar in philosophy but differ in the coverage of the phase space of the emitted partons.

All the generators we have presented so far start from the splitting probabilities described in section 3.1 and improve them to take into account, as much as possible, all regions of the multi-parton phase space. Another set of algorithms starts from the probability for the emission of soft gluons which, in the limit of a large number of colours (large- N_c), can be written in a closed form [68] and gives rise to a branching equation, which admits an iterative solution. The branching algorithm involves ‘dipoles’ as basic objects. In fact, a soft gluon is emitted by pairs of partons, each pair being a dipole. When the gluon is emitted, a new dipole is formed, which can in turn emit one more gluon, and so on. Since gluons are emitted with the correct probability, coherence is automatically taken into account by such branching algorithms, called ‘dipole’ showers. Dipole showers differ in the way in which they accommodate collinear splittings. The first program implementing these ideas was ARIADNE [76], a widely used tool in e^+e^- annihilation. Dipole showers are now the basis of the Monte Carlo event generator VINCIA [77]. A more ambitious programme of improving parton-shower event generators involves starting from QCD amplitudes, instead of from branching probabilities [78].

Another relevant direction of improvement is in the generation of the hard event. The branching algorithms described so far need as a starting point a given set of hard partons that initiate collinear branchings. In their basic version, all event generators produce these partons at tree-level and all subsequent partons are produced through the branching algorithm. But this does not properly account for events in which new hard jets are produced. One way to deal with this problem is a merging procedure, in which a jet-resolution parameter is introduced [79, 80]. When a new parton is emitted, if its distance (suitably defined) with respect to the other partons is below the resolution parameter, it will be considered as a soft-collinear parton, otherwise it will be considered as a new hard jet and the event will be given the correct tree-level probability for the production of a new hard parton. With this procedure one can merge different jet multiplicities. This is necessary in all analyses in which the signal we are interested in produces high-energy jets. For instance, supersymmetric particles, in particular squarks and gluinos, are expected to produce many jets at high transverse momentum through their decays into coloured particles. Therefore, a correct estimate of multi-jet emission probability is essential for such searches. There are cases in which the particle we are looking for is typically accompanied by at most one extra jet. In this case it is important to precisely determine the rate of production of the particle, i.e. compute it at least at NLO. There are procedures through which it is possible to generate NLO events with a modified weight, so that they can be used as the starting point of a parton-shower event generator. Subsequent partons are produced in such a way that no double counting occurs and that the inclusive sum of all the weights gives the correct cross section at NLO.

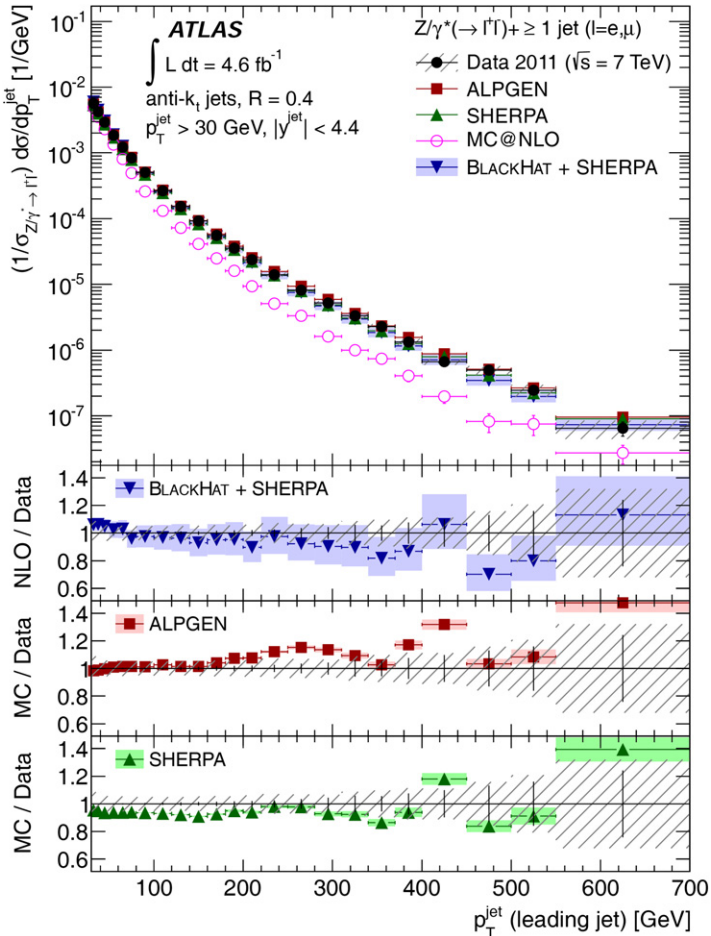


Figure 3.10. The transverse momentum distribution of the leading jet in Z production, as measured by the ATLAS collaboration [4].

Such procedures, called ‘NLO matching’, are implemented in the public programs MC@NLO [81] and POWHEG [82]. An example of the performance of different parton-shower event generators is given in figure 3.10, showing the transverse momentum of the leading jet associated with a Z boson [4]. The data are compared to the NLO program BLACKHAT + SHERPA [33], to the two parton-shower event generators SHERPA [75] and ALPGEN [83], and to MC@NLO [11]. MC@NLO is set up in such a way that the total Z production cross section is correct at NLO. This means that the first jet produced in the branching is correctly produced at LO accuracy, whereas all other jets are produced by the parton shower, which is accurate in the collinear limit only. In fact, the calculation of MC@NLO is basically equivalent to the LO calculation illustrated in section 3.2.1, which explains why it underestimates the data, especially at high transverse momentum. The correct normalisation is accounted for, within theoretical uncertainties, by the NLO calculation provided by BLACKHAT + SHERPA. Note that SHERPA and

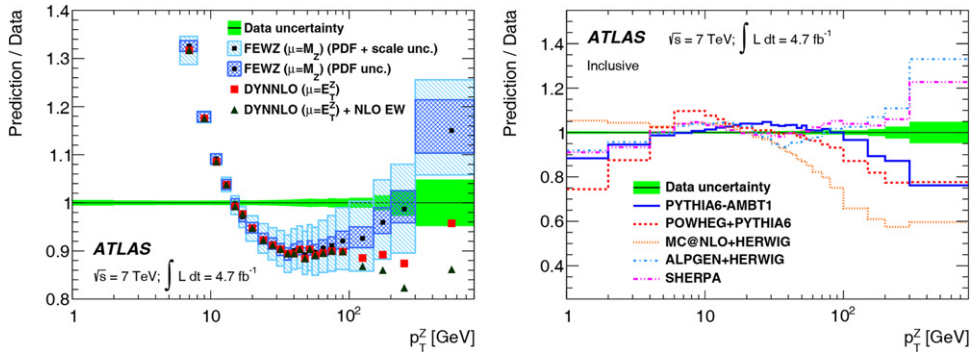


Figure 3.11. Ratio of ATLAS data [84] for the transverse momentum distribution of a Z boson to fixed-order predictions (left) and results obtained from various parton-shower event generators (right).

ALPGEN, implementing the tree-level merging procedures of [79] and [80], respectively, give the correct normalisation despite the fact that they do not have the full virtual corrections, but only the approximate value given by the Sudakov form factor. The message we extract is that, for this process, the main role of virtual corrections is that of cancelling divergences of real-emission contributions, and that leftover finite terms are quite small and contained within theoretical uncertainties. Parton-shower event generators are instead crucial for describing observables that are sensitive to multiple soft and collinear emissions, as is the case for the distribution in the transverse momentum p_T^Z of a Z boson at low p_T^Z . A comparison of fixed-order calculations with experimental data (see figure 3.11, left panel) shows that theory predictions break down at small values of the Z transverse momentum, due to the presence of large logarithms $\ln(M_Z/p_T^Z)$. This is not the case for all parton-shower event generators (see figure 3.11, right panel), although their normalisation does not perfectly agree with data at small values of p_T^Z . Observables such as the Z transverse momentum distributions thus have significant scope in assessing the performance of various approaches to parton showers.

In addition to improvements in branching algorithms and the matching of more and more processes at NLO, more sophisticated parton-shower event generators aim at merging different jet multiplicities in such a way that the rate of each multiplicity is NLO accurate [85, 86]. For instance, through the MiNLO procedure, it became possible to merge for the first time Higgs events with zero and one jet at NLO. Furthermore, with a simple re-weighting of zero-jet events, events generated with MiNLO add up to the total Higgs cross section at NNLO [87]! The MiNLO procedure therefore represents the first example of a parton shower matched to NNLO.

Parton-shower event generators are leaving their traditional role of tools for approximate simulation of collider events, to become more and more precise tools, also being able to predict jet distributions with a reliable normalisation and to account to some extent for their own theoretical uncertainties. This has been possible also because parton-shower generators have incorporated many theoretical advances in analytical calculations. For instance, to achieve NLO accuracy for two different jet multiplicities in Higgs production it was necessary to improve the Sudakov form factor in such a way that logarithmically enhanced contributions in the transverse

momentum of the Higgs were described at very high accuracy. Fortunately, these logarithms were known already from analytical calculations. Therefore, there is an interplay between the accuracy of parton-shower event generators and progress in analytical calculations, which will be discussed in the following.

Analytical resummations. Let us consider again the case of the invariant mass of a hemisphere in e^+e^- annihilation (or of a jet, if we consider an event in hadronic collisions) as a relevant example of a jet observable. We have already seen that the probability $\Sigma(Q_0^2)$ that the jet mass is less than a given resolution Q_0^2 is roughly a Sudakov form factor $\Delta_q(Q^2, Q_0^2)$. The Sudakov form factor is an exponent

$$\Delta_q(Q^2, Q_0^2) \sim e^{-\alpha_s L^2}, \quad L = \ln \frac{Q}{Q_0}, \quad (3.36)$$

that contains at most one more power of the logarithm L than the powers of α_s . In fact, the Sudakov form factor aims at resumming all the so-called ‘leading logarithmic’ (LL) terms, those of the form $\alpha_s^n L^{n+1}$ in the *logarithm* of the mass distribution. Since most events lie in the region $\alpha_s L \sim 1$, LL terms are not enough to constrain jet-observable distributions and better logarithmic accuracy is needed. In the region $\alpha_s L \sim 1$, it is customary to reorganise the perturbative series for $\Sigma(Q_0^2)$ (as well as that for any other jet observable) as follows

$$\Sigma(Q_0^2) = e^{Lg_1(\alpha_s L) + g_2(\alpha_s L) + \alpha_s g_3(\alpha_s L) + \dots}. \quad (3.37)$$

The function g_1 resums all LL terms, of the form $\alpha_s^n L^{n+1}$, g_2 resums next-to-LL (NLL) terms, $\alpha_s^n L^n$, g_3 resums next-to-NLL terms (NNLL), $\alpha_s^n L^{n-1}$, and so on. It is instructive to rewrite the perturbative series in the form

$$\Sigma(Q_0^2) = e^{Lg_1(\alpha_s L)} [G_2(\alpha_s L) + \alpha_s G_3(\alpha_s L) + \dots] \sim e^L [1 + \alpha_s + \dots]. \quad (3.38)$$

For $\alpha_s L \sim 1$ we have that all functions g_i are of order one, so that the only contribution that needs to exponentiate is that arising from g_1 . The other contributions build up a new perturbative series, which starts from the NLL contribution which is of order 1, with higher logarithmic corrections suppressed by more and more powers of the QCD coupling. When it comes to resummation an important clarification is in order. While in fixed-order calculations moving from one order to the next is just a matter of computing more and more Feynman diagrams (which of course might be very complicated from a technical point of view), each logarithmic order already involves the summation of an infinite number of diagrams. Moving from one logarithmic order to the next requires understanding which sets of diagrams, or, better yet, which physical effects, are relevant at that order and computing the corresponding contributions at the necessary accuracy. Here lies a crucial difference between analytic resummations and parton-shower event generators. The latter might contain all the relevant effects to achieve a given logarithmic accuracy, for instance NLL, but their predictions will also contain many subleading contributions, which are basically impossible to disentangle. In contrast, analytic resummations aim to have control of a specific set of logarithmically enhanced contributions, completely neglecting all subleading effects.

As an example, we discuss how NLL can be achieved for the jet mass distribution $\Sigma(Q_0^2)$, and other jet observables related to this quantity. A good starting point [88] is the evolution equation (3.32) which, as we have seen, is able to account for leading logarithms in the invariant mass distribution, but misses relevant NLL contributions arising from soft emissions. As explained in [88, 89], accounting for NLL logarithms in the mass distribution $J_q(Q^2, k^2)$ requires only a small modification of (3.32). In fact, one only needs to change the evolution variable from the invariant mass produced in each splitting to the relative angle θ of each splitting, embedding the fact that coherence of soft QCD radiation is automatically taken into account if collinear splittings occur with decreasing angles. The resulting evolution equation reads

$$\begin{aligned} J_q(Q^2, k^2) = & \tilde{\Delta}_q(Q^2, 0)\delta(k^2) + \int_0^{Q^2} \frac{d\tilde{q}^2}{\tilde{q}^2} \tilde{\Delta}_q(Q^2, \tilde{q}^2) \int_0^1 dz P_{qq}(z) \frac{\alpha_s^{\text{CMW}}[z(1-z)\tilde{q}]}{2\pi} \\ & \times \int_0^\infty dq_1^2 J_q(z^2\tilde{q}^2, q_1^2) \int_0^\infty dq_2^2 J_g((1-z)^2\tilde{q}^2, q_2^2) \\ & \times \delta\left(k^2 - z(1-z)q^2 - \frac{q_1^2}{z} - \frac{q_2^2}{1-z}\right), \end{aligned} \quad (3.39)$$

where $\tilde{q}^2 = \theta^2 Q^2 / 4$ is a dimensionful variant of the splitting angle θ and $\tilde{\Delta}_q$ is the Sudakov form factor corresponding to angular ordering. To ensure NLL accuracy, the QCD coupling has to be evaluated in the physical CMW renormalisation scheme (see footnote 2 for the explanation of what a renormalisation scheme is), related to the widely used $\overline{\text{MS}}$ scheme by

$$\alpha_s^{\text{CMW}} = \alpha_s^{\overline{\text{MS}}} \left(1 + K \frac{\alpha_s^{\overline{\text{MS}}}}{2\pi} \right), \quad K = C_A \left(\frac{67}{18} - \frac{\pi^2}{6} \right) - \frac{10}{9} T_F n_f. \quad (3.40)$$

The iterative solution of (3.39) leads to the coherent branching algorithm that is implemented in the parton-shower generator HERWIG. Note that the Sudakov form factor is different from (3.31) and reads

$$\tilde{\Delta}_q(Q^2, Q_0^2) = \exp \left[- \int_{Q_0^2}^{Q^2} \frac{d\tilde{q}^2}{\tilde{q}^2} \int_0^1 dz P_{qq}(z) \frac{\alpha_s^{\text{CMW}}[z(1-z)\tilde{q}]}{2\pi} \right]. \quad (3.41)$$

For the sake of analytical calculations, the Sudakov form factor is expanded in powers of α_s and the evolution equation for $J_q(Q^2, k^2)$ is rewritten as follows:

$$\begin{aligned} J_q(Q^2, k^2) = & \delta(k^2) + \int_0^{Q^2} \frac{d\tilde{q}^2}{\tilde{q}^2} \int_0^1 dz P_{qq}(z) \frac{\alpha_s^{\text{CMW}}[z(1-z)\tilde{q}]}{2\pi} \\ & \times \left[\int_0^\infty dq_1^2 J_q(z^2\tilde{q}^2, q_1^2) \int_0^\infty dq_2^2 J_g((1-z)^2\tilde{q}^2, q_2^2) \right. \\ & \left. \times \delta\left(k^2 - z(1-z)\tilde{q}^2 - \frac{q_1^2}{z} - \frac{q_2^2}{1-z}\right) - J_q(\tilde{q}^2, k^2) \right]. \end{aligned} \quad (3.42)$$

This is a non-linear equation whose full solution is not needed to compute $J_q(Q^2, k^2)$ at NLL accuracy. In fact, coherence forces the angle of a subsequent branching of the gluon $q_2^2/(1-z)^2$ to be less than \tilde{q}^2 . Therefore, q_2^2 gives a non-negligible contribution to the delta function in (3.42) only for $q_2^2 \simeq (1-z)^2\tilde{q}^2$, which gives a correction of relative order α_s and hence NNLL. Neglecting this correction, one can integrate $J_g((1-z)^2\tilde{q}^2, q_2^2)$ freely over q_2^2 . This integration gives 1, because it corresponds to a total probability, so that in the end we obtain a linear equation. Furthermore, since $P_{qq}(z)$ is singular at $z = 1$, one can set $z \rightarrow 1$ in all smooth functions of z , up to NNLL corrections. One then obtains the linear equation

$$\begin{aligned} J_q(Q^2, k^2) &= \delta(k^2) + \int_0^{Q^2} \frac{d\tilde{q}^2}{\tilde{q}^2} \int_0^1 dz P_{qq}(z) \frac{\alpha_s^{\text{CMW}}[(1-z)\tilde{q}]}{2\pi} \\ &\times \left[J_q(\tilde{q}^2, k^2 - (1-z)\tilde{q}^2) - J_q(\tilde{q}^2, k^2) \right], \end{aligned} \quad (3.43)$$

which can be solved analytically via an integral transform. Note that a parton-shower event generator will not perform these approximations, but will just provide a solution of the full non-linear equation, thus capturing not only all NLL contributions, but also a number of subleading corrections, in general not under control. Whether (3.43) accounts for all NLL contributions to jet mass distributions in e^+e^- annihilation depends on the specific observable we consider. A way to probe the invariant mass of jets is through the two variables thrust and heavy-jet mass. In two-jet events, one minus the thrust is approximately the sum of the (squared) invariant masses of the two hemispheres (normalised to Q^2), whereas the heavy-jet mass is the (squared) invariant mass of the heavier hemisphere (again normalised to Q^2). Both are examples of event-shape variables, because their value gives an idea of the shape of the energy-momentum flow of hadronic events. Let us consider the cumulative distributions $\Sigma(\tau)$, the fraction of events for which one minus the thrust is less than τ . When τ is close to zero, events contain two pencil-like jets, whereas for large τ events are more symmetric, quasi-spherical. In the two-jet limit, i.e. if τ is close to zero, $\Sigma(\tau)$ is related to $J_q(Q^2, k^2)$ as follows

$$\Sigma(\tau) = \int_0^{\tau Q^2} dq_1^2 J_q(Q^2, q_1^2) \int_0^{\tau Q^2} dq_2^2 J_q(Q^2, q_2^2) \Theta(\tau Q^2 - q_1^2 - q_2^2), \quad (3.44)$$

with q_1^2 and q_2^2 the (squared) invariant masses of the two hemispheres. Similarly, for $\Sigma(\rho_H)$, the fraction of events for which the heavy-jet mass is less than ρ_H , we have

$$\Sigma(\rho_H) = \int_0^{\rho_H Q^2} dq_1^2 J_q(Q^2, q_1^2) \int_0^{\rho_H Q^2} dq_2^2 J_q(Q^2, q_2^2) \Theta(\rho_H Q^2 - \max\{q_1^2, q_2^2\}). \quad (3.45)$$

If we consider instead the cumulative distribution in the invariant mass of a single hemisphere, unfortunately (3.43) is not enough to achieve full NLL accuracy. This

is because, in the coherent branching formalism, $J_q(Q^2, k^2)$ accounts for the branchings that occur inside the hemisphere containing the quark. There are, however, configurations in which soft emissions falling into the opposite hemisphere coherently emit a softer gluon that contributes to the mass of the observed hemisphere [90]. For observables such as the single-jet mass, such configurations give an NLL contribution, whereas for the thrust or the heavy-jet mass they give subleading effects. These NLL contributions are called non-global logarithms, because they appear whenever the region in which measurements are performed is restricted. In fact, gluons emitted in the unobserved region have energies that are logarithmically distributed between the jet resolution Q_0 and the hard scale of the process Q , giving rise to single-logarithmic contributions to all orders. For the single-jet mass distribution $\Sigma(\rho)$, the probability that the (squared) invariant mass of one jet is less than ρQ^2 , we obtain

$$\Sigma(\rho) = \int_0^{\rho Q^2} dq^2 J_q(Q^2, q^2) \int_0^{\rho Q} dk S_{q\bar{q}}(Q, k) \Theta(\rho Q^2 - q^2 - kQ), \quad (3.46)$$

where $S_{q\bar{q}}(Q, k)$ embodies the contribution of non-global logarithms. An evolution equation such as (3.43) has been written for the scalar sum of transverse momenta within a jet, which led to the NLL resummation of the total and wide-jet broadenings, two relevant event shapes in e^+e^- annihilation, giving an idea of the width of jets [91, 92]. The distribution in the single-jet broadening is affected by non-global logarithms, and hence cannot be expressed in terms of the distribution in the scalar sum of transverse momenta within a jet.

Non-global logarithms deserve a special mention. First of all, they are single logarithms, i.e. they have a power of α_s for each power of the resummed logarithm. They originate from soft emissions, which cannot be taken into account via a simple probabilistic picture. However, such a picture does exist in the large- N_c limit. In that limit, one can write an evolution equation whose solution provides the resummation of non-global logarithms [93]. The equation was solved first via a Monte Carlo iteration [90, 94] and later through other numerical techniques [95]. Currently, the evolution equation for non-global logarithms has been extended beyond the large- N_c limit [96] and some terms beyond NLL accuracy have been computed [97–100]. However, due to these complications, to ensure that analytic resummation can be performed with the highest possible accuracy, one preferably considers global observables. This is what we will do in the rest of our discussion on resummation.

The limitation of the coherent branching formalism is that it is tied to a probabilistic picture of QCD collinear splitting, which might not be adequate to capture corrections beyond NLL accuracy. A more general analytic approach is based on soft-collinear effective theory (SCET) [101]. In SCET one considers all Feynman diagrams that contribute to a given observable and divides them according to how the loop momenta scale with respect to the physical scales of the problem. For instance, in the case of the thrust distribution the relevant scales

are Q^2 , τQ^2 and $\tau^2 Q^2$. It is then possible to show that, in SCET the thrust distribution for $\tau \ll 1$ can be written as [102]

$$\begin{aligned} \Sigma(\tau) \simeq & H(Q^2, \mu) \int dq_1^2 dq_2^2 dk_s J(q_1^2, \mu) J(q_2^2, \mu) S(k_s, \mu) \\ & \times \Theta(\tau Q^2 - q_1^2 - q_2^2 - k_s Q). \end{aligned} \quad (3.47)$$

The hard function $H(Q^2, \mu)$ contains the contribution of all loop momenta of the order of the e^+e^- centre-of-mass energy Q . This implies that only virtual corrections can contribute to H , because a real emission with a large momentum would give a jet with a large invariant mass, which cannot contribute to $\Sigma(\tau)$ in the two-jet limit. The *jet functions* $J(q_1^2, \mu)$ and $J(q_2^2, \mu)$ contain loop momenta which are energetic, but have a small invariant mass, of order $q_1^2 \sim q_2^2 \sim \tau Q^2$, as is typical for collinear, but energetic, emissions. The *soft function* $S(k_s, \mu)$ contains loop momenta whose components are all small and of order $k_s \sim \tau Q$. There are many other possible scalings of loop momenta, but they all lead to dimensionless integrals, which vanish when evaluated in dimensional regularisation. All these functions, in particular the jet and soft functions contributing to the thrust, are all defined in terms of operators in the effective theory, even beyond perturbation theory, and have a well-defined expansion in powers of the QCD coupling. Furthermore, each function depends on an unphysical scale μ on which the thrust distribution $\Sigma(\tau)$ cannot depend. Taking the derivative with respect to μ gives an equation relating H , J and S , which leads to the emergence of the Sudakov form factor as the solution of a linear differential equation, rather than from probabilistic arguments. Also, each of the three functions satisfies a linear differential equation by itself and this is enough to fully constrain $\Sigma(\tau)$ at all logarithmic orders. SCET has been successfully applied to many final-state observables in e^+e^- and hadron–hadron collisions, reaching an accuracy that is difficult to obtain with other approaches. This is also due to the fact that evolution equations for hard, soft and jet functions can be studied separately and in some cases the results can be already found in the literature from unrelated studies. For instance, the hard function $H(Q^2, \mu)$ is just the absolute value squared of the on-shell quark form factor, a well-known object in quantum field theory which has been computed up to three orders in α_s [103, 104] and its functional form is known at all orders [105]. Also, the evolution equations for H , J and S all involve the so-called ‘cusp anomalous dimension’, which is another important object in quantum field theory, whose expansion in powers of the QCD coupling is known up to three orders [106]. Despite this success, SCET has some limitations. First, the relevant expansion modes, and hence the needed effective theory, might differ from one observable to the next and at the moment there exists no general criterion that associates an effective theory to a given observable. Second, the observable constraint, e.g. $\Theta(\tau Q^2 - q_1^2 - q_2^2 - k_s Q)$ should not correlate the relevant modes in a non-trivial way, which would make an analytic treatment of the observable infeasible.

The main limitation posed by evolution equations is that physical observables need to be written in some factorised form. In fact, this is not the case for most

final-state observables, especially for jet rates, which result from algorithmic procedures involving all final-state particles in a highly non-trivial way. However, the physics content of the coherent branching equations needed to achieve NLL resummation for the thrust and jet broadening distributions is that relevant QCD emissions at that accuracy are just soft and collinear gluons widely separated in angle. These gluons are independently emitted from the hard quark and antiquark produced in e^+e^- annihilation and subsequent collinear splittings of the emitted gluons contribute beyond NLL accuracy. This corresponds to integrating away $J_g((1-z)^2\tilde{q}^2, q_2^2)$ in (3.42). Consider now a generic final-state observable $V(\{\tilde{p}\}, k_1, \dots, k_n)$ in e^+e^- annihilation, where $\{\tilde{p}\}$ represents the primary quark and antiquark produced in the collision and k_1, \dots, k_n being secondary partons. Suppose also that V vanishes when no emissions are present, i.e. $V(\{\tilde{p}\}) = 0$. If relevant emissions at NLL accuracy are the same as for the thrust and jet broadening, it is possible to write a general NLL resummation formula for $\Sigma(v)$, the fraction of events with $V(\{\tilde{p}\}, k_1, \dots, k_n) < v$.

$$\Sigma(v) = e^{-\int [dk]M^2(k)} \sum_{n=0}^{\infty} \frac{1}{n!} \int \prod_{i=1}^n [dk_i] M^2(k_i) \Theta(v - V(\{\tilde{p}\}, k_1, \dots, k_n)), \quad (3.48)$$

where $M^2(k_i)$ is an effective emission probability for soft and/or collinear gluons widely separated in angle and $[dk_i]$ a suitable Lorentz invariant phase space for gluon k_i . The fact that for suitable observables $\Sigma(v)$ can be written in a closed form makes it possible to compute it with a Monte Carlo integration procedure, even if the observable cannot be handled analytically [107]. In fact, one just needs to know the function $V(\{\tilde{p}\}, k_1, \dots, k_n)$ for an arbitrary set of final-state momenta. It is also possible, given $V(\{\tilde{p}\}, k_1, \dots, k_n)$, to establish if (3.48) is enough to obtain an NLL resummation for $\Sigma(v)$. The set of requirements that $V(\{\tilde{p}\}, k_1, \dots, k_n)$ needs to satisfy are known as ‘continuous globalness’ (a stronger condition than globalness) and ‘recursive IRC (rIRC) safety’ [108]. These are more restrictive constraints with respect to standard IRC safety and are related to the scaling behaviour of $V(\{\tilde{p}\}, k_1, \dots, k_n)$ in the presence of multiple soft and/or collinear emissions. It is possible to show that the NLL resummation for any continuously global rIRC final-state observable is given by a general master formula, obtained from (3.48), whose ingredients can be extracted by evaluating $V(\{\tilde{p}\}, k_1, \dots, k_n)$ with suitable ensembles of soft and/or collinear emissions. This evaluation can be efficiently performed by a computer and is encoded in the numerical code Computer Automated Expert Semi-Analytical Resummer (CAESAR) [109]. The CAESAR approach is very effective in handling contributions arising from multiple soft-collinear emissions. These are computed through a simplified parton-shower event generator, which produces an arbitrary number of soft and collinear emissions and feeds them into a computer subroutine that computes $V(\{\tilde{p}\}, k_1, \dots, k_n)$. However, the cancellation of infrared and collinear singularities between real and virtual corrections has to be performed analytically. At NLL accuracy, this simply leads to the exponent $e^{-\int [dk]M^2(k)}$ in (3.48). The exponent contains virtual corrections, and unresolved real emissions, which give no contribution to $V(\{\tilde{p}\}, k_1, \dots, k_n)$ (for instance, because they are too soft) and is in fact the Sudakov form factor for the observable V . From NNLL

accuracy onwards, a general expression for the all-order contribution of virtual corrections and unresolved emissions is not known and one has to work out the cancellation of IRC singularities for each observable. Once this is done, however, all NNLL corrections induced by real radiation can be computed with Monte Carlo event generators. This has been achieved for event shapes for which cancellation of singularities between virtual and real corrections works in the same way as for the thrust and jet broadening [109]. A clear advantage of having a resummation formula in terms of actual emissions rather than as the solution of a differential equation is that one has a clear picture of what approximations on the multi-parton emission probabilities and phase space are needed to achieve a given logarithmic accuracy. This is important to establish the logarithmic accuracy of parton-shower event generators: one needs to check the approximations according to which partons are produced by the corresponding branching algorithm. This is one of the benefits of the cross-talk between analytic resummation and the development of parton shower event generators.

3.4 At the boundary of perturbative QCD

The theoretical methods employed to describe the jet observables introduced in the previous sections consider jets as being made up of quarks and gluons, the basic degrees of freedom of QCD, rather than hadrons, as is the case in reality. The appropriateness of a perturbative QCD analysis of jet properties depends crucially on the observables we consider. If we ask how many hadrons of a given type (e.g. pions or protons) we will observe on average in a jet of a given transverse momentum, it is obvious that the answer will depend on the details of the hadronisation process. However, if we look at the distribution in the transverse momentum of a jet originating from an energetic quark, we expect that the reshuffling of final-state momenta due to hadronisation will not dramatically change the total transverse momentum of the jet. Let us make this argument more rigorous. Suppose we have a generic cross section σ that depends on a typical scale Q , (e.g. the transverse momentum of a jet) and on the masses of the quarks involved m_q . Collinear divergences are regulated by the quark masses and we also introduce a fake gluon mass m_g to regulate soft divergences. For $Q^2 \gg m_q^2, m_g^2$, the dependence of σ on the relevant scales involved is given by

$$\sigma(\alpha_s(\mu), \mu^2, Q^2, m_i^2) = \frac{1}{Q^2} F\left(\frac{Q^2}{\mu^2}, \frac{m_i^2}{\mu^2}, \alpha_s(\mu)\right), \quad i = q, g. \quad (3.49)$$

If soft and collinear divergences cancel completely between real and virtual corrections, then this cross section can be computed in the limit in which all masses are set to zero. Hence we can write [110]

$$F\left(\alpha_s(\mu), \frac{Q^2}{\mu^2}, \frac{m_i^2}{\mu^2}\right) = \hat{F}\left(\alpha_s(\mu), \frac{Q^2}{\mu^2}, 0\right) \left[1 + \mathcal{O}\left(\frac{m_i^2}{Q^2}\right)^p\right], \quad (3.50)$$

where p is a positive power. This means that when $Q^2 \gg m_q^2, m_g^2$, it is enough to compute \hat{F} , since what we are losing are power-suppressed corrections. It is these corrections that account for hadronisation effects, so we can say that, when the typical hard scale of a process is much bigger than small quark and gluon masses, hadronic cross sections can simply be computed using the quark–gluon language of perturbative QCD. Also, when Q is extremely large, radiation from hard partons is forced to be extremely collimated, hence we can safely assume that one jet is obtained per hard parton produced.

For moderate energies, however, hadronisation corrections do play a role and have to be quantified. This is normally achieved through hadronisation models available in parton-shower event generators. These models are phenomenological tools, encoding heuristic, though not simplistic, ideas of how hadronisation works. They contain many parameters, which have to be determined by comparing predictions for suitable observables, sensitive to hadronisation (such as hadron multiplicities inside jets, event-shape mean values and distributions), to experimental data. Then, hadronisation corrections to IRC safe observables (e.g. jet cross sections) can be evaluated by simply taking the ratio of the predictions of a parton-shower event generator at hadron level and at parton level (with hadronisation switched off). Such a procedure is not inappropriate, in that the fact that hadronisation corrections are power-suppressed suggests that the phenomena underlying the formation of hadrons are largely decoupled from the energetic parton branching giving rise to the energy–momentum pattern of jets.

Local parton–hadron duality. It is possible to estimate the size of hadronisation corrections with analytical methods. Totally inclusive quantities, such as the total cross section $e^+e^- \rightarrow \text{hadrons}$, can be expressed in terms of Fourier transforms of the expectation values of products of operators in quantum field theory, for instance

$$\sigma(e^+e^- \rightarrow \text{hadrons}) \sim \int d^4x e^{iqx} \langle 0 | J(x) \cdot J(0) | 0 \rangle, \quad (3.51)$$

where the four-vector $J(x)$ is a local operator representing the conserved quark electromagnetic current and q is the total four-momentum of the incoming e^+e^- pair. The quantity in (3.51) is a function of the invariant $Q^2 = q^2$, and can be expanded in inverse powers of Q^2 . The leading term in $1/Q^2$, the so-called ‘leading-twist’ term, gives precisely what we would obtain in massless QCD. Higher powers of $1/Q^2$, called ‘higher-twist’ terms, can be systematically accounted for in this expansion and consist of products of coefficients, calculable using the quark–gluon language, and expectation values of local operators, which have to be extracted from data or computed with non-perturbative methods, e.g. discretising QCD on a lattice. Note that this expansion, called operator product expansion (OPE), is rigorously defined for $Q^2 < 0$ and must necessarily be truncated at a given order. Its analytic continuation into the physical region $Q^2 > 0$ misses completely non-perturbative effects such as the production of hadronic resonances, but captures very well the

continuum background on top of them. This analytic continuation corresponds physically to the assumption that at high energies hadronic physics is mostly accounted for by the dynamics of quarks and gluons, with hadronisation giving just a reshuffling of parton momenta into the observed hadrons. This hypothesis is known as local parton–hadron duality (LPHD) and is assumed to hold also for non-inclusive observables for which an OPE does not exist (see e.g. [111, 112]). LPHD is the philosophy underlying parton-shower event generators, which produce quarks and gluons until a cut-off value in the evolution variable is reached, after which a hadronisation model transforms all produced partons into hadrons [67, 113].

Hadronisation corrections through an effective coupling. An interesting development of LPHD is the idea of describing hadronisation through the notion of a QCD effective coupling at low momentum scales [114]. There are observables such as event-shape distributions in which leading hadronisation corrections are due to soft hadrons, at large angles with respect to the leading jets. Despite the fact that, at each order in perturbation theory, gluons emitted in this kinematic region give a very small contribution, it turns out that the resulting perturbative series is factorially divergent. To overcome this problem, introducing a merging scale μ_I has been suggested, such that only emissions with energy above μ_I are treated perturbatively and in fact they lead to a convergent perturbative expansion [115, 116]. Emissions with energies below μ_I are treated as soft hadrons, having the same emission probability as soft gluons, except for the coupling which is a non-perturbative extension of the CMW coupling introduced in (3.39). For instance, consider a generic event-shape $V(\{\tilde{p}\}, k_1, \dots, k_n)$ in e^+e^- annihilation, to which a non-perturbative emission at large angles contributes by an amount

$$\delta V(\{\tilde{p}\}, k) \simeq (1 - z)f_V(\theta), \quad (3.52)$$

with $(1 - z)Q/2$ the energy of the non-perturbative gluon. In the CAESAR approach, the contribution of this emission to the probability $\Sigma(v)$ that $V(\{\tilde{p}\}, k_1, \dots, k_n) < v$ is given by

$$\begin{aligned} \delta\Sigma(v) \simeq 2C_F \int_0^1 \frac{dz}{1 - z} \frac{\alpha_s^{\text{NP}}[(1 - z)\theta Q]}{\pi} \int \frac{d\theta^2}{\theta^2} \Theta(\mu_I - (1 - z)\theta Q) \\ \times e^{-\int [dk]M^2(k)} \sum_{n=0}^{\infty} \frac{1}{n!} \int \prod_{i=1}^n [dk_i] M^2(k_i) \\ \times [\Theta(v - V(\{\tilde{p}\}, k_1, \dots, k_n)) - \delta V(\{\tilde{p}\}, k)) - \Theta(v - V(\{\tilde{p}\}, k_1, \dots, k_n))], \end{aligned} \quad (3.53)$$

where the difference in step functions represents the fact that soft emission k can be either real or virtual. Note that all emissions except k have transverse momenta much bigger than μ_I and can thus be considered as quarks and gluons. Since δV is small with respect to v , one can expand the theta function and obtain

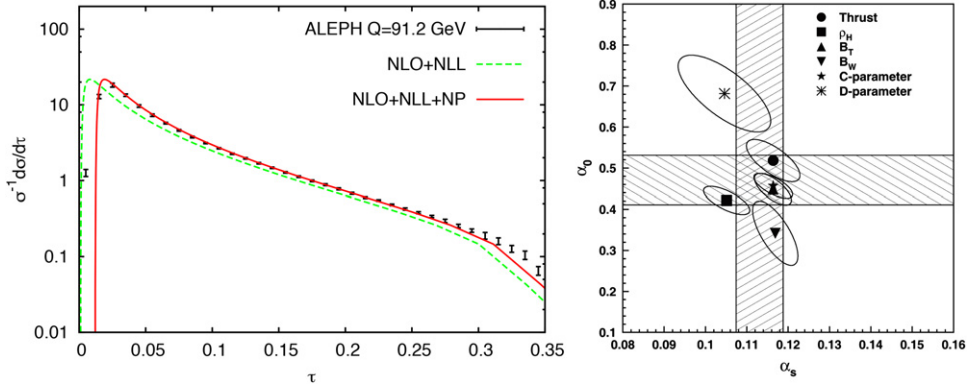


Figure 3.12. Left: theoretical predictions for the distribution in one minus the thrust τ without [89] (green, dashed) and with (solid, red) hadronisation corrections [115], compared to ALEPH data [117]. The corresponding theoretical predictions have been matched by the author to exact NLO provided by the program EVENT2 [27]. Right: simultaneous fit of $\alpha_s(M_Z)$ and $\alpha_0(2 \text{ GeV})$ performed by the L3 collaboration [118].

$$\begin{aligned} \delta\Sigma(v) \simeq & -2C_F \int_0^1 \frac{dz}{1-z} \frac{\alpha_s^{\text{NP}}[(1-z)\theta Q]}{\pi} \int \frac{d\theta^2}{\theta^2} \delta V(\{\tilde{p}\}, k) \Theta(\mu_I - (1-z)\theta Q) \\ & \times e^{-\int [dk] M^2(k)} \sum_{n=0}^{\infty} \frac{1}{n!} \int \prod_{i=1}^n [dk_i] M^2(k_i) \delta(v - V(\{\tilde{p}\}, k_1, \dots k_n)) \\ & \equiv -\langle \delta V \rangle_{\text{NP}} \frac{d\Sigma(v)}{dv}. \end{aligned} \quad (3.54)$$

The contribution above represents the leading hadronisation correction to $\Sigma(v)$, including which we have

$$\Sigma(v) \rightarrow \Sigma(v) - \langle \delta V \rangle_{\text{NP}} \frac{d\Sigma(v)}{dv} \simeq \Sigma(v - \langle \delta V \rangle_{\text{NP}}). \quad (3.55)$$

Since $\langle \delta V \rangle_{\text{NP}} \sim \mu_I/Q$, hadronisation corrections to such final-state observables amount in a power-suppressed shift in the corresponding distributions. This is actually observed in data, as illustrated for instance in the left-hand panel of figure 3.12. There one sees that the perturbative resummed distribution for one minus the thrust τ (the green dashed curve) has a shape that is roughly consistent with the data, but it needs to be shifted in order to be able to describe the ALEPH data (see the red curve, containing leading hadronisation corrections). The fact that non-perturbative corrections are expressed in terms of the same integral of the universal coupling α_s^{NP} makes it possible to extract this non-perturbative parameter, known as $\alpha_0(\mu_I)$ from the data. This parameter is defined from the relation [115]

$$A(\mu_I) \equiv \int_0^{\mu_I} dk \frac{\alpha_s^{\text{NP}}(k)}{\pi} = \frac{\mu_I}{\pi} \left[\alpha_0(\mu_I) - \alpha_s(Q) + \mathcal{O}(\alpha_s^2) \right]. \quad (3.56)$$

What is actually performed are simultaneous fits of $\alpha_0(\mu_t)$ and $\alpha_s(M_Z)$. These fits, an example of which is shown in the right-hand panel of figure 3.12, shows that α_0 is approximately universal, thus confirming the appropriateness of the effective coupling approach to describe hadronisation corrections to jet observables. It has to be noted that other approaches give the same result: leading power-suppressed corrections to event shapes are of order $1/Q$ and can be expressed in terms of a single universal parameter. Also, at the moment the form of hadronisation corrections to jet rates is not known. Phenomenological studies with parton-shower event generators show that they are much smaller than those of event shapes. This is one of the reasons why defining observables in terms of jets is preferred to using individual hadrons.

Underlying event. In hadron collisions there is an additional source of non-perturbative corrections, the so-called underlying event (UE). When two hadrons collide at high energies they break apart and a single parton is extracted out of each of them. The remnants have themselves a colour charge and can therefore interact strongly. A rare occurrence is a secondary hard scattering of two partons from the remnants. This is called double-parton scattering, and gives rise to a secondary hard event, for instance the production of two or more jets with high transverse momenta. The most likely situation is that low-energy collisions occur, producing a cloud of low transverse-momentum hadrons, with a distribution that is roughly uniform in rapidity and azimuth. In practice, it is difficult to distinguish between the two situations, because there might be more than one secondary collision and some secondary collisions will produce such low transverse momentum jets that the resulting event cannot be distinguished from a uniform hadron background. This is why many parton-shower event generators, e.g. PYTHIA, model the UE as multi-parton interactions (MPI), where proton remnants can undergo one or more secondary collisions. The default version of HERWIG produces soft hadrons uniformly in rapidity and azimuth [69, 70]. However, since this does not account properly for hadron production in the presence of the UE, the package JIMMY, which encodes a model for MPI, has been devised to be interfaced with HERWIG [119]. The main quantity one is interested in when studying jet physics is ρ , the average transverse momentum per unit rapidity and unit azimuth produced by the UE. How this quantity can be extracted from data, and how its fluctuations from one event to the other can be assessed, are still the subject of debate and beyond the scope of this book [120, 121]. An analogous quantity ρ_{PU} represents the average transverse momentum per unit rapidity and unit azimuth produced by pile-up (PU) events, secondary hadronic collisions that occur at each beam crossing. UE and PU are unavoidable in hadronic collisions and contaminate any jet observable. It is therefore important to quantify how much they affect physical observables and find strategies to assess, and hopefully subtract, their contribution. The method of jet areas makes it possible to perform this task for quantities related to the total transverse momentum of jets, as discussed in section 2.1.3. Further methods to eliminate a uniform background will be discussed in the next chapter, dealing with how jets can be exploited to discover new particles.

Bibliography

- [1] Ellis R K, Stirling W J and Webber B R 1996 *Camb. Monogr. Part. Phys. Nucl. Phys. Cosmol.* **8** 1
- [2] Dissertori G, Knowles I G and Schmelling M 2009 *Quantum Chromodynamics (International Series of Monographs on Physics* vol 17) (Oxford: Oxford University Press)
- [3] Pfeifenschneider P *et al* (ADE and OPAL Collaborations) 2000 *Eur. Phys. J. C* **17** 19
- [4] Aad G *et al* (ATLAS Collaboration) 2013 *J. High Energy Phys.* JHEP07(2003)032
- [5] <http://mcfm.fnal.gov>
- [6] Lai H L, Guzzi M, Huston J, Li Z, Nadolsky P M, Pumplin J and Yuan C-P 2010 *Phys. Rev. D* **82** 074024
- [7] Nogueira P 1993 *J. Comput. Phys.* **105** 279
- [8] Hahn T 2001 *Comput. Phys. Commun.* **140** 418
- [9] Belyaev A, Christensen N D and Pukhov A 2013 *Comput. Phys. Commun.* **184** 1729
- [10] Press W H, Teukolsky S A, Vetterling W T and Flannery B P 1992 *Numerical Recipes in FORTRAN: The Art of Scientific Computing* (Cambridge: Cambridge University Press)
- [11] Lepage G P 1978 *J. Comput. Phys.* **27** 192
- [12] Stelzer T and Long W F 1994 *Comput. Phys. Commun.* **81** 357
- [13] Alwall J *et al* 2014 *J. High Energy Phys.* JHEP07(2014)079
- [14] De Causmaecker P, Gastmans R, Troost W and Wu T T 1982 *Nucl. Phys. B* **206** 53
- [15] Berends F A, Kleiss R, De Causmaecker P, Gastmans R, Troost W and Wu T T 1982 *Nucl. Phys. B* **206** 61
- [16] Parke S J and Taylor T R 1986 *Phys. Rev. Lett.* **56** 2459
- [17] Witten E 2004 *Commun. Math. Phys.* **252** 189
- [18] Cachazo F, Svrcek P and Witten E 2004 *J. High Energy Phys.* JHEP09(2014)006
- [19] Kosower D A 2005 *Phys. Rev. D* **71** 045007
- [20] Berends F A and Giele W T 1988 *Nucl. Phys. B* **306** 759
- [21] Caravaglios F and Moretti M 1995 *Phys. Lett. B* **358** 332
- [22] Draggiotis P, Kleiss R H P and Papadopoulos C G 1998 *Phys. Lett. B* **439** 157
- [23] Britto R, Cachazo F and Feng B 2005 *Nucl. Phys. B* **715** 499
- [24] Britto R, Cachazo F, Feng B and Witten E 2005 *Phys. Rev. Lett.* **94** 181602
- [25] Mangano M L and Parke S J 1991 *Phys. Rep.* **200** 301
- [26] Frixione S, Kunszt Z and Signer A 1996 *Nucl. Phys. B* **467** 399
- [27] Catani S and Seymour M H 1997 *Nucl. Phys. B* **485** 29
Catani S and Seymour M H 1998 *Nucl. Phys. B* **510** 503 (erratum)
- [28] Nagy Z 2003 *Phys. Rev. D* **68** 094002
- [29] Passarino G and Veltman M J G 1979 *Nucl. Phys. B* **160** 151
- [30] Ossola G, Papadopoulos C G and Pittau R 2007 *Nucl. Phys. B* **763** 147
- [31] Ellis R K, Kunszt Z, Melnikov K and Zanderighi G 2012 *Phys. Rep.* **518** 141
- [32] Ellis R K, Giele W T, Kunszt Z, Melnikov K and Zanderighi G 2009 *J. High Energy Phys.* JHEP01(2009)012
- [33] Andersen J R *et al* 2014 *PoS LL* **2014** 079
- [34] Cullen G *et al* 2014 *Eur. Phys. J. C* **74** 3001
- [35] Bevilacqua G, Czakon M, Garzelli M V, van Hameren A, Kardos A, Papadopoulos C G, Pittau R and Worek M 2013 *Comput. Phys. Commun.* **184** 986
- [36] Bern Z, Dixon L J, Febres Cordero F, Höche S, Ita H, Kosower D A, Maître D and Ozeren KJ 2013 *Phys. Rev. D* **88** 014025

- [37] Ita H, Bern Z, Dixon L J, Febres Cordero F, Kosower D A and Maitre D 2012 *Phys. Rev. D* **85** 031501
- [38] Bern Z *et al* 2012 *Phys. Rev. Lett.* **109** 042001
- [39] Cullen G *et al* 2013 *Phys. Rev. Lett.* **111** 131801
- [40] Bevilacqua G, Czakon M, Papadopoulos C G, Pittau R and Worek M 2009 *J. High Energy Phys.* JHEP09(2009)109
- [41] Denner A, Dittmaier S, Kallweit S and Pozzorini S 2012 *J. High Energy Phys.* JHEP10 (2012)110
- [42] Caola F, Henn J M, Melnikov K and Smirnov V A 2014 *J. High Energy Phys.* JHEP09 (2014)043
- [43] Gehrmann T, von Manteuffel A, Tancredi L and Weihs E 2014 *J. High Energy Phys.* JHEP06(2014)032
- [44] Bärnreuther P, Czakon M and Fiedler P 2014 *J. High Energy Phys.* JHEP02(2014)078
- [45] Anastasiou C, Gehrmann T, Oleari C, Remiddi E and Tausk J B 2000 *Nucl. Phys. B* **580** 577
- [46] Somogyi G, Trocsanyi Z and Del Duca V 2007 *J. High Energy Phys.* JHEP01(2007)070
- [47] Del Duca V, Duhr C, Somogyi G, Tramontano F and Trócsányi Z 2015 *J. High Energy Phys.* JHEP04(2015)036
- [48] Gehrmann-De Ridder A, Gehrmann T and Glover E Q N 2005 *J. High Energy Phys.* JHEP09(2005)056
- [49] Gehrmann-De Ridder A, Gehrmann T, Glover E W N and Heinrich G 2007 *J. High Energy Phys.* JHEP12(2007)094
- [50] Currie J, Gehrmann-De Ridder A, Glover E W N and Pires J 2014 *J. High Energy Phys.* JHEP01(2014)110
- [51] Binotto T and Heinrich G 2000 *Nucl. Phys. B* **585** 741
- [52] Anastasiou C, Melnikov K and Petriello F 2004 *Phys. Rev. D* **69** 076010
- [53] Anastasiou C, Melnikov K and Petriello F 2004 *Phys. Rev. Lett.* **93** 262002
- [54] Melnikov K and Petriello F 2006 *Phys. Rev. D* **74** 114017
- [55] Czakon M 2010 *Phys. Lett.B* **693** 259–68
- [56] Czakon M, Fiedler P and Mitov A 2013 *Phys. Rev. Lett.* **110** 252004
- [57] Boughezal R, Caola F, Melnikov K, Petriello F and Schulze M 2015 *Phys. Rev. Lett.* **115** 082003
- [58] Catani S and Grazzini M 2007 *Phys. Rev. Lett.* **98** 222002
- [59] Catani S, Cieri L, Ferrera G, de Florian D and Grazzini M 2009 *Phys. Rev. Lett.* **103** 082001
- [60] Ferrera G, Grazzini M and Tramontano F 2015 *Phys. Lett. B* **740** 51
- [61] Ferrera G, Grazzini M and Tramontano F 2014 *J. High Energy Phys.* JHEP04(2014)039
- [62] Gehrmann T, Grazzini M, Kallweit S, Maierhöfer P, von Manteuffel A, Pozzorini S, Rathlev D and Tancredi L 2014 *Phys. Rev. Lett.* **113** 212001
- [63] Cascioli F *et al* 2014 *Phys. Lett. B* **735** 311
- [64] Boughezal R, Focke C, Giele W, Liu X and Petriello F 2015 *Phys. Lett. B* **748** 5
- [65] Gaunt J, Stahlhofen M, Tackmann F J and Walsh J R 2015 *J. High Energy Phys.* JHEP09 (2015)058
- [66] Brown N and Stirling W J 1990 *Phys. Lett. B* **252** 657
- [67] Marchesini G and Webber B R 1984 *Nucl. Phys. B* **238** 1
- [68] Bassetto A, Ciafaloni M and Marchesini G 1983 *Phys. Rep.* **100** 201

- [69] Marchesini G and Webber B R 1988 *Nucl. Phys. B* **310** 461
- [70] Corcella G, Knowles I G, Marchesini G, Moretti G, Odagiri K, Richardson P, Seymour M H and Webber B R 2001 *J. High Energy Phys.* JHEP01(2001)010
- [71] Sjostrand T, Mrenna S and Skands P Z 2006 *J. High Energy Phys.* JHEP05(2006)026
- [72] Sjostrand T and Skands P Z 2005 *Eur. Phys. J. C* **39** 129
- [73] Sjöstrand T *et al* 2015 *Comput. Phys. Commun.* **191** 159
- [74] Bahr M *et al* 2008 *Eur. Phys. J. C* **58** 639
- [75] Gleisberg T, Hoeche S, Krauss F, Schalicke A, Schumann S and Winter J C 2004 *J. High Energy Phys.* JHEP02(2004)056
- [76] Lonnblad L 1992 *Comput. Phys. Commun.* **71** 15
- [77] Ritzmann M, Kosower D A and Skands P 2013 *Phys. Lett. B* **718** 1345
- [78] Nagy Z and Soper D E 2014 *J. High Energy Phys.* JHEP06(2014)097
- [79] Catani S, Krauss F, Kuhn R and Webber B R 2001 *J. High Energy Phys.* JHEP11(2001)063
- [80] Mangano M L, Moretti M and Pittau R 2002 *Nucl. Phys. B* **632** 343
- [81] Frixione S and Webber B R 2002 *J. High Energy Phys.* JHEP06(2002)029
- [82] Nason P 2004 *J. High Energy Phys.* JHEP11(2004)040
- [83] Mangano M L, Moretti M, Piccinini F, Pittau R and Polosa A D 2003 *J. High Energy Phys.* JHEP07(2003)001
- [84] Aad G *et al* (ATLAS Collaboration) 2014 *J. High Energy Phys.* JHEP09(2014)145
- [85] Hamilton K, Nason P and Zanderighi G 2012 *J. High Energy Phys.* JHEP10(2012)155
- [86] Gehrmann T, Hoche S, Krauss F, Schonherr M and Siegert F 2013 *J. High Energy Phys.* JHEP01(2013)144
- [87] Hamilton K, Nason P, Oleari C and Zanderighi G 2013 *J. High Energy Phys.* JHEP05(2013)082
- [88] Catani S, Webber B R and Marchesini G 1991 *Nucl. Phys. B* **349** 635
- [89] Catani S, Trentadue L, Turnock G and Webber B R 1993 *Nucl. Phys. B* **407** 3
- [90] Dasgupta M and Salam G P 2001 *Phys. Lett. B* **512** 323
- [91] Catani S, Turnock G and Webber B R 1992 *Phys. Lett. B* **295** 269
- [92] Dokshitzer Y L, Lucenti A, Marchesini G and Salam G P 1998 *J. High Energy Phys.* JHEP01(1998)011
- [93] Banfi A, Marchesini G and Smye G 2002 *J. High Energy Phys.* JHEP08(2002)006
- [94] Dasgupta M and Salam G P 2002 *J. High Energy Phys.* JHEP03(2002)017
- [95] Schwartz M D and Zhu H X 2014 *Phys. Rev. D* **90** 065004
- [96] Hagiwara Y, Hatta Y and Ueda T 2015 arXiv: [1507.07641](#)
- [97] Larkoski A J, Moult I and Neill D 2015 *J. High Energy Phys.* JHEP09(2015)143
- [98] Caron-Huot S 2015 arXiv: [1501.03754](#)
- [99] Neill D 2015 arXiv: [1508.07568](#)
- [100] Becher T, Neubert M, Rothen L and Shao D Y 2015 arXiv: [1508.06645](#)
- [101] Bauer C W, Pirjol D and Stewart I W 2002 *Phys. Rev. D* **65** 054022
- [102] Becher T and Schwartz M D 2008 *J. High Energy Phys.* JHEP07(2008)034
- [103] Moch S, Vermaseren J A M and Vogt A 2005 *Phys. Lett. B* **625** 245
- [104] Gehrmann T, Glover E W N, Huber T, Ikizlerli N and Studerus C 2010 *J. High Energy Phys.* JHEP06(2010)094
- [105] Magnea L 2001 *Nucl. Phys. B* **593** 269
- [106] Moch S, Vermaseren J A M and Vogt A 2004 *Nucl. Phys. B* **688** 101
- [107] Banfi A, Salam G P and Zanderighi G 2002 *J. High Energy Phys.* JHEP01(2002)018

- [108] Banfi A, Salam G P and Zanderighi G 2005 *J. High Energy Phys.* JHEP03(2005)073
- [109] Banfi A, McAslan H, Monni P F and Zanderighi G 2015 *J. High Energy Phys.* JHEP05 (2015)102
- [110] Brock R *et al* (CTEQ Collaboration) 1995 *Rev. Mod. Phys.* **67** 157
- [111] Shifman M A 2001 Quark hadron duality *At the Frontier of Particle Physics* vol 3, ed M A Shifman (Singapore: World Scientific) pp 1447–94
- [112] Dokshitzer Y L, Khoze V A, Mueller A H and Troian S I (ed) 1991 *Basics of Perturbative QCD* (Gif-sur-Yvette: Editions Frontières)
- [113] Andersson B, Gustafson G, Ingelman G and Sjostrand T 1983 *Phys. Rep.* **97** 31
- [114] Dokshitzer Y L, Marchesini G and Webber B R 1996 *Nucl. Phys. B* **469** 93
- [115] Dokshitzer Y L, Lucenti A, Marchesini G and Salam G P 1998 *J. High Energy Phys.* JHEP05(1998)003
- [116] Korchemsky G P and Sterman G F 1999 *Nucl. Phys. B* **555** 335
- [117] The ALEPH Collaboration 2004 *Eur. Phys. J C* **35** 457–86
- [118] Achard P *et al* (L3 Collaboration) 2004 *Phys. Rep.* **399** 71
- [119] Butterworth J M, Forshaw J R and Seymour M H 1996 *Z. Phys. C* **72** 637
- [120] Field R D (CDF Collaboration) 2001 *eConf C* **010630** P501
- [121] Cacciari M, Salam G P and Sapeta S 2010 *J. High Energy Phys.* JHEP04(2010)065

Hadronic Jets

An introduction

Andrea Banfi

Chapter 4

Jets as discovery tools

As we have seen in the previous chapter, QCD, the theory of strong interactions, predicts the occurrence of jets in high-energy collisions. Using perturbative QCD it is possible to predict observables involving jets with high accuracy. This is especially true at very high scales, since non-perturbative corrections (e.g. hadronisation) are suppressed by inverse powers of the characteristic energy of each process. Therefore, the most natural use of jets is as a means of testing perturbative QCD, for instance by measuring the QCD running coupling. One such measurement is the inclusive transverse momentum distribution of a jet in hadron collisions, obtained by binning the transverse momentum of every detected jet. The plot in the left-hand panel of figure 4.1 shows such measurements performed by the ATLAS collaboration at the LHC [1]. One sees very good agreement between the data and NLO QCD predictions obtained with the program NLOJET++ [2], so that an extraction of the QCD coupling α_s as well as fits of parton distribution functions are possible. Inclusive jet transverse momentum spectra are just an example of the many jet observables that are currently used for α_s measurements. A comprehensive plot showing a summary of the most precise measurements of α_s [3] is shown in the right-hand panel of figure 4.1. There is a striking agreement of all the measurements with the running of the coupling predicted by QCD, thus confirming its reliability as a theory of strong interactions at high energies. Note also that not only do jet observables provide most of the measurements in the plot (jets in electron–proton collisions e^+e^- jets and shapes, $pp, p\bar{p} \rightarrow$ jets), but also make it possible to explore different energy scales, which is not possible with full inclusive observables such as τ decays, which are characterised by a single hard scale. This is why it is very important to refine theoretical methods as much as possible to compute jet observables with higher and higher precision.

However, using jets as a means of testing perturbative QCD is just one of the ways in which they can be exploited. Another important application of jet physics is the search for new particles, especially in hadron colliders. To understand how this can be achieved, let us start again with an example, taken from [4]. Suppose we are

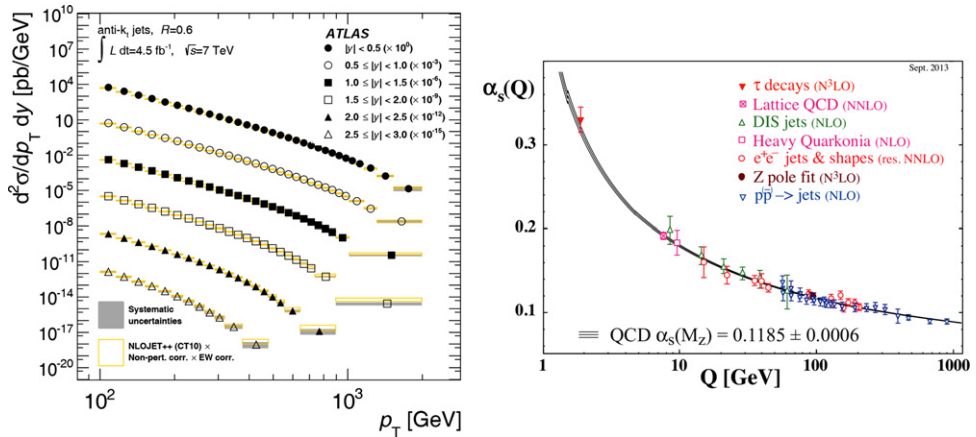


Figure 4.1. The inclusive transverse momentum spectra of jets, as measured by the ATLAS collaboration in different rapidity bins (left) [1] and the running of the QCD coupling, as determined by various measurements (right) [3].

looking for a new heavy particle that decays into quarks. The latter will give rise to jets in the final state. The relevant question is how to distinguish jets originating from new-particle decays from those produced directly in a hard collision. The main philosophy is to devise suitable observables whose distributions are different for signal and background events, thus acting as discriminators. The choice of these observables may be guided by a trial–error procedure, e.g. simulating signal and backgrounds with parton-shower event generators and examining the outcome until a satisfactory signal-to-background ratio is obtained. This approach is reasonable and highlights how important it is that parton-shower event generators accurately describe most of the features of jet production. However, one may complement this information with theoretical considerations. For instance, consider the simple scenario in which one looks for a heavy electrically neutral vector boson, let us call it Z' , that decays into a quark–antiquark pair. The natural way to look for such an object at the LHC is to reconstruct a pair of jets at high transverse momentum, say with the anti- k_t algorithm with a given radius R , and look for a peak in the invariant mass distribution of the two jets. The choice of the jet radius plays an important role in such analyses. In fact, partons from Z' decay can radiate outside the jet radius, the dijet pair hence loses mass and instead of a peak we may observe a broad distribution, indistinguishable from the continuum background. If, in contrast, we increase the radius too much, we catch many secondary hadrons from pile-up (PU) and from the underlying event (UE), again spoiling the resolution of the mass peak. This effect can be appreciated in figure 4.2, where (simulated) jets originating from the decay of a Z' with a mass of 2 TeV are reconstructed with the anti- k_t algorithm and different jet radii. There one clearly sees a degradation of the reconstruction quality of the mass peak when one moves away from $R = 0.6$, which represents somehow an optimal radius for this analysis. The trial–error procedure here consists in reconstructing the mass peaks for all possible algorithms and jet values, and this would have to be repeated for each new analysis. Furthermore,

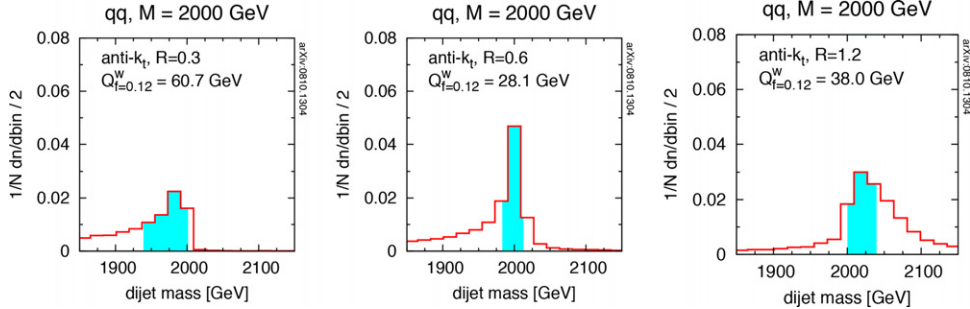


Figure 4.2. The distribution in the invariant mass of two quark jets in hadron collisions with UE, but no PU, obtained from [5].

relying on the outcome of parton-shower event generators implicitly assumes that these tools are able to capture the main features of the physics involved. A theoretically more sound approach consists in assessing the impact of perturbative and non-perturbative effects on jet-based analyses, and checking whether parton-shower event generators reproduce the main features that the theory predicts. The thus-validated event generators can be reliably used in a more refined trial-error procedure. In this chapter we will discuss how QCD has helped in devising better procedures to discriminate signal events, e.g. the hadronic decay of a heavy particle, from background events arising from QCD jet production. In particular, in section 4.1 we will discuss how the energy-momentum content of a jet of a given radius is affected by QCD radiation and non-perturbative effects such as hadronisation and UE. In section 4.2 we will present an overview of searches for boosted particles, whose decay products tend to fall into the same jet. Finally, in section 4.3 we will discuss methods to distinguish whether a jet is initiated by a quark or a gluon, highlighting why this is important for new physics searches in colliders.

4.1 Optimising the jet radius

Consider again the problem of a Z' decaying into two jets, where we are looking for a peak in the dijet invariant mass distribution $d\sigma/dM_{jj}^2$. Assuming the two jets p_1 and p_2 are almost massless, their invariant mass squared is given by

$$M_{jj}^2 \simeq 2p_{t1}p_{t2}[\cosh(y_1 - y_2) - \cos(\phi_1 - \phi_2)]. \quad (4.1)$$

If p_1 and p_2 are just a quark and an antiquark, their invariant mass will be the mass of the new boson $M_{Z'}$. However, the quark and antiquark will transform into jets, whose momenta will not be the same as those of the original quark and antiquark. This gives rise to a broad distribution, peaked around $M_{Z'}^2$ and with a width given approximately by

$$\begin{aligned} \delta M_{jj}^2 &\simeq 2(\langle \delta p_{t1} \rangle p_{t2} + p_{t1} \langle \delta p_{t2} \rangle)[\cosh(y_1 - y_2) - \cos(\phi_1 - \phi_2)] \\ &\simeq M_{jj}^2 \left(\frac{\langle \delta p_{t1} \rangle}{p_{t1}} + \frac{\langle \delta p_{t2} \rangle}{p_{t2}} \right), \end{aligned} \quad (4.2)$$

where $\langle \delta p_t \rangle$ is the difference between the transverse momentum of a jet p_t and that of the parton that has initiated it, averaged over all possible final-state configurations. Here we have assumed that jet directions stay more or less unchanged. There are three main effects contributing to $\langle \delta p_t \rangle$: QCD radiation, hadronisation, and PU and/or UE. Here we will present the main features of each contribution. For a more detailed analysis, the reader is referred to the original source [6].

QCD radiation. Consider one of the two jets produced by the decay of a Z' into a quark–antiquark pair, for instance the one initiated by the quark. When a gluon is emitted from the quark, it can escape the jet, so that the jet transverse momentum after the splitting is less than the quark transverse momentum. Suppose also that our candidate jet is the one with the highest transverse momentum, which is reasonable because we want to avoid following soft jets. In quasi-collinear kinematics, the transverse momentum of the hardest jet after the splitting will be $\max(z, 1 - z)p_t$, with p_t the transverse momentum of the parent quark. Therefore, the quantity $\delta p_t = -\min(z, 1 - z)p_t$ represents the transverse momentum lost in the splitting. The average decrease $\langle \delta p_t \rangle$ is obtained by integrating δp_t over the phase space of the emitted gluon, with the condition that the latter is not clustered with the outgoing quark. This condition depends in general on the jet algorithm. However, for generalised k_t algorithms, a gluon escapes a jet if and only if its distance ΔR in the y – ϕ plane from the final-state quark is bigger than the jet radius R . For small angles, ΔR is approximately equal to the splitting angle θ , so that we have

$$\begin{aligned} \langle \delta p_t \rangle_{q,\text{PT}} &\simeq \frac{\alpha_s}{2\pi} \int_{R^2}^1 \frac{d\theta^2}{\theta^2} \int_0^1 dz P_{qq}(z) [-\min(z, 1 - z)p_t] \\ &= -C_F \left(2 \ln 2 - \frac{3}{8} \right) p_t \frac{\alpha_s}{\pi} \ln \frac{1}{R} \simeq -1.35 p_t \frac{\alpha_s}{\pi} \ln \frac{1}{R}, \end{aligned} \quad (4.3)$$

where $P_{qq}(z)$ is the splitting function related to the elementary process $q \rightarrow qg$, defined in (3.5). Given the fact that the splitting probability is positive, we have a transverse momentum loss, as expected. Note that this quantity is logarithmically enhanced in the jet radius, a consequence of the collinear singularity $d\theta/\theta$ in the gluon emission probability. This means that the smaller the jet radius, the more the jet will lose transverse momentum due to QCD radiation. This effect will in turn spoil the resolution of an invariant mass peak.

For jets initiated by gluons, one needs to consider a gluon splitting into two gluons or n_f quark–antiquark pairs. This gives

$$\begin{aligned} \langle \delta p_t \rangle_{g,\text{PT}} &\simeq \frac{\alpha_s}{2\pi} \int_{R^2}^1 \frac{d\theta^2}{\theta^2} \int_0^1 dz [P_{gg}(z) + n_f P_{qg}(z)] [-\min(z, 1 - z)p_t] \\ &= - \left(\left(2 \ln 2 - \frac{43}{96} \right) C_A + \frac{7}{48} T_F n_f \right) p_t \frac{\alpha_s}{\pi} \ln \frac{1}{R} \\ &\simeq -(2.82 + 0.08n_f) p_t \frac{\alpha_s}{\pi} \ln \frac{1}{R}. \end{aligned} \quad (4.4)$$

By comparing the size of the two contributions one sees that gluon-initiated jets lose roughly twice as much transverse momentum with respect to quark-initiated jets. The ratio $\langle \delta p_t \rangle_g / \langle \delta p_t \rangle_q$ is driven by the ratio of the corresponding Casimir factors C_A/C_F , because the splitting probabilities are dominated by the universal soft singularity $dz/(1-z)$.

Note that, for small jet radii, the logarithms of the jet radius in (4.3) and (4.4) can become large, thus endangering the convergence of the QCD perturbative expansion. Logarithms of the jet radius can be resummed at all orders by exploiting the coherent branching formalism and considering a cascade of collinear splittings with decreasing angles, which stops when the angle of the most collinear splitting reaches the jet radius R . Such resummation has been carried out in [7].

Hadronisation. Suppose some soft hadrons at large angles escaped the jet. As explained in section 3.4, it is useful, and phenomenologically accurate, to treat such hadrons as gluons emitted with an effective coupling $\alpha_s^{\text{NP}}(k_t)$, where k_t is the relative transverse momentum of the emitted non-perturbative gluon with respect to the emitter. For a gluon taking a fraction $1-z$ of jet transverse momentum, we have $k_t \simeq (1-z)\theta p_t$. The loss of these soft hadrons will not change appreciably the transverse momentum of the leading jet, so that the transverse momentum loss due to hadronisation is always $\delta p_t \simeq -(1-z)p_t$. This gives, for a quark-initiated jet

$$\begin{aligned} \langle \delta p_t \rangle_{q,\text{had}} &\simeq \int_{R^2}^1 \frac{d\theta^2}{\theta^2} \int_0^1 dz \frac{2C_F}{1-z} \left[-(1-z)p_t \right] \frac{\alpha_s^{\text{NP}} \left[(1-z)\theta p_t \right]}{2\pi} \\ &\simeq -\frac{2C_F}{\pi} p_t \int_R^1 \frac{d\theta}{\theta^2} \int_0^{\mu_1} dk_t \alpha_s^{\text{NP}}(k_t). \end{aligned} \quad (4.5)$$

Note that we are entitled to use the most singular part (for $z \rightarrow 1$) of the splitting function only, because the remaining parts give a correction that is suppressed by a higher power of the jet transverse momentum. We have also cut off the relative transverse momentum k_t with a scale $\mu_1 \simeq 2 \text{ GeV}$, which represents the boundary between perturbative and non-perturbative physics, as explained in section 3.4. The average transverse momentum loss can be further expressed in terms of the same parameter $\alpha_0(\mu_1)$ that enters hadronisation corrections to event-shape distributions and means as follows

$$\frac{\langle \delta p_t \rangle_{q,\text{had}}}{p_t} \simeq -\frac{2C_F}{\pi} \frac{1}{R} \frac{\mu_1}{p_t} \left[\alpha_0(\mu_1) - \alpha_s(p_t) + \mathcal{O}(\alpha_s^2) \right] \equiv -\frac{2C_F}{R} \frac{A(\mu_1)}{p_t}, \quad (4.6)$$

where the parameter $A(\mu_1)$, introduced in (3.56) and defined precisely in [6], is the same as entering hadronisation corrections to event-shape distributions and means in e^+e^- annihilation. For a gluon jet the answer is almost identical, one needs to replace C_F by C_A . Since $C_A \simeq 2C_F$, it turns out that a gluon jet loses on average twice as much transverse momentum with respect to a quark jet through hadronisation. Note also that the relative p_t loss scales as one inverse power of the jet transverse momentum. As expected, hadronisation corrections become negligible at very high transverse momenta.

The leading $1/R$ behaviour of hadronisation corrections is reproduced by parton-shower event generators [6]. This is not surprising, since a similar correction appears in event-shape distributions and means, and all hadronisation models in event generators are tuned so as to reproduce e^+e^- data for event shapes.

Pile-up and/or underlying event. The common characteristics of the p_t -loss induced by QCD radiation and hadronisation is that they increase with decreasing radius. However, in hadron colliders, a better resolution cannot be obtained by just increasing the jet radius, because of contamination from PU and UE. These contributions can be somehow unified by considering that they produce a distribution in transverse momentum which is roughly uniform in rapidity and azimuth. Note that, in this context, a further contamination with the same characteristics is given by soft, yet perturbative, radiation from the initial-state partons. In our discussion then we will simply consider a generic source of background, producing a uniform average transverse momentum ρ_{bkg} per unit rapidity and unit azimuth. It follows immediately that such a background produces an average increase $\langle \delta p_t \rangle_{\text{bkg}}$ of the transverse momentum of a jet, getting larger with the jet radius. Assuming E -scheme recombination for the jets, the change in transverse momentum δp_t due to background hadrons having a total transverse momentum \vec{k}_t can be estimated as follows

$$\delta p_t = |\vec{p}_t + \vec{k}_t| - p_t \simeq \frac{\vec{k}_t \cdot \vec{p}_t}{p_t} \simeq k_t \cos \phi, \quad (4.7)$$

with ϕ the azimuthal angle between \vec{p}_t and \vec{k}_t . If we are interested only in the leading dependence on the jet radius, we can take the limit of small R and hence $\cos \phi \simeq 1$, so that $\delta p_t \simeq k_t$. If we average over all possible values of k_t and integrate over the region in rapidity and azimuth corresponding to the area of the jet, we obtain [6]

$$\langle \delta p_t \rangle_{\text{bkg}} \simeq \pi R^2 \rho_{\text{bkg}},$$

with πR^2 the active area of the anti- k_t jet. Note that, for small R , the same result holds for the Cambridge/Aachen and the k_t algorithms.

If one considers events with no PU, parton-shower event generators do reproduce the R^2 dependence of the contribution of the UE. However, while for hadronisation corrections there is a reasonable agreement among different parton showers themselves, as well as with the calculation in (4.6), the size of ρ_{bkg} depends on the model of the UE implemented in each generator, as shown in the plot in the left-hand panel of figure 4.3. However, we recall that the contamination due to a uniform background can be removed by means of the subtraction procedure of (2.8). To apply that equation one needs to find an estimator of ρ_{bkg} itself using data, for instance that defined in (2.11).

The simple calculations we have presented convey a clear message. The dominant effect of QCD final-state radiation (perturbative or non-perturbative) is that of degrading the transverse momentum of a jet, the larger the decrease the smaller the

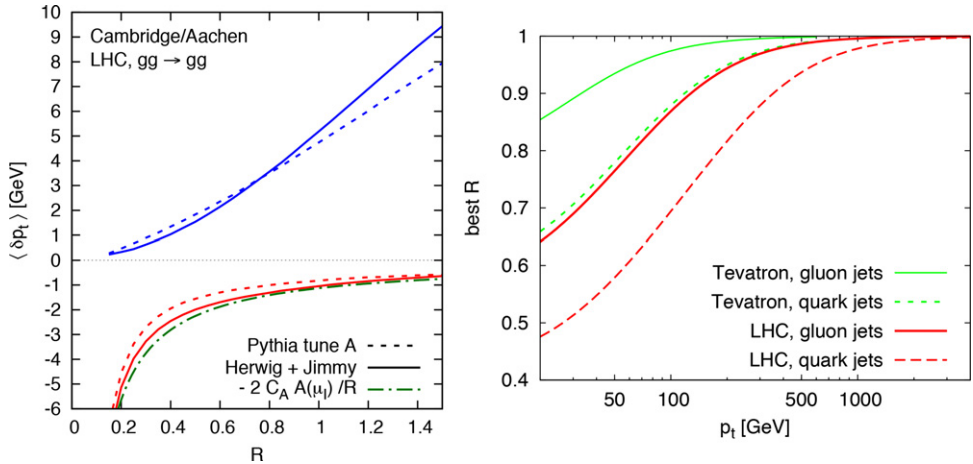


Figure 4.3. Left: the average transverse momentum difference induced by hadronisation (bottom) and UE (top) for gluon jets at the LHC. Right: the radius R that minimises $\langle \delta p_t^2 \rangle$, as a function of the jet transverse momentum p_t , for quark and gluon jets at the Tevatron and at the LHC [6].

jet radius. In contrast, sources of a uniform background in rapidity and azimuth, such as initial-state QCD radiation, PU or UE, cause an increase in a jet's transverse momentum, the larger this is the larger the jet radius. It is therefore possible to find an optimal jet radius for which the combination of the two effects is minimised. This minimisation is particularly useful specifically in new physics searches, where one wants to preserve as much information as possible on the partons that have initiated each jet. Furthermore, since the effect of QCD radiation is proportional to the charge of the parton giving rise to the jet, whereas the contribution of the UE is independent of it, one expects that the optimal radius will be roughly double for gluon jets than for quark jets. These naive considerations have been confirmed by more thorough theoretical analyses. For instance, the authors of [6] minimised the positive-definite quantity $\langle \delta p_t^2 \rangle$, estimated using parton-shower event generators with no PU. The results, shown in the right-hand panel of figure 4.3, confirm our naive expectation. Note that the optimal jet radius is smaller at the LHC than at the Tevatron due to the larger activity of the UE, which makes it necessary to reduce the jet radius. The pioneering study of [6] does not investigate what happens if the contribution of a uniform background is subtracted off before optimising the jet radius. This is carried out for instance in [4], where more sophisticated quantities have been proposed to assess the quality of jet reconstruction for different algorithms and jet sizes.

To conclude, finding the optimal jet radius is one of the crucial problems when using jets as discovery tools and remains a matter of debate. In this section we have discussed the main sources that determine the difference between the transverse momentum of a jet and that of the parton that has initiated it. Similar arguments can be applied to the search for boosted objects, whose decay products fall into the same jet. This topic will be covered in the next section.

4.2 Boosted objects and jet substructure

The LHC makes it possible, for the first time, to access in a controlled way energy scales that are larger than those typical of electroweak interactions, which are of the order of a few hundreds of giga-electron-volts. In this situation, a massive particle can have a transverse momentum considerably larger than its mass and its decay products will receive a huge boost along the particle direction. As a consequence, if a heavy particle decays into partons, these will be likely clustered inside the same jet. In fact, for a jet of mass m_{jet} , the distance ΔR_{12} in the rapidity-azimuth plane between two quasi-parallel constituents, carrying a fraction z and $1 - z$ of the jet transverse momentum $p_{t,\text{jet}}$, is given by

$$\Delta R_{12} \simeq \frac{m_{\text{jet}}}{\sqrt{z(1-z)p_{t,\text{jet}}}}, \quad (4.8)$$

which, for fixed m_{jet} , becomes smaller and smaller the larger the jet transverse momentum. Boosted analyses thus consider a candidate jet and look for a peak in the distribution in the invariant mass of that jet. Various problems arise in this situation. The first is how to distinguish such jets from standard QCD jets, whose invariant mass is dynamically generated through parton branching. The peak of the mass distribution of a QCD jet is at around 10% of the transverse momentum of the jet. Therefore, for a jet of the transverse momentum of 1 TeV, we expect a peak at around 100 GeV, right at the electroweak scale! The other problem is to clean the jet in such a way that only the hadrons originated by the decay of the heavy particle are used to compute the jet invariant mass. Here the same considerations apply as for the mass resolution of dijet pairs, discussed in the previous section. Partons lose energy due to QCD radiation, so using too few jet constituents results in a lower invariant mass than expected. In contrast, enlarging the jet constituents increases contamination from uniform sources of background, such as initial-state radiation, PU or the UE. Therefore, one needs to find an optimal procedure to clean the candidate jet down to its relevant constituents.

The methods used to search for jets arising from the decay of heavy particles are generally called ‘jet substructure techniques’. They were introduced for the first time in [8], in the context of the search for a heavy Higgs boson decaying into a pair of W bosons, one of which decays hadronically. The basic idea of the proposed analysis was to consider a jet with a large radius, which we now call a ‘fat’ jet, measure the invariant mass of its two hardest subjets and look for a peak corresponding to the mass of the W boson. To reduce contamination from the UE it was also proposed to recluster hadrons inside a fat jet with a smaller jet radius, whose size was optimised according to the desired resolution in the fat-jet invariant mass. In the following we give an overview of the most used methods to search for boosted heavy objects inside fat jets. For simplicity, we will concentrate on two-prong decays, in which a heavy particle decays into two coloured particles, referring the reader to the recent literature on the subject [9, 10] for the generalisation to three-prong decays (e.g. top-quark taggers [11–13]).

4.2.1 Groomers and taggers

The most widely used procedures for jet substructure studies perform two different kinds of actions on a jet. One is grooming, aimed at cleaning a jet of soft constituents, whose output is always a jet which might be very different from the original jet. These soft constituents can have any origin, can be for instance soft gluons radiated by the hard partons that have initiated the jet, as well as contamination from initial-state radiation, PU or UE. The second action is tagging, through which a jet can either be kept or discarded, according to whether it satisfies certain criteria, specific to the particle we are looking for. The first two procedures we will discuss, trimming [14] and pruning [15], are relevant examples of groomers. The third one, the mass-drop tagger (MDT) [16], is mainly a tagger, but also includes some grooming procedures, such as filtering. The last one we will present, which is also the most recent, is the soft drop [17] which can be used both as a groomer and as a tagger. It has to be noted that a tagger can always be supplemented by additional grooming procedures. This is the case for the original version of the MDT, which came together with a filtering procedure, which is in fact a groomer.

Trimming. The aim of this procedure is to clean all hard jets (i.e. those above some transverse momentum threshold) by eliminating softer constituents [14]. Once jets have been reconstructed, each jet is reclustered with a radius R_{sub} , smaller than the jet radius. One then looks inside each jet and discards all subjets p_j having a transverse momentum $p_{tj} < z_{\text{cut}} \Lambda_{\text{hard}}$, where z_{cut} is a free parameter and Λ_{hard} a typical hard scale, for instance the transverse momentum of the parent jet. The surviving subjets constitute the trimmed jet. Figure 4.4 illustrates pictorially how the trimming algorithm works with a jet containing two hard and two soft constituents. At the end of the procedure, one obtains a hard jet of radius R_{sub} containing the two hard constituents only.

Pruning. This procedure aims to eliminate soft large-angle constituents of jets by trying to follow the hardest branch of a jet [15]. This is achieved by performing a reclustering of the constituents of each jet with a sequential algorithm such that,

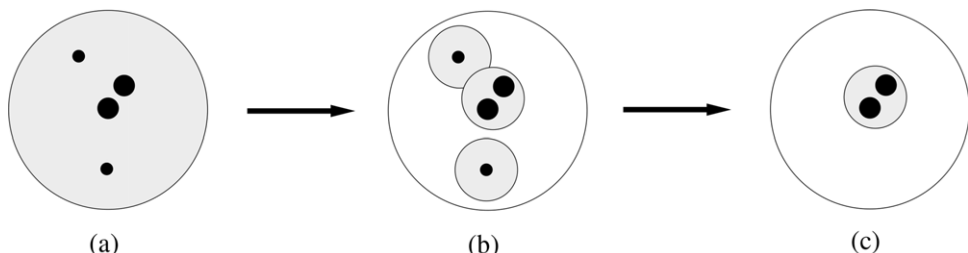


Figure 4.4. (a) A jet of large radius R containing two hard constituents (the big black circles) and two soft constituents (the small black circles). (b) The jet is reclustered with radius $R_{\text{sub}} < R$, and three subjets are found. (c) All subjets such that $p_{tj} < z_{\text{cut}} \Lambda_{\text{hard}}$ are discarded and only the subject containing the two hardest constituents survives.

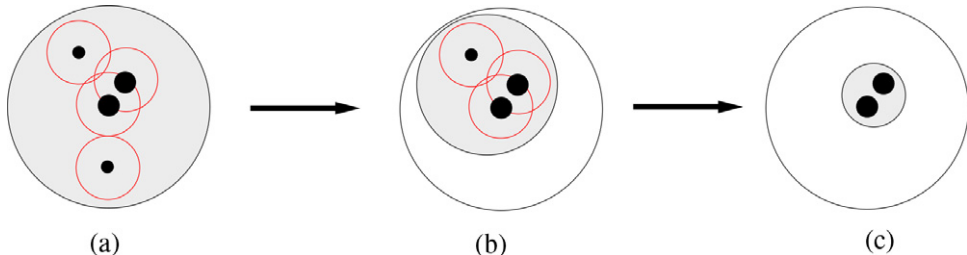


Figure 4.5. (a) The same jet considered in figure 4.4, where circles of radius R_{prune} are drawn around each constituent. (b) The first stage of the clustering: the soft jet at the bottom is discarded. (c) The second stage of the clustering: the soft jet at the top is discarded and one is left with a jet of R_{prune} with the two hardest constituents only.

whenever two constituents p_i and p_j are to be recombined, one checks whether they meet the conditions

$$\frac{\min(p_{ti}, p_{tj})}{|\vec{p}_{ti} + \vec{p}_{tj}|} < z_{\text{cut}}, \quad \text{and} \quad \Delta R_{ij} > R_{\text{prune}}. \quad (4.9)$$

If this is the case, the two constituents are not merged into a single jet, but the one with smaller transverse momentum is discarded. The set of all surviving subjets constitutes the *pruned* jet. The value of R_{prune} is not fixed, but is set dynamically. A common choice is $R_{\text{prune}} = m_{\text{jet}}/p_{t,\text{jet}}$, where m_{jet} and $p_{t,\text{jet}}$ are the jet invariant mass and transverse momentum, respectively. The behaviour of pruning is pictorially illustrated in figure 4.5 for the same configuration considered for trimming. Again, the final result is a jet containing only the two hardest constituents.

Mass-drop tagger and filtering. The MDT is itself a mixture of a groomer and a tagger. In its original version [16], it aims to find a hard jet that originates from the two-body decay of a massive particle, such as the Higgs or a vector boson. One starts by clustering an event into fat jets. Then, one reclusters each fat jet using the Cambridge/Aachen algorithm, whose clustering sequence is close to reversing the angular-ordered branching predicted by QCD. For each fat jet, the last step of the clustering is then undone, giving two subjets p_1 and p_2 , with masses m_{j1} and m_{j2} . In the original version of the MDT, one then checks the following conditions

$$\frac{\min(p_{t1}^2, p_{t2}^2)}{m_{\text{jet}}^2} \Delta R_{12}^2 > y_{\text{cut}}, \quad \text{and} \quad \min(m_{j1}, m_{j2}) < \mu m_{\text{jet}}. \quad (4.10)$$

If they are both met, the two subjects are kept and the procedure stops, otherwise the subject with the smaller invariant mass is eliminated and one undoes one more step of the clustering procedure. The first condition in (4.10) is in fact a groomer. It aims to eliminate soft large-angle constituents from the jet, in particular checking for asymmetric splittings which are typical of QCD radiation. The second relation is the actual mass-drop condition, and acts as a tagger, in that if it is not satisfied at any stage of the clustering, the jet is discarded as a whole. The mass-drop condition

implements a basic property of the decay of a heavy particle into two hard massless objects. In fact, whenever these two massless constituents are split into two different subjets, one observes a significant difference, effectively a drop, between the mass of each subjet and that of the parent jet. Similarly, the procedure stops when it has identified a pair of constituents one of which is quasi-massless. If one expects a two-prong decay, i.e. the heavy particle decays into two partons only, the procedure can end here. For three-prong decays, such as those of the top quark, one can consider the subjet with larger mass and undo the clustering further until another mass drop is found. The mass-drop procedure can be then generalised to more complicated decays. Note that, following the study of [18], the MDT has been slightly modified with respect to its original version. In the updated version, if any of the conditions in (4.10) are not met, the jet p_j with the largest transverse mass $m_{tj} = \sqrt{m_j^2 + p_{tj}^2}$ is discarded. This is to avoid following a soft subjet whose mass is generated dynamically by soft-collinear parton branching. This procedure is again explained pictorially in figure 4.6. At the end of the procedure, using the same configuration as in figures 4.4 and 4.5, one obtains a jet that contains only the two hardest constituents. At this point, the mass-drop procedure can be supplemented by filtering. This technique was introduced for the first time in combination with the MDT, but it could be applied to trimmed or pruned jets as well. Once the hardest constituents of a jet have been found, it might be possible that some of the soft subjets that have been discarded were due to soft radiation from the primary hard partons that initiated the fat jet. Losing them would result in spoiling the resolution of the jet mass peak, as discussed in section 4.1. Filtering specifically aims to restore the soft constituents that originated from soft radiation, while at the same time trying to exclude spurious soft jets from a uniform background. This is achieved by reclustering the tagged jet with a smaller radius R_{filt} and measuring the distribution in the invariant mass of only n_{filt} subjets, as the quantity that is supposedly closer to the mass of the heavy particle that originated the jet. Using similar arguments as in section 4.1, it is possible to show that perturbative QCD radiation causes a loss in the

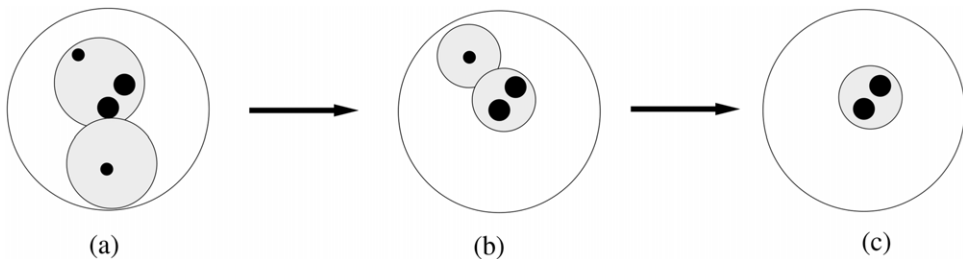


Figure 4.6. (a) The same jet considered in figure 4.4. The last stage of the clustering is undone and two subjets are found. (b) The mass-drop condition is not satisfied, so the soft jet at the bottom is discarded. A further stage of the clustering is undone, and one is left with two subjets. Then the soft jet at the top is discarded because of the failure of the mass-drop condition. (c) If one eliminates either of the remaining hard subjets, one is left with a single massless constituent. At this stage, the mass-drop condition is met and the procedure stops, leaving a tagged jet containing only the two hardest constituents.

jet mass that follows $\ln(1/R_{\text{filt}})$, hadronisation corrections also provide a loss, proportional to $1/R_{\text{filt}}$, whereas a uniform background provides an enhancement in the jet mass that follows R_{filt}^2 [16]. It is therefore possible to find an optimal radius that minimises the jet-mass width δM . If we are looking for a colourless particle, such as the Higgs decaying into a $b\bar{b}$ pair, QCD coherence offers an extra handle to look for the optimal filtering radius. In fact, suppose the MDT, or another procedure, has found two subjets separated by a distance R_{jj} . Then, the coherence properties of QCD radiation will force an extra soft gluon to be radiated within two cones of radius R_{jj} , centred in each of the two hard subjets (see figure 4.7). Therefore, R_{filt} will have to be presumably a fraction of R_{jj} . A study to optimise the quantity R_{filt} has been performed for the case of Higgs production into a $b\bar{b}$ pair and can be confidently applied to the production of any two-body decay of a colourless massive particle [19]. For $n_{\text{filt}} = 3$, one sees a minimum in the jet mass resolution δM as a function of $\eta = R_{\text{filt}}/R_{\text{jj}}$, located at $\eta = 0.3$ (see figure 4.8, left panel). This is roughly consistent with the value $R_{\text{filt}} = \min\{0.3, R_{b\bar{b}}/2\}$ and $n_{\text{filt}} = 3$ proposed by the pioneering publication [16], in which the MDT/filtering technique was introduced for the first

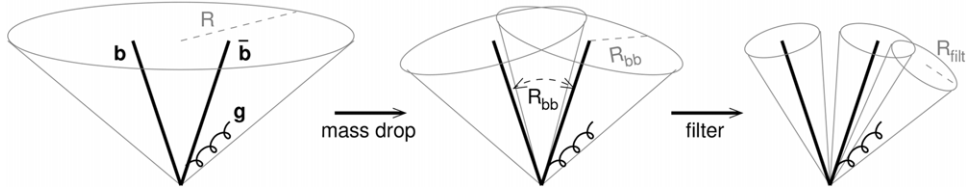


Figure 4.7. Pictorial illustration of the filtering procedure, taken from [16]. A fat jet of radius R contains a $b\bar{b}$ pair and a soft gluon radiated by the pair (left). The MDT found the $b\bar{b}$ pair but might have excluded the soft gluon. The soft gluon is radiated within two cones of radius $R_{b\bar{b}}$, centred around each of the b quarks (middle). With the filtering procedure, the fat jet is reclustered with a radius $R_{\text{filt}} < R_{b\bar{b}}$ and three subjets are considered in the calculation of the invariant mass of the jet, so as to re-include the soft gluon (right).

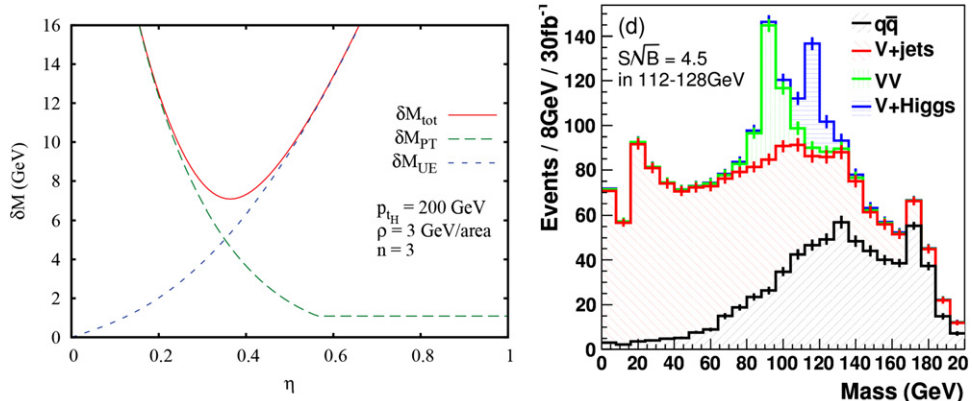


Figure 4.8. The filtered-jet mass width δM as a function of $\eta = R_{\text{filt}}/R_{\text{jj}}$ for $n_{\text{filt}} = 3$, as computed in [19] (left). The invariant mass of a filtered Higgs-candidate jet selected with the MDT procedure, taken from the pioneering study of [16] (right).

time to look for a boosted Higgs boson decaying into a $b\bar{b}$ pair and produced in association with a vector boson at the LHC with $\sqrt{s} = 14$ TeV. The result of that analysis was that it was possible to find a candidate fat jet that survived the MDT procedure and whose mass distribution after filtering showed a nice peak around the Higgs mass, taken to be 115 GeV in [16] (see figure 4.8, right).

Soft drop. Along the same line of thought, a further improvement of the modified MDT (mMDT) is the ‘soft drop’ [17]. Its first step proceeds exactly as with the MDT, in that it reclusters a jet with the Cambridge/Aachen algorithm and undoes the last step of the clustering of a jet, finding two subjets p_1 and p_2 . Then, one checks if they satisfy the soft-drop condition

$$\frac{\min(p_{t1}, p_{t2})}{p_{t1} + p_{t2}} > z_{\text{cut}} \left(\frac{\Delta R_{12}}{R} \right)^{\beta}, \quad (4.11)$$

where β is a parameter that can take any value. If the soft-drop condition is not met, then the subjet with lower transverse momentum is removed. A peculiarity of the soft-drop procedure is that it acts as a groomer or a tagger, according to the value of β . Specifically, for $\beta > 0$ it removes the soft constituents of a jet, with β essentially controlling the angular size of the groomed jet. The output of the procedure for $\beta > 0$ is a jet with a reduced radius, so that the algorithm behaves as a groomer. In contrast, for $\beta < 0$, the soft-drop condition implicitly forces the two subjets to have a large-angle separation and hence selects only jets that contain at least two hard, well-separated subjets, as is typical for two-prong decays. In fact, for $\beta < 0$ the algorithm behaves as a tagger. The case $\beta = 0$ corresponds to the asymmetry condition of the MDT, which in fact can be rewritten as

$$\frac{\min(p_{t1}^2, p_{t2}^2)}{m_{\text{jet}}^2} \Delta R_{12}^2 \simeq \frac{\min(p_{t1}^2, p_{t2}^2)}{p_{t1} p_{t2}} \simeq \frac{\min(p_{t1}^2, p_{t2}^2)}{z(1-z)(p_{t1} + p_{t2})^2} > y_{\text{cut}}, \quad (4.12)$$

where we have assumed that the two subjets p_1 and p_2 are very close in angle. In fact, (4.12) represents a soft-drop condition with $z_{\text{cut}} = \sqrt{z(1-z)}y_{\text{cut}}$. Furthermore, for $\beta = 0$, the soft-drop condition corresponds to the mMDT, because only the subjet with larger transverse momentum is kept if the asymmetry condition fails and not the one with the larger invariant mass as in the original version of the MDT. The soft-drop condition for $\beta < 0$, i.e. in tagging mode, avoids the need for the mass-drop check altogether.

The above ideas have been refined over the years and now we have a considerable number of taggers for boosted objects, the description of which goes beyond what can be covered in this book. A yearly report on the state-of-the-art of existing taggers can be found in the proceeding of the BOOST conferences (see [9, 10] for the most recent conference proceedings). In the rest of this section we will instead concentrate on how a quantitative understanding of the various taggers using perturbative QCD can be exploited to improve their performance. The last subsection of this section is devoted to an overview of recent experimental studies on jet substructure.

4.2.2 Groomers and taggers in QCD

Given the variety of methods available to investigate jet substructure, it is natural to ask the question of how to assess their performance. One way of doing this is to study their behaviour using perturbative QCD, as proposed in [18]. There the authors considered the invariant mass of a QCD jet, more specifically the dimensionless variable $\rho = m_{\text{jet}}^2/(p_{t,\text{jet}}^2 R^2)$, after trimming, pruning or MDT. The main idea is that not only should a tagger be able to identify the relevant constituent in a signal jet, but also it should reduce the number of background jets that pass the tagger. Also, ideally one would prefer the mass distribution of a QCD jet to be featureless, without peaks that can mimic a signal peak. For instance, the plain jet mass distribution, which has a peak at around 10% of the jet transverse momentum, may not be the ideal for boosted object searches. The peak is a consequence of the fact that QCD radiation that dominates the mass distribution at large invariant masses, is then suppressed and vanishes at low invariant masses due to the presence of a Sudakov form factor, as explained in section 3.3. We call this feature a Sudakov peak. A first interesting result of a QCD analysis of the ρ distribution is that, after trimming or pruning, it still shows features. This can be seen in figure 4.9, which shows the ρ distribution for trimmed (left) and pruned (right) quark jets. In particular, it is interesting to investigate the behaviour of the distribution $\rho d\sigma/d\rho$ for decreasing values of ρ . As expected, the distribution starts with an increase, due to the jet being dominated by a single gluon emission. Then, at around $\rho \simeq 0.1$, the distribution becomes almost flat until a turning point at $\rho \simeq 0.01$, which, unfortunately, for 1 TeV jets just coincides with the electroweak scale, where the masses of interesting particles lie! The plots in the figure were obtained using the Monte Carlo event generator PYTHIA 6, but the same features are obtained with an analytic calculation. This feature can be easily understood for a

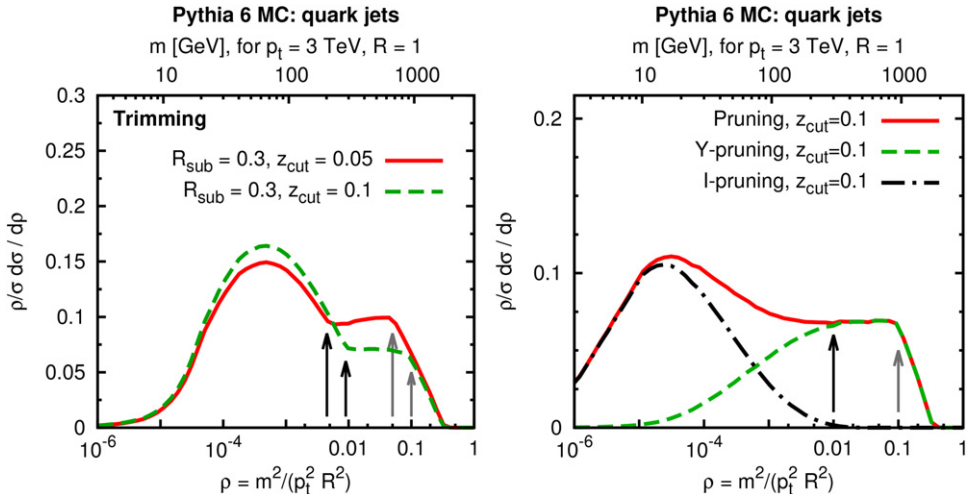


Figure 4.9. The distribution $\rho d\sigma/d\rho$ for a trimmed (left) and a pruned (right) quark jet with $p_t = 3$ TeV [18]. The plots report also the corresponding value of the jet mass, here denoted by m .

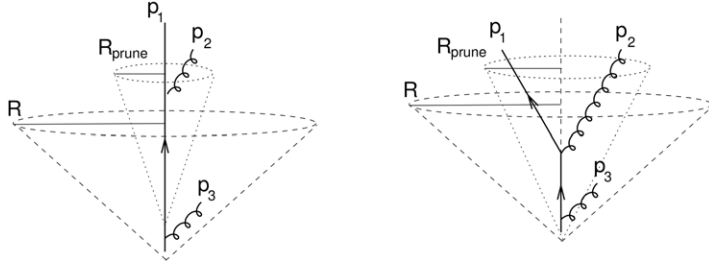


Figure 4.10. Configurations at $\mathcal{O}(\alpha_s^2)$ that give rise to a I-pruning (left) and Y-pruning (right). Left: soft gluon p_3 sets R_{prune} and is then pruned away. Right: R_{prune} is set by hard gluon p_2 and soft gluon p_3 is simply pruned away. Both pictures have been drawn by the author, inspired by the pictures in [18].

trimmed jet, which differs from the original jet only in that it has a smaller radius. This gives a peak that is moved to lower values of ρ with respect to that of the plain jet mass distribution. In the case of pruning the situation is more complicated. In fact it turns out that this procedure actually selects two kinds of jets. If one does not find in any of the clusterings a pair of subjets p_i and p_j such that $\Delta R_{ij} > R_{\text{prune}}$ and $\min(p_{ti}, p_{tj}) > z_{\text{cut}} |\vec{p}_{ti} + \vec{p}_{tj}|$, it means that the jet mass m_{jet} , and hence $R_{\text{prune}} = m_{\text{jet}}/p_{t,\text{jet}}$ is set by the energy of the soft large-angle constituent that is pruned away (see figure 4.10, left panel). Therefore, the mass of the pruned jet will be just the mass of a jet of radius R_{prune} , which has a peak at some low value of ρ , which is what is seen in figure 4.9. These narrow jets are called I-pruned jets, due to their shape. If, however, one finds at least one clustering with $\Delta R_{ij} > R_{\text{prune}}$ and $\min(p_{ti}, p_{tj}) > z_{\text{cut}} |\vec{p}_{ti} + \vec{p}_{tj}|$, the jet will have a two-prong structure and its invariant mass, and hence R_{prune} , will be basically unaffected by extra soft radiation (see figure 4.10, right panel). Such jets are called Y-pruned jets, again due to their shape. I-pruned jets can be discarded by looking at the clustering sequence, leaving only Y-pruned jets. The mass distribution of Y-pruned jets no longer has a Sudakov peak, but vanishes smoothly with ρ . Interestingly, while I-pruning is essentially a groomer, Y-pruning is in fact a tagger, since only two-prong structures are kept. Concerning MDT, the analysis of [18] discovered a flaw in the original procedure, which has now been replaced by the mMDT described in the text. In fact, suppose the mass-drop condition has to be checked on two subjets one of which is energetic but almost massless, and the other is massive but its mass results from multiple splittings of a soft gluon (see figure 4.11, left panel). In this case, the algorithm will discard the hard subjet and follow the soft subjet until it finds two massless constituents. This occurrence is rare, because soft subjets are normally eliminated by the asymmetry condition, the first of (4.10). However, this is clearly an unwanted feature of the MDT and can be avoided by just discarding the subjet with the lower transverse mass, instead of that with the lower invariant mass. Another possibility is to follow the branch with the larger transverse momentum, as is done by the soft-drop procedure. One more interesting feature of the MDT, particularly of its modified version, is that it is possible to tune its parameter y_{cut} in such a way that the mass distribution of a tagged jet does not have

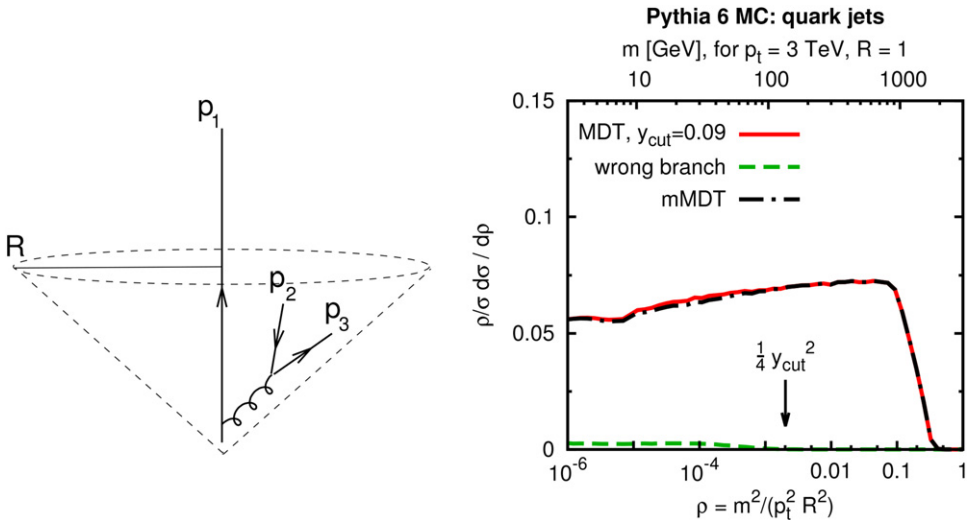


Figure 4.11. Left: a configuration that leads the original mass-drop procedure to follow an incorrect branch; in this case the original algorithm discards the subjet made up of a single quark because it is energetic, but massless. The picture has been drawn by the author, and is similar to the corresponding picture in [18]. Right: the distribution $\rho d\sigma/d\rho$ for a jet tagged with the MDT procedure [18].

the characteristic Sudakov peak, being more or less flat from the point at which the MDT condition sets in (see figure 4.11, right panel). Such featureless mass distribution is ideal to distinguish signal from background. From this analysis one sees that an analytical understanding of groomers and taggers from the point of view of perturbative QCD can lead to improvements that would be difficult to devise through a trial-error procedure. Similarly, one can investigate the behaviour of the soft-drop tagger as a function of β . As already stated, for $\beta > 0$ the procedure is basically equivalent to trimming or pruning, for $\beta = 0$ it roughly corresponds to the mMDT, whereas for $\beta < 0$, the extreme tagging mode, its behaviour resembles that of Y-pruning. The performance of the various taggers can be assessed by studying the acceptance efficiency for the signal ϵ_S (the number of tagged signal jets over the total number of signal jets) versus that for the background ϵ_B . In figure 4.12 we find a couple of examples of such studies for the tagging of a boosted W boson. The one on the left is taken from [18], and shows $\epsilon_S/\sqrt{\epsilon_B}$ as a measure of the signal significance, as a function of the tagged jet transverse momentum. There one can see the better performance of taggers with respect to groomers. In particular, Y-pruning seems to outperform the other taggers at large p_t . The plot on the right, taken from [17], shows instead ϵ_S/ϵ_B as a function of the jet transverse momentum, for different variants of the soft-drop procedure, corresponding to different values of the parameter β . The pattern is very similar, with taggers performing better than groomers. Also, variants with negative β outperform the one with $\beta = 0$, which corresponds roughly to the mMDT. Their performance is similar to that of Y-pruning. This is not surprising, in that setting $\beta < 0$ de facto removes jets that are very collimated, thus leaving two-prong structures only, the more aggressive the cut the more negative β is.

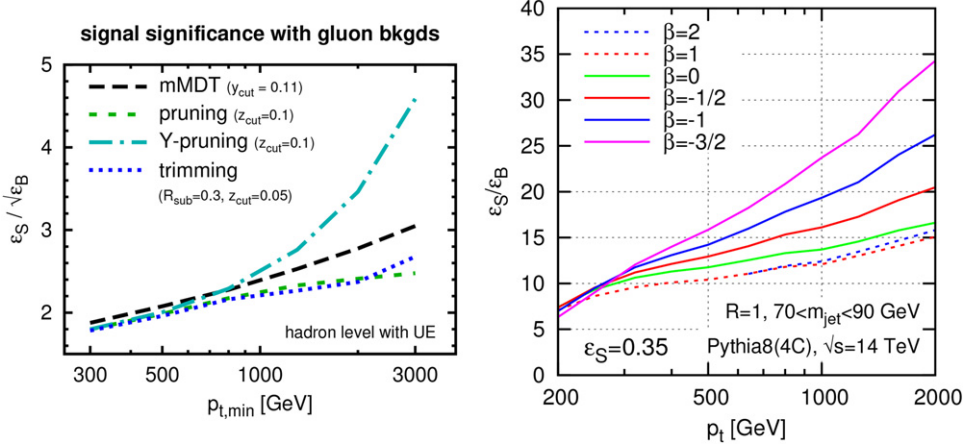


Figure 4.12. Estimate of signal versus background tagging efficiency for various taggers as a function of the minimum transverse momentum of the tagged jet $p_{t,\min}$ [18] (left) and of the soft-drop tagger for various values of β , as a function of the tagged jet transverse momentum p_t [17] (right).

4.2.3 Event shapes for jet-substructure studies

The procedures we have seen so far are based on the declustering of a jet and subsequent elimination of jet constituents. A complementary approach is to use event shapes, or jet resolution parameters, using the constituents of a fat jet as inputs. Suppose that one reclusters a fat jet using the k_t algorithm. Then, a single jet will have a one-jet resolution y_1 that is of order one. If a jet is made up of two energetic subjets, then the two-jet resolution y_2 will also be of order one. A QCD jet instead will tend to have a small two-jet resolution. Therefore, the distribution in y_2/y_1 will be peaked at lower values for QCD jets than for jets originating from hadronic decays of a heavy particle. One can then separate signal from background by simply performing a cut in y_2/y_1 . For two-prong decays, this is similar to the asymmetry condition for the MDT in (4.10). Similarly, one can look for three-prong decays by performing a cut on y_3/y_2 , and so on. This is the basis of the tagging procedure encoded in the program Y-splitter [20]. Jet resolutions are just an example of a discriminating variable. More recent studies use the N -subjettiness variable [21, 22], defined after declustering a jet of radius R into N subjets as

$$\tau_N^{(\beta)} = \frac{1}{d_0} \sum_{i \in \text{jet}} p_{ti} \min\{(\Delta R_{1i})^\beta, (\Delta R_{2i})^\beta, \dots, (\Delta R_{Ni})^\beta\}, \quad d_0 = \sum_{i \in \text{jet}} p_{ti} R^\beta. \quad (4.13)$$

The parameter β gives then the extra freedom to vary the relative importance of soft and collinear radiation, as happened in the case of the soft drop. The sums in the above expression run over all jet constituents and ΔR_{jk} is the $y-\phi$ distance between the jet momentum p_j , with $j = 1, \dots, N$, and the jet constituent p_k . The use of N -subjettiness is similar to that of the Y-splitter: looking for a N -prong decay requires a suitable cut on τ_N / τ_{N-1} (with $\tau_N \equiv \tau_N^{(1)}$). N -subjettiness is more tractable than the Y-splitter from an analytical point of view, because of the existence of all-order factorisation formulae in

SCET, at least for its global variant N -jettiness [23]. Another example of variables that can be used to investigate jet substructure is ratios of generalised energy-correlation functions (ECFs) $\text{ECF}(N, \beta)$ [24], defined by the relations

$$\begin{aligned}\text{ECF}(0, \beta) &= 1 \\ \text{ECF}(1, \beta) &= \sum_{i \in \text{jet}} p_{ti} \\ \text{ECF}(2, \beta) &= \sum_{i < j \in \text{jet}} p_{ti} p_{tj} (\Delta R_{ij})^\beta, \\ \text{ECF}(N, \beta) &= \sum_{i_1, i_2, \dots, i_n \in \text{jet}} \left(\prod_{a=1}^N p_{ti_a} \right) \left(\prod_{b=1}^{N-1} \prod_{c=b+1}^N \Delta R_{i_b i_c} \right)^\beta.\end{aligned}\tag{4.14}$$

For instance, for two-prong decays one can consider the ratio $C_1^{(\beta)}$, defined as

$$C_1^{(\beta)} = \frac{\text{ECF}(2, \beta) \text{ECF}(0, \beta)}{\text{ECF}(1, \beta)^2},\tag{4.15}$$

where by comparing (4.14) and (4.13), one sees that $C_1^{(\beta)}$ is related to the 1-subjettiness variable defined in (4.13). A comparison of the performance of generalised ECFs and N -subjettiness can be found in [24]. ECFs will be discussed further in the context of separation between quark and gluon jets.

4.2.4 The role of interjet radiation

Let us consider again the case of a boosted Higgs decaying into a $b\bar{b}$ pair and suppose that, after some tagging procedure, we are left with a jet cleaned of all its soft constituents, showing two subjets, both tagged as b jets (see figure 4.7). An irreducible background to our signal originates from a gluon splitting into a $b\bar{b}$ pair. Due to the collinear singularity of gluon splitting, it is presumable that such a background will be reduced by a suitable cut, such as the asymmetry cut in (4.10). However, QCD radiation is more probable than any electroweak process we wish to observe, so many events with two well-separated b jets arising from gluon splitting will probably survive the cuts. A way to reduce this background is to observe that a gluon carries a colour charge, whereas a Higgs does not. Therefore, due to the coherence properties of QCD radiation, in the case of $H \rightarrow b\bar{b}$, radiation coming from the $b\bar{b}$ pair will be roughly contained inside the fat jet (see figure 4.7), whereas in the gluon case there will be a considerable amount of radiation outside as well. A way of exploiting this information is to veto additional jets in the event. In fact, final-state radiation at angles larger than the jet radius will produce additional jets, so that vetoing this activity suppresses the background through a Sudakov form factor, whereas no such price is paid for the signal. However, both signal and background events are affected by initial-state radiation, so that Sudakov form factors will suppress the signal as well. Imposing vetoes on extra jets is a way to exploit the angular distribution of energy-momentum flow in QCD and Higgs jets. In fact, in $H \rightarrow b\bar{b}$, QCD radiation will be contained in the region between the two b jets (we say in this case that the b and anti- b are ‘colour connected’), whereas in the

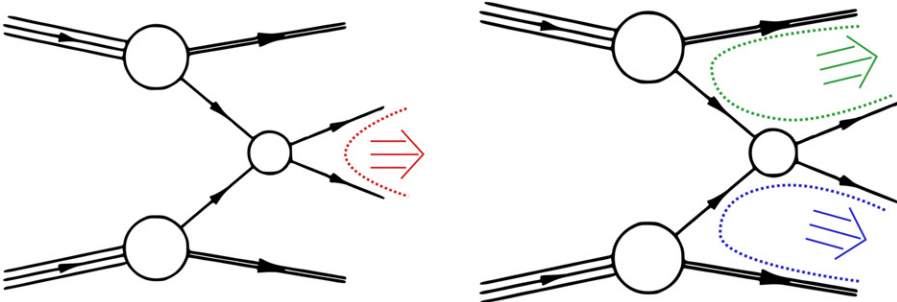


Figure 4.13. A pictorial representation of the preferred directions of QCD radiation (the big arrows) in an event in which a $b\bar{b}$ pair is produced via the decay of a colourless particle (left) or through the splitting of a coloured particle, for instance a gluon (right) [25].

case of a QCD event, radiation will preferably occupy the region between each jet and the closest beam. This is pictorially illustrated in figure 4.13. A way of specifically quantifying this effect is through a physical quantity called the ‘pull’ vector, which is a property of each jet and gives an idea of the direction in which the colour flow of an event is ‘pulled’. For any particle p_i in the jet ‘J’ of momentum p_J , one considers the two-dimensional distance vector $\vec{\eta}_i = (y_i - y_J, \phi_i - \phi_J)$. In terms of this quantity the pull vector of jet ‘J’ is defined as

$$\vec{v}_p^J \equiv \sum_{i \in J} \frac{p_{ti} |\vec{\eta}_i|}{p_{tJ}} \vec{\eta}_i. \quad (4.16)$$

An interesting quantity to look at is the pull angle θ_p that the pull vector forms with respect to a reference axis. In [25] the reference axis was chosen to be that of one of the beams. The expectation was that the distribution in the pull angle of a b jet in signal and background events would be peaked at $\theta_t = 0, \pm\pi$ for background events and at the position of the other b jet for signal events. That this variable is indeed an event-by-event probe of colour connections has been confirmed by an experimental analysis performed by the ATLAS collaboration [26], which considers two jets coming from the decay of a W boson from the decay of a top quark. The measured quantity is the pull angle of one of the jets with respect to the axis of the other jet (see figure 4.14, left panel). The distribution in the pull angle (see figure 4.14, right panel) is then compared to the output of different Monte Carlo event generators, one of which has flipped colour connections, so that one of the quarks coming from the decay of the W is not colour-connected to the other antiquark, but rather to the b quark coming from the decay of the top. As expected, the pull angle distribution is peaked around zero. This behaviour is reproduced by a standard colour connection (labelled ‘SM $t\bar{t}$ ’ in figure 4.14), but not by the flipped colour connection (labelled ‘Flipped $t\bar{t}$ ’ in figure 4.14).

4.2.5 Quantum jets and volatility

As we have seen in section 2.2, it is possible to run traditional jet algorithms in quantum mode [27]. This is done by repeating the jet clustering procedure N_{tree} times

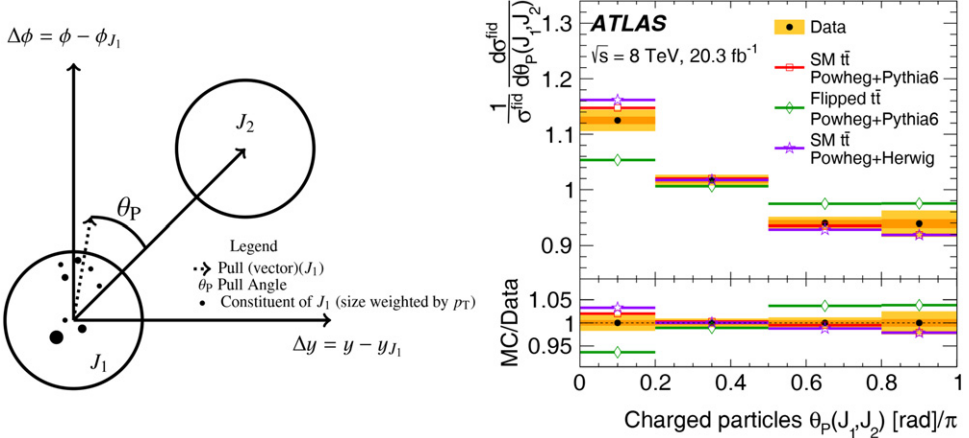


Figure 4.14. The pull angle measured by the ATLAS collaboration in [26] (left) and its differential distribution obtained with charged tracks only, compared to different predictions obtained with parton-shower event generators (right).

for each event, each time giving a different probability to the clustering sequence. In practice, each event will not be clustered unambiguously into jets, but we will instead obtain N_{tree} different sets of jet momenta, each with a different assigned probability. For instance, if we run a sequential algorithm inside a fat jet applying a pruning procedure, we will obtain a probability distribution for the pruned mass instead of a single value. Once one considers all possible events, one obtains very different distributions for quantum versus classical pruned jets, as shown in figure 2.13 of section 2.2.

A first consequence of the existence of multiple interpretations for an event is that signal events that look background-like can be clustered in different ways and then they have the chance of being kept rather than rejected, as might happen by enforcing a single interpretation. This has the overall effect of increasing the significance of the signal over the background.

Quantum jets also offer the possibility of defining new observables that would be just zero at the classical level. For instance, given the mass of a jet m_{jet} , one can define the volatility of a jet as [27]

$$\mathcal{V} \equiv \frac{\sqrt{\langle m_{\text{jet}}^2 \rangle - \langle m_{\text{jet}} \rangle^2}}{\langle m_{\text{jet}} \rangle}, \quad (4.17)$$

where the average has to be taken over all possible interpretations of an event. For instance, if we wish to distinguish between W jets and QCD jets, we expect the former to have a smaller volatility. This is because these jets will have a mass close to the W mass, which will fluctuate less over multiple interpretations. This is what is observed in the left-hand panel of figure 4.15, which shows the distribution in volatility for W and QCD jets. Therefore, performing a cut on volatility is a viable way to discriminate between signal and background. The performance of this

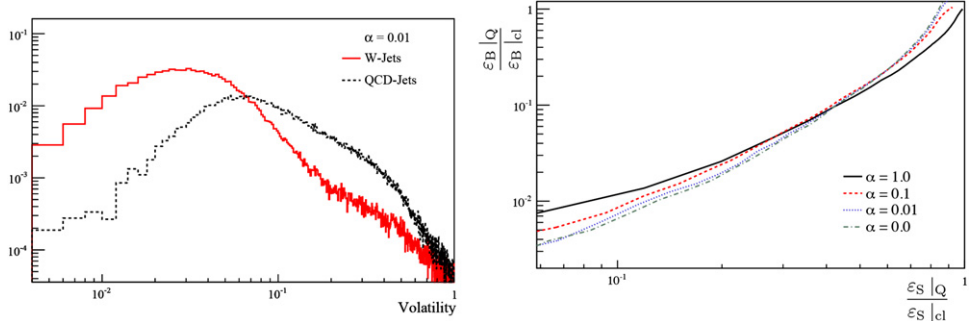


Figure 4.15. Left: the distribution in the volatility for W and QCD jets corresponding to a rigidity parameter $\alpha = 0.01$. Right: the efficiency for background acceptance (normalised to the classical value) versus that for the signal (also normalised to the classical value) [27].

discriminator is shown in the plot of the right-hand panel of figure 4.15, where one can see the efficiency for background acceptance versus that for the signal, both normalised to the corresponding classical limit, for various values of the rigidity parameter α controlling the quantum jet algorithm. The plots correspond to a cut $\mathcal{V} < 0.03$. It is interesting to note that allowing multiple interpretations overall decreases the efficiency for signal and background with respect to the classical case. However, the resulting efficiency for the background can be reduced by a factor of ten more than that for the signal, thus giving a larger significance of the signal over the background. In fact, for the point with the best performance, located around (0.25, 0.03) in the plot, the significance of the signal is doubled with respect to the classical case. For a comprehensive study of the use of quantum jets for signal and background discrimination the reader is referred to [28].

4.2.6 Jet substructure studies at the LHC

Ultimately, the effectiveness of all the procedures described so far has to be validated using real data, before they can be used in actual searches. This can be achieved by considering events in which the decaying heavy particle is known (a so-called ‘pure sample’) and performing jet-substructure studies on that sample.

The first run of the LHC has been an excellent playground to test the performance of different jet-substructure techniques. A large number of Z and W bosons, as well as top quarks, have offered the possibility to have reasonably pure samples of heavy particles generating two- and three-prong hadronic decays. And of course, a large amount of jet data is the ideal laboratory to investigate the properties of pure QCD jets. Here we will focus on experimental studies of two-prong decays, namely those of W and Z bosons. The reader interested in boosted top decays can find a comprehensive study in [29]. The study compares the performance of various jet-substructure procedures for top, W and QCD jets. This source also contains a detailed description of how to perform the calibration of highly boosted jets. This is particularly important in view of the fact that the target observable for jet substructure studies is the jet invariant mass, and also that many taggers and

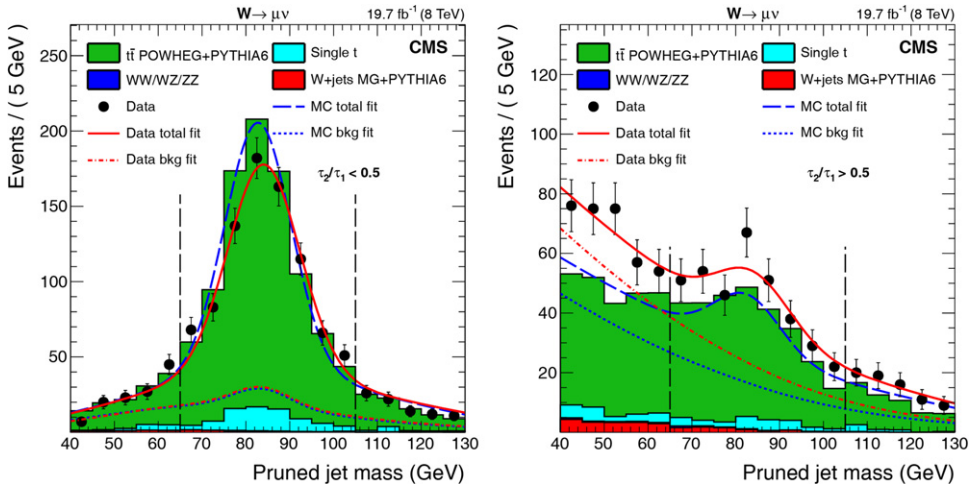


Figure 4.16. The distribution in the invariant mass of a pruned jet in semi-leptonic $t\bar{t}$ events for $\tau_2/\tau_1 < 0.5$ (left) and $\tau_2/\tau_1 > 0.5$ (right), as measured by the CMS collaboration [30].

groomers need ratios of transverse momenta and invariant masses between pairs of subjets to be precisely measured.

The CMS Collaboration has considered a pure sample of W bosons originating from semi-leptonic top decays [30]. This means that the W from one of the tops decays into leptons, i.e. giving a charged lepton (electron or muon) and a neutrino, whereas the other W decays hadronically. The study includes pruning, the MDT in its original version, event shapes such as N -subjettiness and moments of ECFs, Q-jets volatility and the jet charge [31]. A combined study of these variables has shown that pruning the W jet and imposing a cut on τ_2/τ_1 provides an efficient separation between the signal and QCD background. In particular, $\tau_2/\tau_1 < 0.5$ selects predominantly W jets, cutting off most of the QCD background. The effectiveness of the cut can be seen from the distribution in the pruned mass for $\tau_2/\tau_1 < 0.5$ (figure 4.16, left panel) and for $\tau_2/\tau_1 > 0.5$ (figure 4.16, right panel), for events in which a W boson decays into a muon and a neutrino. For $\tau_2/\tau_1 < 0.5$ the pruned mass distribution does show a peak in correspondence to the W mass, but this peak has a very poor resolution. This is not the case for $\tau_2/\tau_1 > 0.5$, where a mass peak is clearly visible.

In [32] ATLAS used a mixed sample of W and Z jets, as well as QCD jets, to measure the invariant-mass distribution of a jet before and after jet grooming with various techniques. These included pruning, trimming, as well as area subtraction, as explained in section 2.13. Figure 4.17 shows a comparison between the distribution in the invariant mass of a jet, both groomed and ungroomed, and the corresponding predictions obtained with parton-shower event generators. As discussed in [18] and reported in section 4.2.2, the main effect of groomers is that of reducing the effective radius of jets, hence pushing the peak in their invariant mass distribution to lower values. Also, the comparison with parton-shower event generators is excellent, thus confirming the reliability of these theoretical tools. Another important result is that, in the presence of PU, the distribution in the invariant mass of groomed jets is

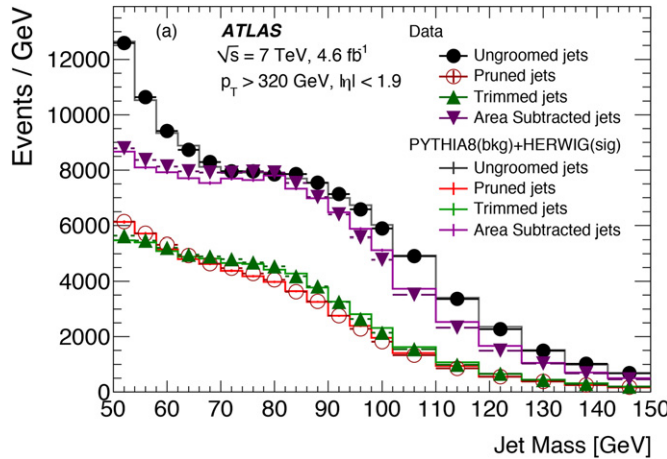


Figure 4.17. The invariant mass of a jet as measured by the ATLAS collaboration [32], with and without grooming.

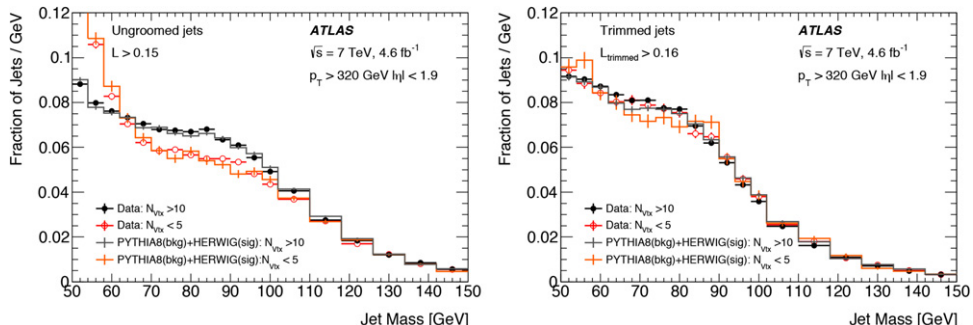


Figure 4.18. The invariant mass distribution of a jet before grooming (left) and after trimming (right), for events with low ($N_{\text{vtx}} < 5$) and high PU ($N_{\text{vtx}} > 10$), as measured by the ATLAS collaboration [32].

basically independent of the number of secondary interaction vertices N_{vtx} , as can be seen in the right-hand panel of figure 4.18 for the specific case of trimming, although all groomers show the same behaviour. This is to be compared to the large dependence on the number of secondary vertices seen for the ungroomed jet mass distribution in the left-hand panel of figure 4.18. This study, as well as that in [30], show that grooming procedures such as trimming and pruning are suitable alternatives to the jet-area method as a means to eliminate PU contamination to boosted jets.

4.3 Quark–gluon jet discrimination

In many new physics searches, it is important to be able to distinguish whether a jet was initiated by a quark or a gluon. For instance, the jets produced in subsequent decays of supersymmetric particles are usually quark jets and the corresponding background largely gluon jets (see e.g. [33]).

4.3.1 Differences between quark and gluon jets

First of all, it is natural to define the flavour of a jet as the net sum of the flavour of all its constituents, i.e. the sum of the quarks minus the sum of the antiquarks, with gluons not contributing to the flavour of a jet [34]. Before hadronisation, the flavour of a jet is a well-defined quantity. If jets are clustered using any IRC safe algorithm, such a definition of flavour is invariant under collinear splittings. However, soft large-angle quark–antiquark pairs might be separated by the clustering procedure and the resulting flavour of jets becomes infrared unsafe. In the case of the k_t algorithm, such unsafety can be removed via a modification of the k_t distance when the softer of the two particles that are to be clustered is a quark. This gives rise to the family of flavour- k_t algorithms, which have various applications in perturbative QCD studies [34, 35]. Such an approach, although theoretically rigorous, cannot be used in practice to determine the flavour of a jet, simply because one does not in general have access to the full information on the flavour of all particles in an event.

The current way to discriminate between quark and gluon jets is to instead use variables whose distributions are different for quark and gluon jets. One then imposes a cut in a discriminating variable and looks at the fraction of gluon jets that do not pass the cut (gluon-jet rejection) as a function of the fraction of quark jets that do survive the cut (quark-jet acceptance). The aim is to find an observable for which both quantities are large. It is thus natural to exploit the fact that gluons radiate roughly twice as much as quarks. Therefore, any observable that is sensitive to QCD radiation can be used for this purpose. Among these variables, one having a good discriminating power is the girth of a jet ‘ J ’¹ [36], defined as

$$g = \sum_{i \in \text{jet}} \frac{p_{ti}}{p_{tJ}} \Delta R_{iJ}. \quad (4.18)$$

Note that this observable is very close to the generalised 1-jettiness variable $\tau_1^{(1)}$, defined in (4.13). Before reviewing the performance of different event-shapes, we discuss the basics of quark-gluon jet discrimination based on colour. The event shapes that we consider here are zero for a single massless particle and acquire a non-zero value dynamically through QCD radiation. As for the jet mass distribution in figure 4.9, the girth distribution has a peak at a non-zero value of g . The position of the peak is different for quark and gluon jets, and at higher values of g for gluon jets than for quark jets. Quark–gluon jet discrimination can be achieved by cutting the girth distribution at a value g_{cut} so as to include the peak of the girth distribution for quark jets and leave out the peak of the same distribution for gluon jets. The fraction of quark and gluon jets surviving the cut is simply given by the two cumulative distributions

$$\Sigma_q(g_{\text{cut}}) \simeq e^{-C_F \frac{\alpha_s}{\pi} \ln^2 g_{\text{cut}}}, \quad \Sigma_g(g_{\text{cut}}) \simeq e^{-C_A \frac{\alpha_s}{\pi} \ln^2 g_{\text{cut}}}, \quad (4.19)$$

where in the analytic evaluation of $\Sigma_{q-g}(g_{\text{cut}})$ we have kept only the leading double logarithms. What one immediately observes here is that, if $\Sigma_q(g_{\text{cut}}) = x$, i.e. one keeps

¹ In studies of event shapes at hadron colliders, the very same variable is known as jet broadening [37].

a fraction x of quark jets, one automatically keeps a fraction x^{C_A/C_F} of gluon jets. This scaling holds at LL accuracy not only for the girth, but for any IRC safe final-state observable whose double logarithms exponentiate. This is due to the fact that, at LL level, both Σ_q and Σ_g are given by Sudakov exponents, proportional to the colour charge of the parton that has initiated the jet. This means that the different discriminating power of event shapes is due to subleading effects, which are generally not very large and moreover are not treated in the same way by parton-shower event generators, which are the tools used in both theoretical and experimental studies of quark–gluon jet discrimination. In particular, beyond LL approximation, the discriminating power of an event shape depends on the relative importance of soft and collinear radiation. ECFs and their ratios have a built-in handle for this, their parameter β . For instance, one can consider [24] the ratio $C_1^{(\beta)}$ of (4.15). Note that, for $\beta = 1$, this variable has the same properties as the girth. Analytical studies of Σ_{q-g} ($C_1^{(\beta)}$) for different values of β suggest that smaller values of this parameter (e.g. $\beta = 0.2$) give a better quark–gluon jet discrimination, although the improvement with respect to the girth is not dramatic, being driven by subleading effects. An example of the performance of different variables is given in figure 4.19. The plot on the left shows the tagging efficiency for quark jets versus the same quantity for gluon jets, obtained through an analytical calculation at NLL + LO accuracy (see [24] for details), for the ratio of moments of ECFs $C_1^{(\beta)}$ (see (4.15)) corresponding to different values of β . For a given quark tagging efficiency, the best discriminator is the one that has the lowest gluon tagging efficiency. At LL accuracy there is no dependence on β , because the ratio between the two efficiencies is determined by colour factors only. Differences start to appear at NLL, where one sees that increasing the importance of collinear versus soft contributions (i.e. decreasing β) increases the discriminatory power of an observable. The same behaviour is seen with Monte Carlo event generators, although numbers differ slightly due to differences in the treatment of subleading effects. The plot on the right shows instead the gluon rejection rate (i.e. one minus the gluon tagging efficiency) corresponding to a 50% quark acceptance rate, as a function of β , both for

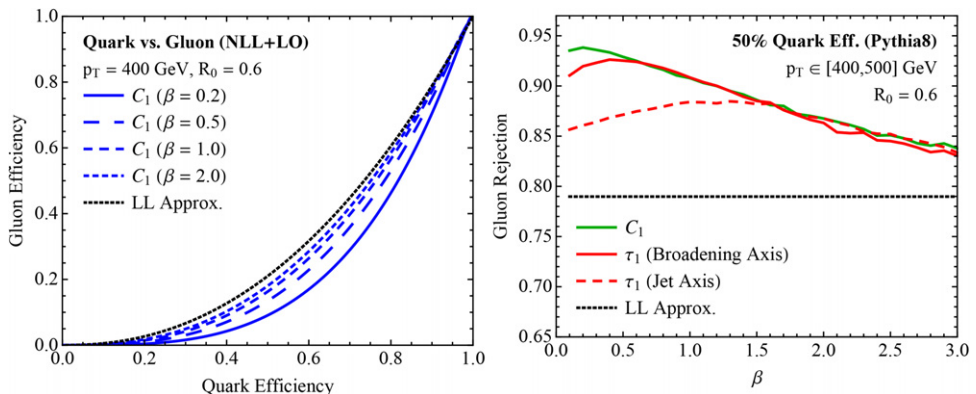


Figure 4.19. Left: gluon jet tagging efficiency versus quark jet tagging efficiency for the ratio of moments of ECFs $C_1^{(\beta)}$ [24]. Right: gluon jet rejection rate corresponding to a 50% quark jet tagging efficiency as a function of the parameter β , for various event shapes [24].

$C_1^{(\beta)}$ and for 1-subjettiness. We note that, while the rejection power for $C_1^{(\beta)}$ increases with decreasing β , it freezes for 1-subjettiness, when the axis with respect to which this variable is computed coincides with the jet axis. This is due to the fact that, for $\beta \leq 1$, 1-subjettiness is mostly sensitive to QCD radiation through recoil, rather than direct emission detection. This is not the case if 1-subjettiness is computed with respect to the axis that minimises 1-subjettiness itself (called the ‘broadening axis’ in the figure). In this case 1-subjettiness is very similar to the corresponding $C_1^{(\beta)}$. The latter observable has, however, the advantage of not requiring a minimisation procedure in order to be computed. In addition to IRC safe observables such as event shapes, one can also consider unsafe ones, such as charged hadron multiplicities, or jet electric charges [31]. These variables are sensitive in many ways to the different QCD radiation patterns of quark and gluon jets. Many of those have various degrees of correlation, so it might be useful to combine different variables and use neural-network methods to find the optimal combination of cuts. Examples of such studies can be found in [10, 36, 38].

4.3.2 Quark and gluon jet discrimination at the LHC

Systematic studies of the properties of quark and gluon jets have been performed at LEP (see e.g. [39, 40]). These analyses exploit three-jet events in which two b-tagged jets fall in the same hemisphere, thus leaving an energetic gluon jet in the other hemisphere to obtain pure samples of gluon jets. This information is used to measure the particle multiplicities inside quark and gluon jets and extract from that the ratio C_A/C_F . In fact, the ratio of hadron multiplicity in quark and gluon jets tends for asymptotically high energies to the ratio of the corresponding colour factors. A preliminary measurement of C_A/C_F has also been performed at the Tevatron [41].

LHC experiments have exploited the ideas illustrated in section 4.3.1 to build statistical discriminants between quark and gluon jets. These use some of the variables defined in section 4.3.1, picking up the ones that are less correlated. ATLAS uses at the scope the number of tracks associated to a jet, the width of the jet, which is in fact the girth or broadening of the jet, as well as $C_1^{(\beta)}$ for different values of the parameter β , referred to as energy-energy-correlation (EEC) angularity [42]. The best performing EEC angularity (the one with $\beta = 0.2$, see figure 4.20) is then discarded in favour of the jet width because it is too correlated with the track multiplicity. A statistical discriminant is then constructed using the differential distribution in these two variables. The result for high p_t jets can be seen in the right-hand panel of figure 4.20. There one sees that the discriminant is able to achieve 50% quark jet efficiency by rejecting 80% of the gluon jets. Similarly, CMS [43] has used a statistical discriminant based on three variables, the multiplicity of jet constituents, an event shape sensitive to the width of a jet, similar to the F-parameter of [44] and a variable $p_T D$, defined as:

$$p_T D = \frac{\left(\sum_{i \in \text{jet}} p_{ti}^2 \right)^2}{\sum_{i \in \text{jet}} p_{ti}}, \quad (4.20)$$

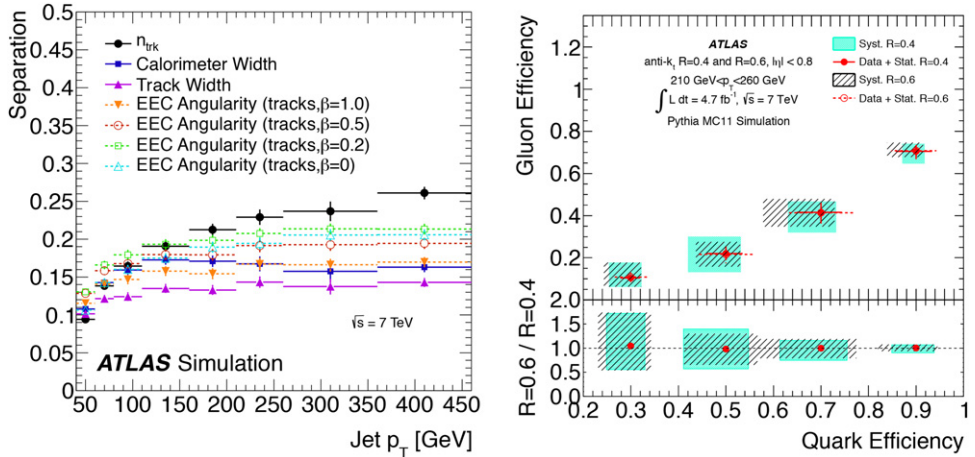


Figure 4.20. Left: the performance of different observables, quantified by a suitable variable called ‘Separation’, as a function of the jet transverse momentum. Right: gluon jet versus quark jet efficiency, for two different values of the jet radius. Both plots are taken from [42].

whose distribution gives an idea of how the energy of a jet is shared among its components. From its definition one sees that $p_T D \rightarrow 1$ for a jet made up of a single particle and $p_T D \rightarrow 0$ for a jet consisting of an infinite number of particles. A preliminary analysis using events with two jets and a Z recoiling against a jet shows that it is possible to accept quark jets with 60% efficiency, while rejecting 70% of gluon jets [43].

Bibliography

- [1] Aad G *et al* (ATLAS Collaboration) 2015 *J. High Energy Phys.* JHEP02(2015)153
- [2] Nagy Z 2001 *Phys. Rev. Lett.* **88** 122003
- [3] Olive K A *et al* (Particle Data Group Collaboration) 2014 *Chin. Phys. C* **38** 090001
- [4] Cacciari M, Rojo J, Salam G P and Soyez G 2008 *J. High Energy Phys.* JHEP12(2008)032
- [5] <http://www.lpthe.jussieu.fr/~salam/jet-quality/>
- [6] Dasgupta M, Magnea L and Salam G P 2008 *J. High Energy Phys.* JHEP02(2008)055
- [7] Dasgupta M, Dreyer F, Salam G P and Soyez G 2015 *J. High Energy Phys.* JHEP04(2015)039
- [8] Seymour M H 1994 *Z. Phys. C* **62** 127
- [9] Altheimer A *et al* 2014 *Eur. Phys. J. C* **74** 2792
- [10] Adams D *et al* 2015 *Eur. Phys. J. C* doi:10.1140/epjc/s10052-015-3587-2
- [11] Kaplan D E, Rehermann K, Schwartz M D and Tweedie B 2008 *Phys. Rev. Lett.* **101** 142001
- [12] Plehn T, Salam G P and Spannowsky M 2010 *Phys. Rev. Lett.* **104** 111801
- [13] Plehn T, Spannowsky M, Takeuchi M and Zerwas D 2010 *J. High Energy Phys.* JHEP10(2010)078
- [14] Krohn D, Thaler J and Wang L T 2010 *J. High Energy Phys.* JHEP02(2010)084
- [15] Ellis S D, Vermilion C K and Walsh J R 2010 *Phys. Rev. D* **81** 094023
- [16] Butterworth J M, Davison A R, Rubin M and Salam G P 2008 *Phys. Rev. Lett.* **100** 242001

- [17] Larkoski A J, Marzani S, Soyez G and Thaler J 2014 *J. High Energy Phys.* JHEP05(2014)146
- [18] Dasgupta M, Fregoso A, Marzani S and Salam G P 2013 *J. High Energy Phys.* JHEP09(2013)029
- [19] Rubin M 2010 *J. High Energy Phys.* JHEP05(2010)005
- [20] Butterworth J M, Cox B E and Forshaw J R 2002 *Phys. Rev. D* **65** 096014
- [21] Thaler J and Van Tilburg K 2011 *J. High Energy Phys.* JHEP03(2011)015
- [22] Thaler J and Van Tilburg K 2012 *J. High Energy Phys.* JHEP02(2012)093
- [23] Jouttenus T T, Stewart I W, Tackman F J and Waalewijn W J 2011 *Phys. Rev. D* **83** 114030
- [24] Larkoski A J, Salam G P and Thaler J 2013 *J. High Energy Phys.* JHEP06(2013)108
- [25] Gallicchio J and Schwartz M D 2010 *Phys. Rev. Lett.* **105** 022001
- [26] Aad G *et al* (ATLAS Collaboration) 2015 *Eur. Phys. J. C* **750** 475–93
- [27] Ellis S D, Hornig A, Roy T S, Krohn D and Schwartz M D 2012 *Phys. Rev. Lett.* **108** 182003
- [28] Kahawala D, Krohn D and Schwartz M D 2013 *J. High Energy Phys.* JHEP06(2013)006
- [29] Aad G *et al* (ATLAS Collaboration) 2013 *J. High Energy Phys.* JHEP09(2013)076
- [30] Khachatryan V *et al* (CMS Collaboration) 2014 *J. High Energy Phys.* JHEP12(2014)017
- [31] Krohn D, Schwartz M D, Lin T and Waalewijn W J 2013 *Phys. Rev. Lett.* **110** 212001
- [32] Aad G *et al* (ATLAS Collaboration) 2014 *New J. Phys.* **16** 113013
- [33] Bechtle P, Phehn T and Sander C 2015 arXiv: [1506.03091](#)
- [34] Banfi A, Salam G P and Zanderighi G 2006 *Eur. Phys. J. C* **47** 113–24
- [35] Banfi A, Salam G P and Zanderighi G 2007 *J. High Energy Phys.* JHEP07(2007)026
- [36] Gallicchio J and Schwartz M D 2011 *Phys. Rev. Lett.* **107** 172001
- [37] Banfi A, Salam G P and Zanderighi G 2004 *J. High Energy Phys.* JHEP08(2004)062
- [38] Gallicchio J and Schwartz M D 2013 *J. High Energy Phys.* JHEP04(2013)090
- [39] Abbiendi G *et al* (OPAL Collaboration) 1999 *Eur. Phys. J. C* **11** 217
- [40] Abreu P *et al* (DELPHI Collaboration) 1999 *Phys. Lett. B* **449** 383
- [41] Pronko A (CDF Collaboration) 2005 *Int. J. Mod. Phys. A* **20** 3723
- [42] Aad G *et al* (ATLAS Collaboration) 2014 *Eur. Phys. J. C* **74** 3023
- [43] CMS Collaboration CMS-PAS-JME-13-002
- [44] Banfi A, Salam G P and Zanderighi G 2010 *J. High Energy Phys.* JHEP06(2010)038